NASA Technical Memorandum 4117

Transonic Aerodynamic Characteristics of a Proposed Assured Crew Return Capability (ACRC) Lifting-Body Configuration

George M. Ware
Langley Research Center
Hampton, Virginia

National Aeronautics and
Space Administration
Office of Management
Scientific and Technical
Information Division

1989

Summary

The investigation was conducted in the Calspan 8-Foot Transonic Wind Tunnel at Mach numbers from 0.6 to 1.2. The 0.07-scale model had a low-aspect-ratio body with a flat undersurface. A center fin and two tip fins were mounted on the aft upper body. The tip fins were rolled outboard 40° from the vertical. Elevon surfaces made up the trailing edges of the outboard fins, and body flaps were located on the upper and lower aft fuselage. Results of the investigation indicated that the model was longitudinally and laterally stable about a center-of-gravity position at 54 percent of the body length. The maximum trimmed lift/drag ratio was about 3.1 at a Mach number of 0.6. The small center fin contributed only a small positive increment to lateral stability but was effective as a yaw control device. The model with pitch controls undeflected had desirable longitudinal trim characteristics.

Introduction

The National Aeronautics and Space Administration (NASA) is considering the requirement of having one or more crew return vehicles docked at the Space Station Freedom. These vehicles will be a safeguard to assure crew return capability. The detailed mission requirements of such a vehicle have not been finalized, but configurations of varying capabilities are under study. One of the return-vehicle concepts has a lifting-body shape that produces moderate lift/drag values over the speed range giving some cross-range performance and offering the option of a conventional landing. The current investigation was undertaken to define the transonic and high-subsonic aerodynamic characteristics of this configuration.

The test was conducted using a 0.07-scale model in the Calspan 8-Foot Transonic Wind Tunnel at Mach numbers from 0.6 to 1.2 at a constant Reynolds number of 6×10^6 based on body length. (The estimated flight Reynolds number would vary from 29×10^6 at a Mach number of 1.2 to 54×10^6 at a Mach number of 0.6.) The model was tested over an angle-of-attack range of about $-5°$ to 25° and an angle-of-sideslip range of $-10°$ to 10°. Control effectiveness of both elevons and body flaps was studied. Tests were also made with center and tip fins removed.

Symbols

The longitudinal data are referred to the stability-axis system, and the lateral-directional data are referred to the body-axis system (fig. 1). All coefficients are based on the dimensions of the basic body without tip fins. The data are normalized by the projected planform area, length, and span of the body. The moment reference center was located at the vehicle center of gravity which was at 54 percent of the body length.

b	body span, in.
C_D	drag coefficient, Drag/qS_{ref}
C_L	lift coefficient, Lift/qS_{ref}
C_l	rolling-moment coefficient, Rolling moment/qbS_{ref}
C_{l_β}	$= \Delta C_l/\Delta\beta$, taken at $\beta = \pm 2°$, per degree
$C_{l_{\delta a}}$	$= \Delta C_l/\Delta\delta_a$, taken at $\delta_a = \pm 5°$ (elevon) and $\pm 10°$ (body flap), per degree
$C_{l_{\delta r}}$	$= \Delta C_l/\Delta\delta_r$, taken at $\delta_r = 0°$ and 5°, per degree
C_m	pitching-moment coefficient, Pitching moment/qlS_{ref}
C_n	yawing-moment coefficient, Yawing moment/qbS_{ref}
$C_{n\beta}$	$= \Delta C_n/\Delta\beta$, taken at $\beta = \pm 2°$, per degree
$C_{n_{\delta a}}$	$= \Delta C_n/\Delta\delta_a$, taken at $\delta_a = \pm 5°$ (elevon) and $\pm 10°$ (body flap), per degree
$C_{n_{\delta r}}$	$= \Delta C_n/\Delta\delta_r$, taken at $\delta_r = 0°$ and 5°, per degree
C_p	pressure coefficient, $(p_{\text{local}} - p_{\text{free stream}})/q$
C_Y	side-force coefficient, Side force/qS_{ref}
C_{Y_β}	$= \Delta C_Y/\Delta\beta$, taken at $\beta = \pm 2°$, per degree
$C_{Y_{\delta a}}$	$= \Delta C_Y/\Delta\delta_a$, taken at $\delta_a = \pm 5°$ (elevon) and $\pm 10°$ (body flap), per degree
$C_{Y_{\delta r}}$	$= \Delta C_Y/\Delta\delta_r$, taken at $\delta_r = 0°$ and 5°, per degree
FS	full size at model scale
L/D	lift/drag ratio
l	length of root chord (body length), in.
M	Mach number
p	pressure, lb/in^2
q	free-stream dynamic pressure, lb/in^2

S_{ref}	basic body planform area (excluding tip fins), in^2
X	longitudinal model body axis
Y	lateral model body axis
Z	vertical model body axis
α	angle of attack, deg
β	angle of sideslip, deg
δ_a	differential control deflection angle, $(\delta_{e,L} - \delta_{e,R})/2$ or $(\delta_{\text{BF},L} - \delta_{\text{BF},R})/2$, deg
δ_{BF}	body-flap deflection angle (positive when deflected downward), deg
δ_e	elevon deflection angle (positive when deflected downward), deg
δ_r	rudder deflection angle (positive when deflected with trailing edge to right), deg

Subscripts:

L	left
max	maximum value
R	right
TRIM	trimmed condition (zero moment)

Description of Model

Sketches and photographs of the model are presented in figures 2 and 3, respectively. Model dimensional information is given in table I. The aluminum model was a 0.07-scale representation of a proposed 24.6-ft-long vehicle. The configuration consisted of a low-aspect-ratio body with a flat undersurface and a blunt base. Three fins were mounted on the upper aft portion of the model. The centerline fin was relatively small, and the larger outboard (tip) fins were rolled outward 40° from the vertical. The fins had a thick flat-plate cross section with a cylindrical leading edge and blunt trailing edge. Control surfaces, referred to as "elevons", made up the trailing edges of the outboard fins. The entire center fin could be pivoted about the midpoint of the root chord to act as a yaw control device. In addition, the model was equipped with four body-flap control surfaces, two on the upper body and two on the lower body. Their surfaces were flush with the body contour and could only be deflected outward.

Apparatus, Tests, and Corrections

Tests were conducted in the Calspan 8-Foot Transonic Wind Tunnel which is a closed-circuit, single-return, variable-density tunnel. Additional information concerning the facility may be found in reference 1. The investigation was conducted at Mach numbers of 0.6, 0.8, 0.9, 0.95, 1.1, and 1.2 at a constant Reynolds number of 3.5×10^6 per foot. The model was sting mounted through its base, and forces and moments were measured with an internally mounted strain-gauge balance (fig. 4). Model angles of attack and sideslip were corrected for the sting and balance deflection under load. Customary tunnel interference corrections were applied to the data. The corrections were small because of the modest size of the model in the 8-ft-square test section (a model/tunnel cross-sectional-area ratio of 0.003). In an attempt to ensure turbulent flow over the model, transition grit was applied in accordance with reference 2 and as shown in figure 5. All drag data presented are gross drag, in that base drag is included. Model base and sting-cavity pressures were measured, however, and are presented as figure 6.

During the test, the model angle of attack was varied from about $-5°$ to 25° and the angle of sideslip from $-10°$ to 10°. Data were obtained as the model was swept from negative to positive angles over the angle-of-attack or angle-of-sideslip range at a rate of approximately 2 deg/sec. The validity of this test method was checked at each Mach number by making a repeat run taking data with the model set at discrete angles (pitch-pause). A typical example of results from the two test methods is presented in figure 7. The data show excellent agreement.

Results and Discussion

Longitudinal Characteristics

Effects of fins. The effects of fins on the longitudinal aerodynamic characteristics of the model are shown in figure 8. As expected, the outboard fins were a large contributor to lift and stability. The body alone was longitudinally unstable and had low values of lift-curve slope over the Mach number range. The tip fins increased the lift-curve slope, primarily at low angles of attack and Mach number. Lift was linear with angle of attack up to about 18° at $M = 0.6$ (fig. 8(a)), but the linear range decreased as Mach number increased. The outboard fins made the configuration longitudinally stable and produced trim conditions at positive lift. With the center fin in place, there was almost no change in the longitudinal characteristics at low Mach numbers. At Mach

numbers approaching sonic, however, the presence of the center fin caused a negative shift in the pitching curve.

The complete configuration was stable about the design center-of-gravity location (54 percent of the body length). At $M = 0.6$ (fig. 8(d)), the model had a 5-percent static margin based on body length. The margin increased rapidly with increasing Mach number such that at $M = 1.2$, the value was about 14.5 percent. This result suggests that the vehicle might benefit from a more aft center-of-gravity position to reduce the level of stability and improve controllability.

Unlike other lifting-body configurations with tip fins (refs. 3 and 4), the test model did not require negative control deflection to produce positive lift values at an angle of attack of 0°. This was accomplished by building an upsweep of about 10° into the basic body on the aft upper section. Although the upsweep is difficult to see because of the blended shape, it can be noted in the photographs of figure 3. The variation of pitching moment with lift coefficient was relatively linear before "breaking unstable" at a maximum C_L value of about 0.6 at $M = 0.6$ and a minimum C_L value of 0.5 at $M = 0.95$. At all test Mach numbers, the destabilizing break occurred at lift values well above trim conditions.

The maximum lift/drag ratio varied from 3.1 at the lowest test Mach number to 2.0 at $M = 1.2$. Research vehicles with values of L/D in this range have been successfully flown and landed but have required special skills (refs. 5 and 6). The model was trimmed at the low Mach numbers at about $(L/D)_{\max}$ with zero control deflection.

Pitch control. Two sets of movable surfaces were tested as pitch controls; elevons made up the trailing edge of the outboard fins and body flaps were located on the upper and lower afterbody. The body flaps could only be deflected outward; therefore, for positive deflection only the lower-surface flaps were moved, and for negative deflection only the upper-surface flaps were moved.

Pitch control characteristics are presented in figure 9. In general, the effectiveness of the body flaps in producing trimming moments was about half that of the elevons at low angles of attack. At the higher angles of attack, however, flap deflection caused the previously mentioned destabilizing break in pitching moment to occur at a lower angle of attack than elevon deflection. Thus, at $M = 0.6$ and 0.8 (fig. 9(c)) with the reduced stability level at the higher angles of attack, the negative body-flap deflection was as effective in trimming the configuration as the elevon deflection. With a deflection of $-10°$, either elevons or body flaps trimmed the model to its highest subsonic lift value before the onset of longitudinal instability. Because of the large increase in longitudinal stability of the model at Mach numbers above 1.0, the control surfaces were not as effective in changing the trim angle of attack.

The lift/drag ratio was reduced by control deflection primarily at the lower angles of attack. Maximum L/D was reduced somewhat, but little change was noted at the higher angles of attack.

Trim characteristics. Values of angle of attack, lift coefficient, and lift/drag ratio for zero pitching moment with controls undeflected are plotted as a function of Mach number in figure 10. The model exhibits favorable trim characteristics. With neutral controls the model trims near $(L/D)_{\max} = 3.1$ at subsonic speeds and at low angles of attack in the transonic range. Glide performance is therefore maximized at landing and transonic buffeting is minimized.

Lateral Characteristics

Basic lateral characteristics. The lateral coefficients C_Y, C_n, and C_l for the complete model measured across an angle-of-sideslip range of $-10°$ to 10° at angles of attack from 0° to 20° are presented in figure 11. In general, the lateral data were linear over the sideslip range except at the higher angles of attack where nonlinearity occurred at sideslip angles greater than ±4°. Therefore, the lateral stability derivatives obtained from tests at sideslip angles of ±2° and presented in the following figures should be valid and representative of the data taken over a somewhat larger sideslip range.

Lateral stability characteristics. The lateral stability derivatives for the model with various fin arrangements are presented in figure 12. The body-alone configuration was, as expected, directionally unstable (negative values of C_{n_β}) over the test Mach number and angle-of-attack ranges. The outboard fins added a large stabilizing moment making the configuration stable over most of the angle-of-attack range. The small center fin also contributed an increment of positive stability. The model with center and outboard fins (complete model) was directionally stable up to an angle of attack of 24° at $M = 0.6$. The stable angle-of-attack range decreased with increasing Mach number until sonic speed was reached. The unstable range, however, occurred at angles of attack above the anticipated vehicle flight angles. At supersonic speeds, the model was directionally stable over the entire test range.

Although the center fin was effective in adding a small positive increment to C_{n_β}, the model with tip fins alone was stable. The center fin, therefore, is not needed for directional stability. The model had positive effective dihedral, $-C_{l_\beta}$ over the test range with or without fins.

Roll control. Roll control was accomplished by differentially deflecting the elevons on the outboard fins or the body flaps. In the body-flap case, a single surface on the upper body was deflected outward at the same time that a diagonally opposed surface on the lower body was deflected outward. The effectiveness of the roll controls is shown in figure 13. Both sets of controls were effective in producing rolling moments. The elevons, with their larger size and outboard location, were much more effective than the body flaps but only at the lower angles of attack. The effectiveness of the elevons decreased with increasing angle of attack, whereas the effectiveness of the body flaps remained approximately constant. At the higher angles of attack, the body flaps were as effective as the elevons.

The elevons produced about as much adverse yawing moment as rolling moment. This is because of the rolled-out fin configuration. Differential deflection of the elevons acted as much like a rudder as ailerons. The yawing moment associated with body-flap deflection, on the other hand, was near zero. Therefore, if the elevons are used for roll control, a control device such as a rudder will be needed to offset the yawing moments produced.

Yaw control. Yaw control was accomplished by pivoting the small center fin about its midchord. Yaw-effectiveness data are given in figure 14. These data were derived from a fin deflection angle of 5°. The effectiveness value per degree of deflection was essentially constant over the angle-of-attack range at each Mach number. Unlike elevon deflection, the center fin produced almost no cross-coupled moment, that is, no rolling moment. The center fin, although not needed for directional stability, is an effective yaw control device.

Concluding Remarks

A wind-tunnel investigation has been made to determine the subsonic-transonic aerodynamic characteristics of a lifting-body configuration considered as a possible return vehicle from the Space Station Freedom. The model was found to be longitudinally and laterally stable about the design center-of-gravity position of 54 percent of the body length. The configuration was controlled in the pitch plane with either elevons on the trailing edge of the rolled-out tip fins or body flaps mounted on the aft fuselage. A small, movable center fin provided yaw control. The configuration with controls undeflected had desirable trim characteristics over the test range. The model trimmed near the maximum lift/drag value (3.1) at subsonic speeds and at low angles of attack through the transonic range. Thus, subsonic glide performance was maximized at landing and transonic buffeting was minimized.

NASA Langley Research Center
Hampton, VA 23665-5225
May 4, 1989

References

1. Peñaranda, Frank E.; and Freda, M. Shannon, eds.: *Aeronautical Facilities Catalogue. Volume 1—Wind Tunnels.* NASA RP-1132, 1985.
2. Braslow, Albert L.; Hicks, Raymond M.; and Harris, Roy V., Jr.: *Use of Grit-Type Boundary-Layer-Transition Trips on Wind-Tunnel Models.* NASA TN D-3579, 1966.
3. Ware, George M.: *Effect of Fin Arrangements on Aerodynamic Characteristics of a Thick 74° Delta Manned Lifting Entry Vehicle at Low-Subsonic Speeds.* NASA TM X-1020, 1965.
4. McKinney, Linwood W.; and Huffman, Jarrett K.: *Subsonic Aerodynamic Characteristics of a Model of the HL-10 Flight Research Vehicle With Basic and Modified Tip Fins.* NASA TM X-2119, 1971.
5. Reeder, John P.: *The Effect of Lift-Drag Ratio and Speed on the Ability To Position a Gliding Aircraft for a Landing on a 5,000-Foot Runway.* NASA MEMO 3-12-59L, 1959.
6. Weil, Joseph: *Review of the X-15 Program.* NASA TN D-1278, 1962.

Table 1. Geometric Characteristics of Model

Body alone:	
Aspect ratio	0.6
Length (reference length), in.	20.6
Span (reference span), in.	9.7
Planform area (reference area), in^2	152.2
Base area (excluding cavity area), in^2	23.2
Cavity area, in^2	4.9
Height (maximum), in.	4.7
Body with fins:	
Aspect ratio	1.5
Length, in.	20.6
Span, in.	16.3
Planform area, in^2	178.6
Base area (excluding cavity area), in^2	23.2
Cavity area, in^2	4.9
Height (to tip of fin), in.	5.9
Elevons:	
Chord, in.	1.1
Span, in.	4.1
Area (each), in^2	3.5
Body flaps:	
Chord, in.	1.5
Span, in.	2.8
Area (each), in^2	4.2

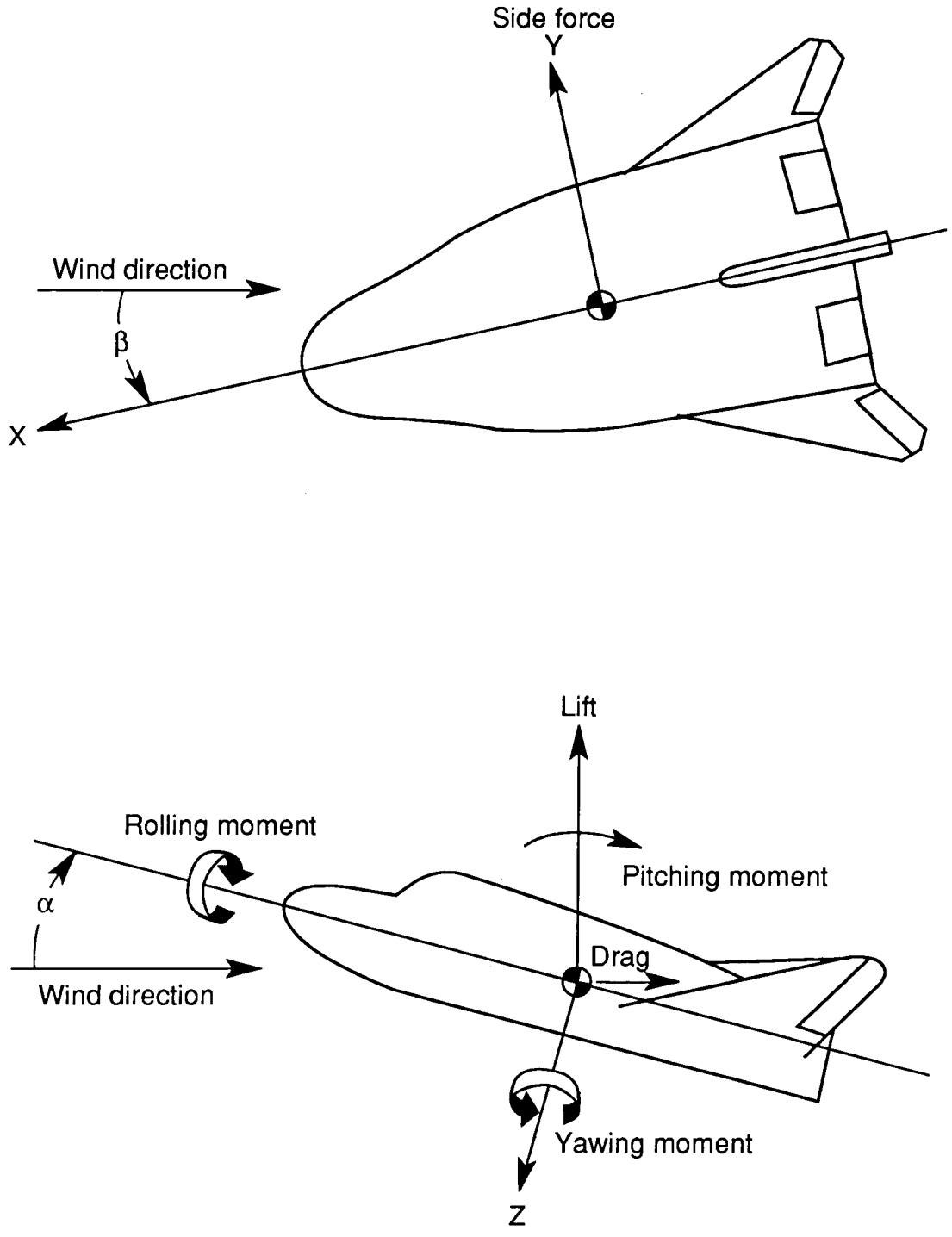

Figure 1. Sketches of systems of axes used in investigation showing positive direction of forces, moments, velocities, and angles.

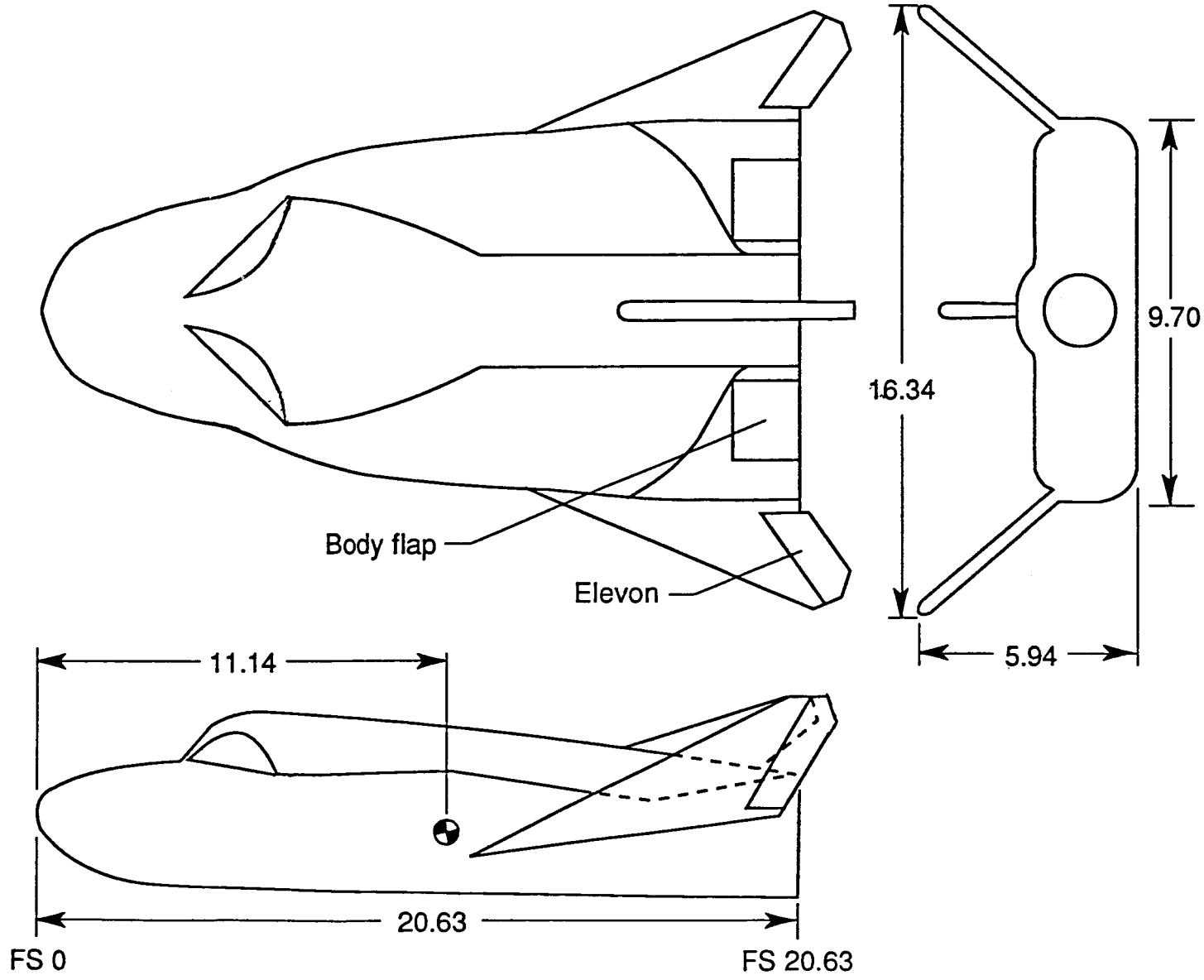

(a) General arrangement.

Figure 2. Sketches of model used in investigation. All dimensions are given in inches.

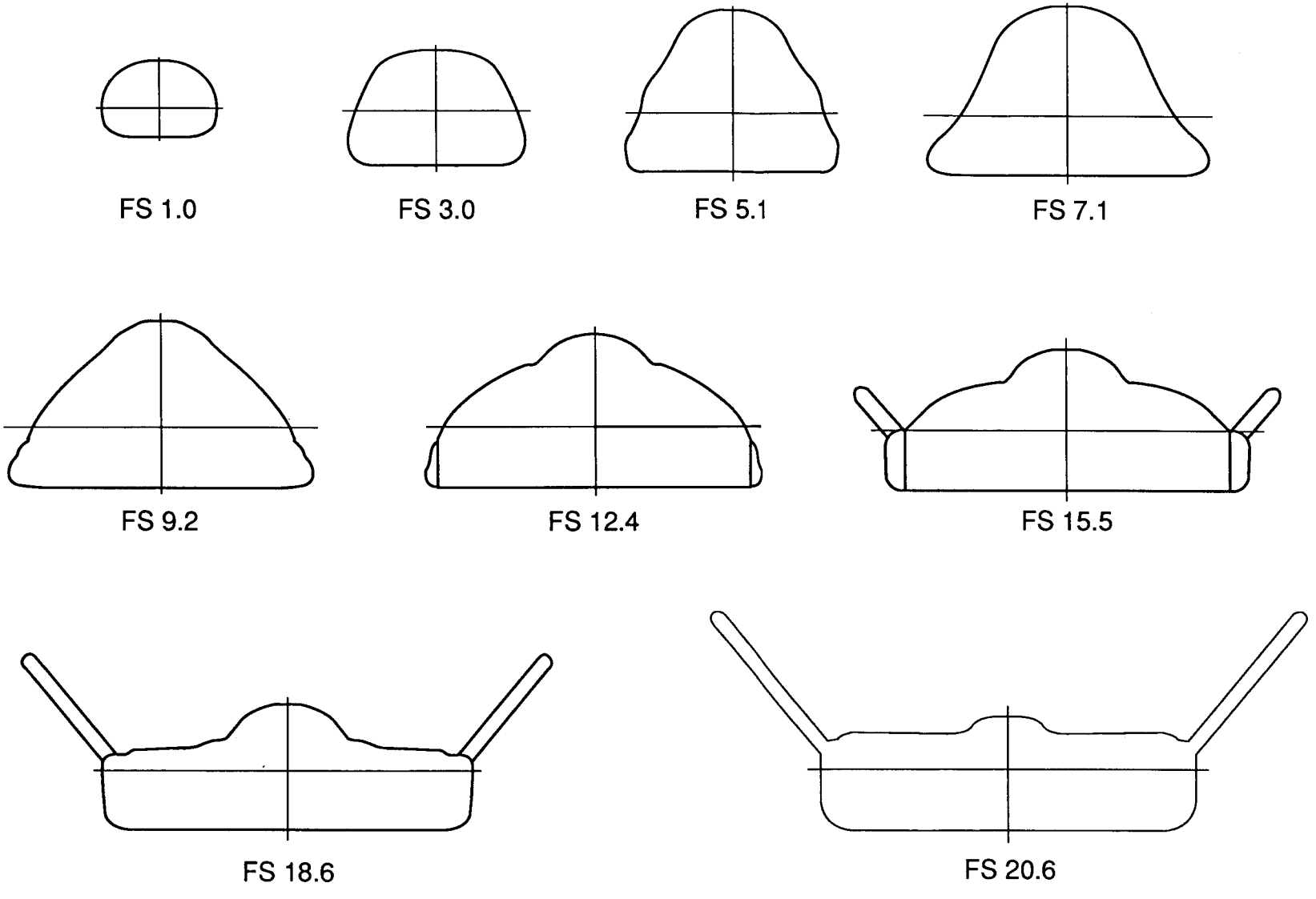

(b) Body cross sections.

Figure 2. Concluded.

ORIGINAL PAGE IS
OF POOR QUALITY

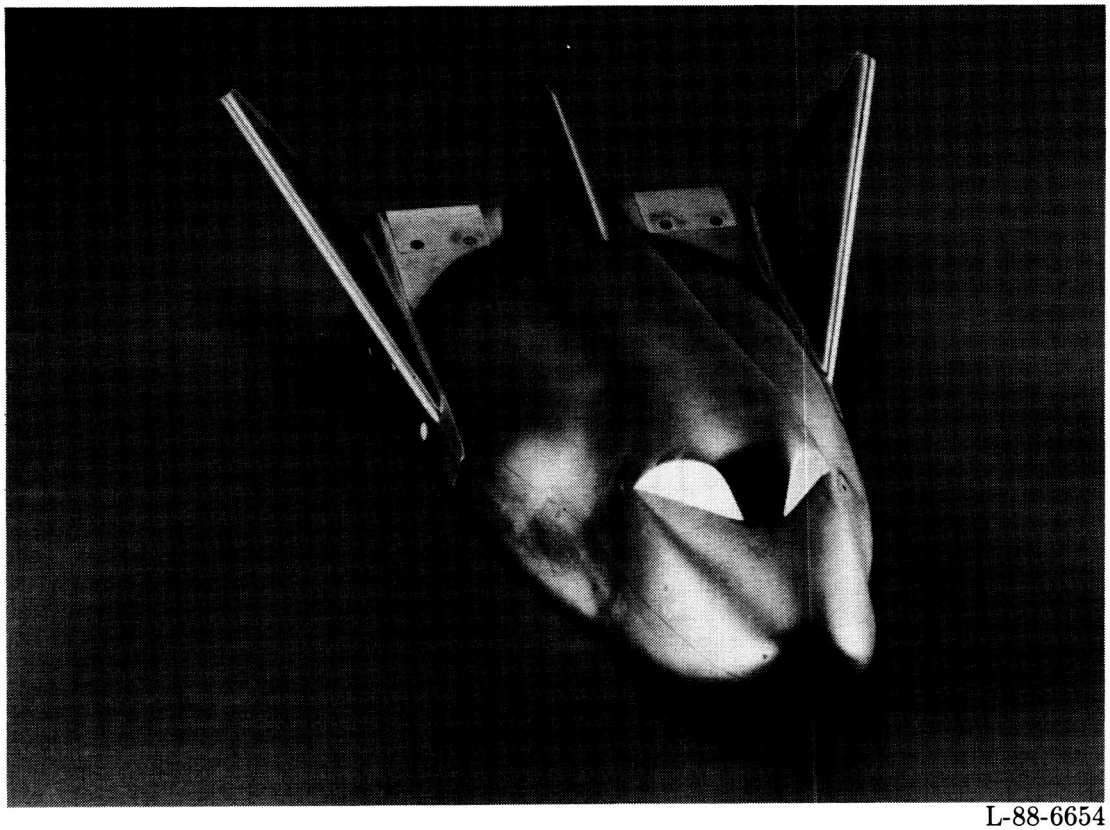

L-88-6654

(a) Side view.

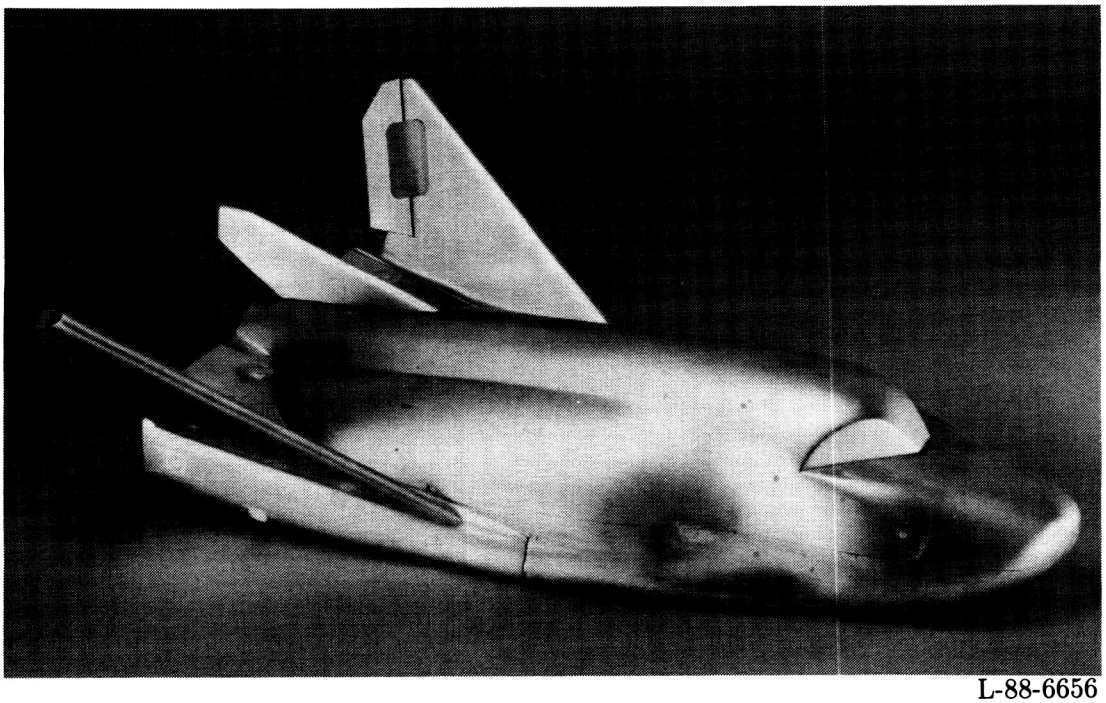

L-88-6656

(b) Front view.

Figure 3. Photographs of model used in investigation.

ORIGINAL PAGE
BLACK AND WHITE PHOTOGRAPH

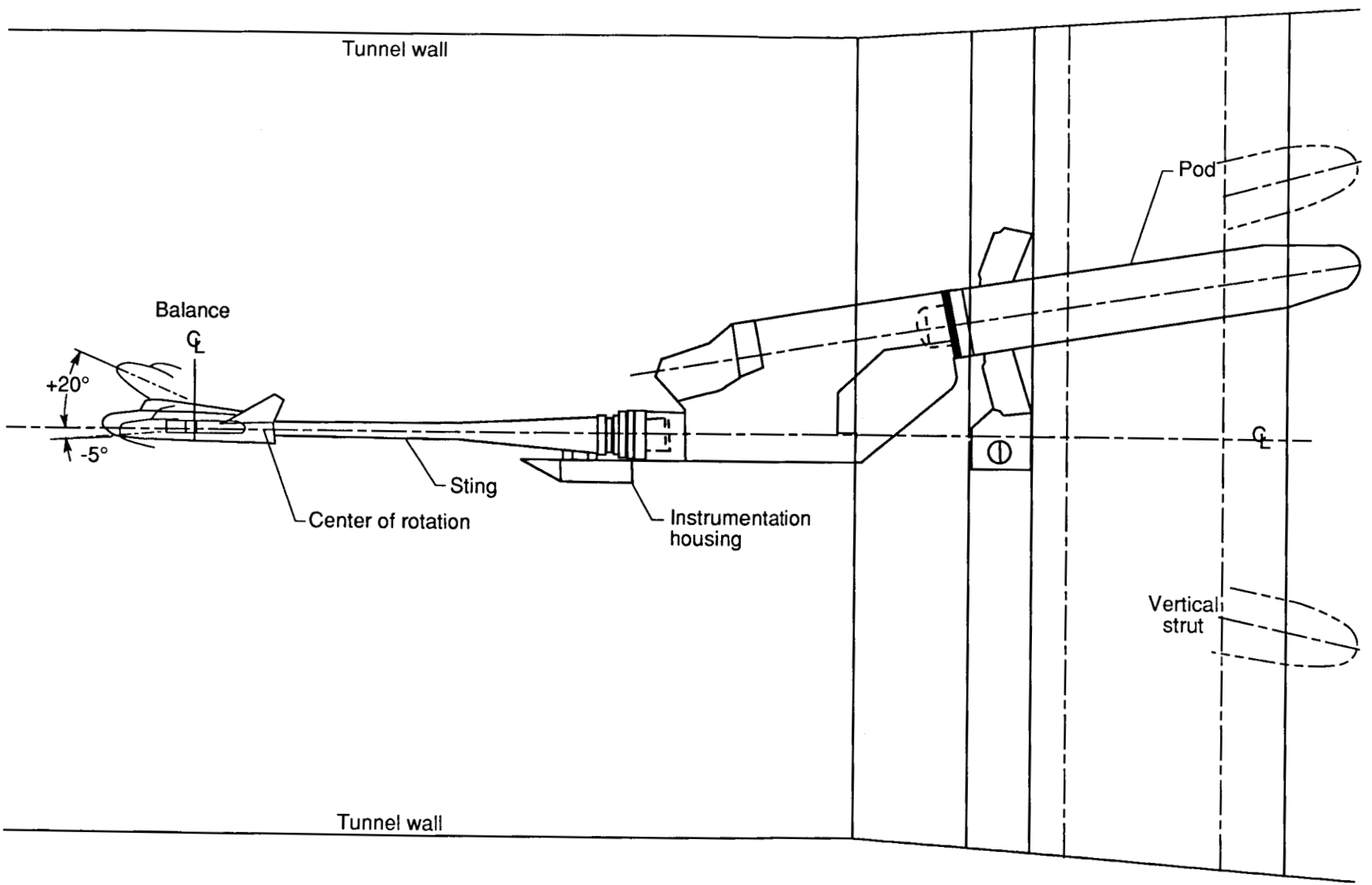

Figure 4. Sketch of model mounted in the Calspan 8-Foot Transonic Wind Tunnel.

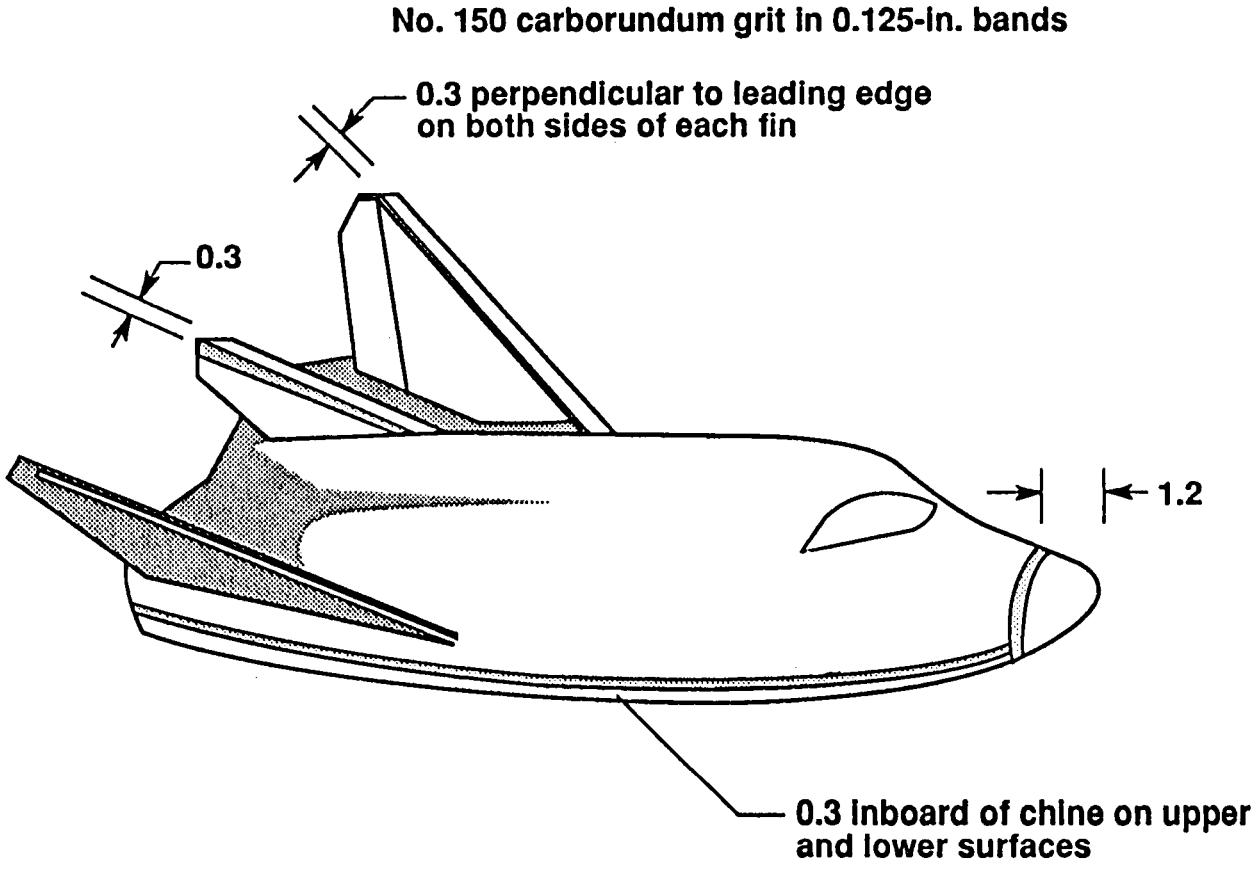

Figure 5. Sketch showing transition grit locations on model. All dimensions are given in inches.

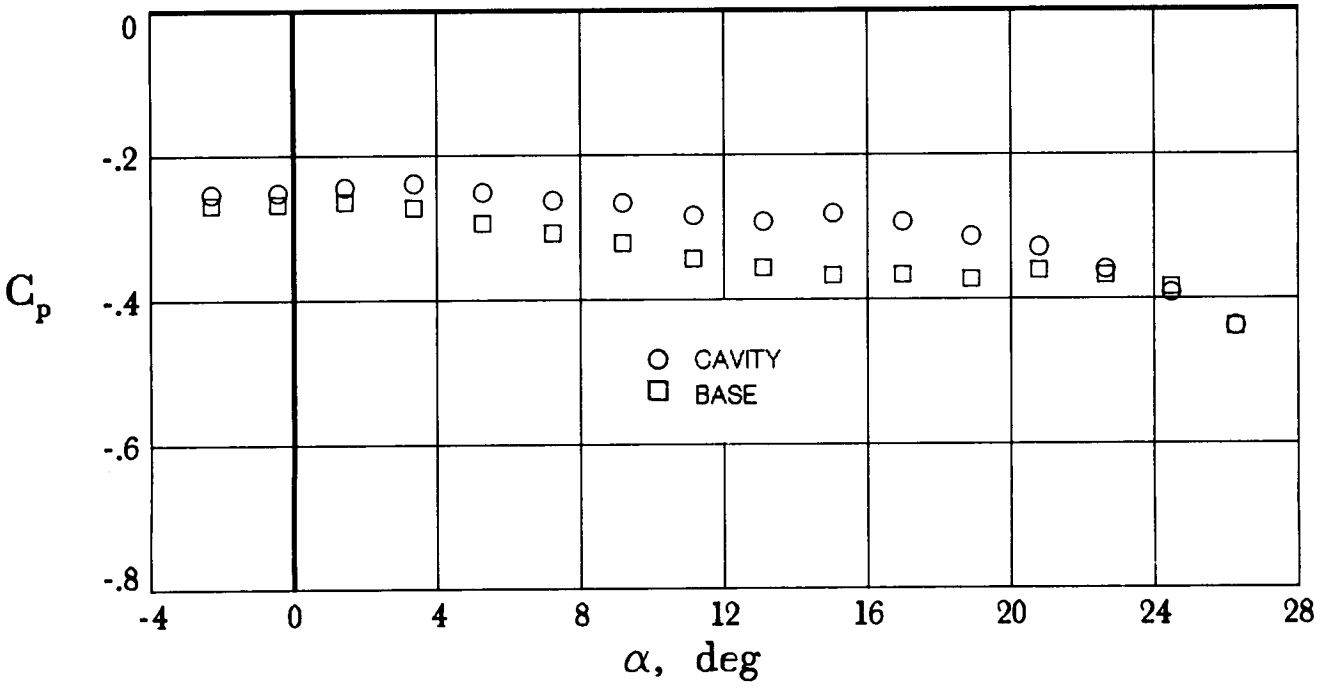

(a) $M = 0.6$.

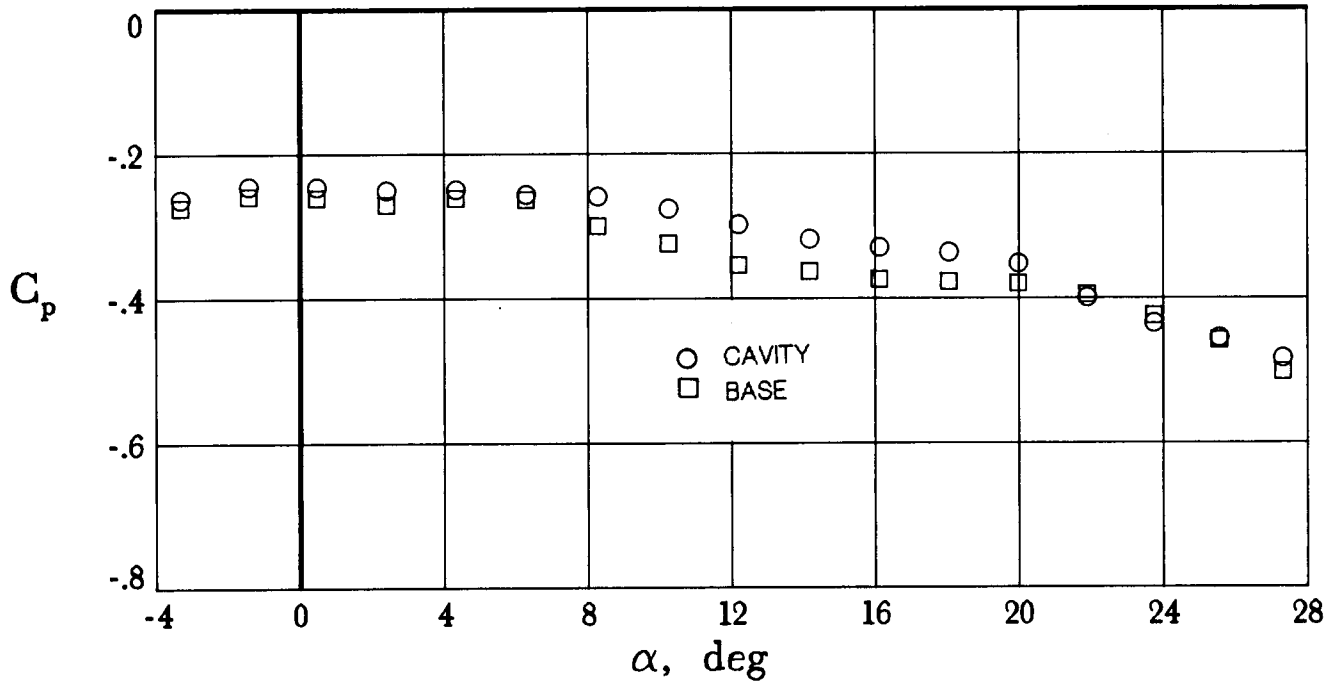

(b) $M = 0.8$.

Figure 6. Model base and sting-cavity pressures measured in investigation.

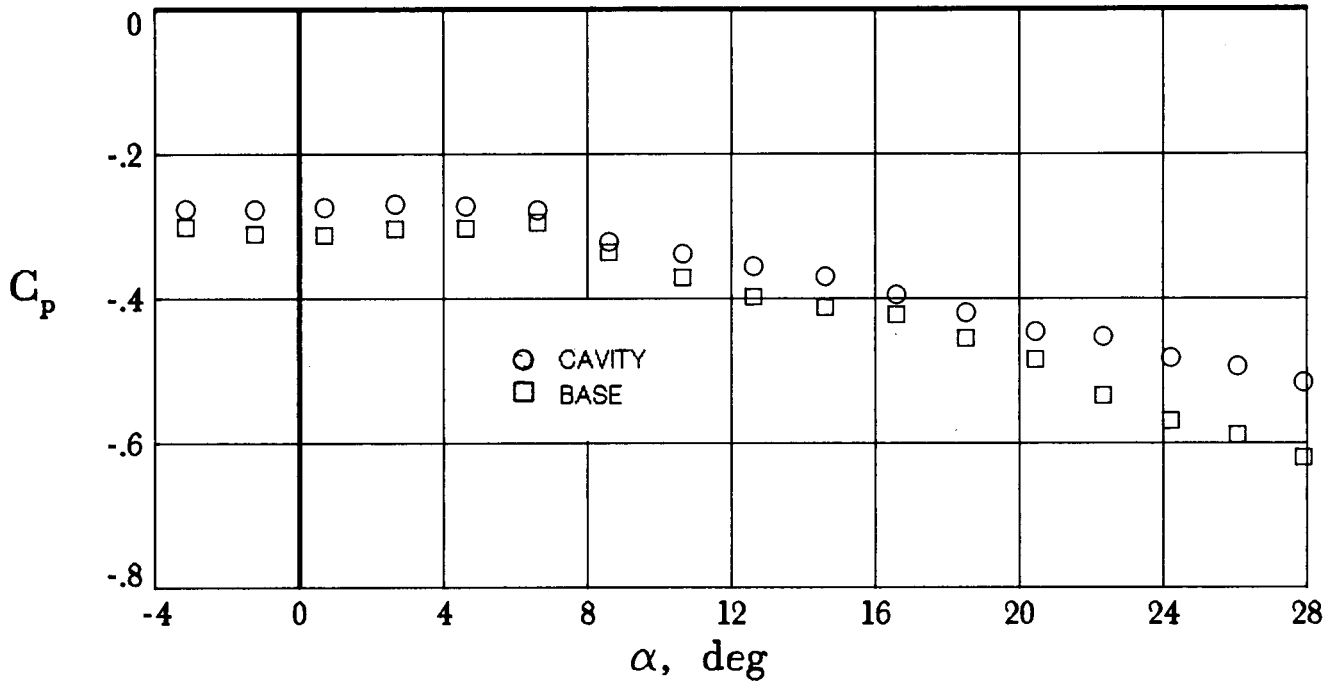

(c) $M = 0.9$.

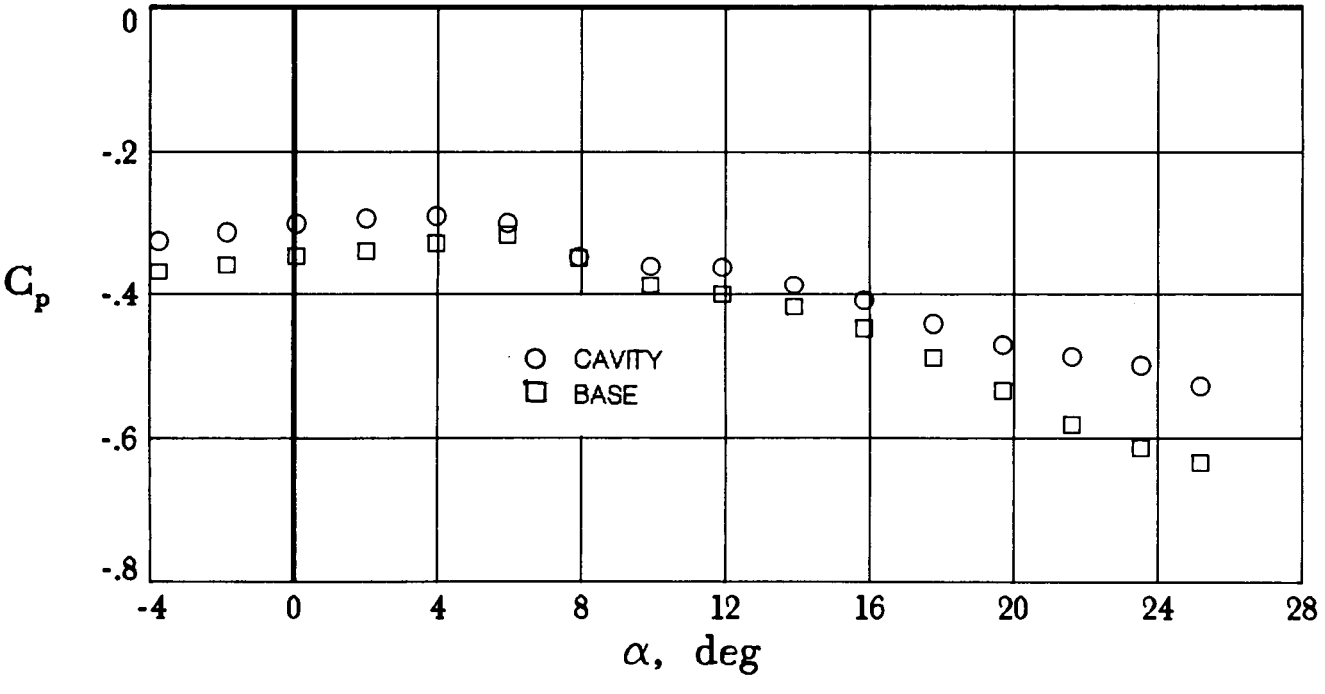

(d) $M = 0.95$.

Figure 6. Continued.

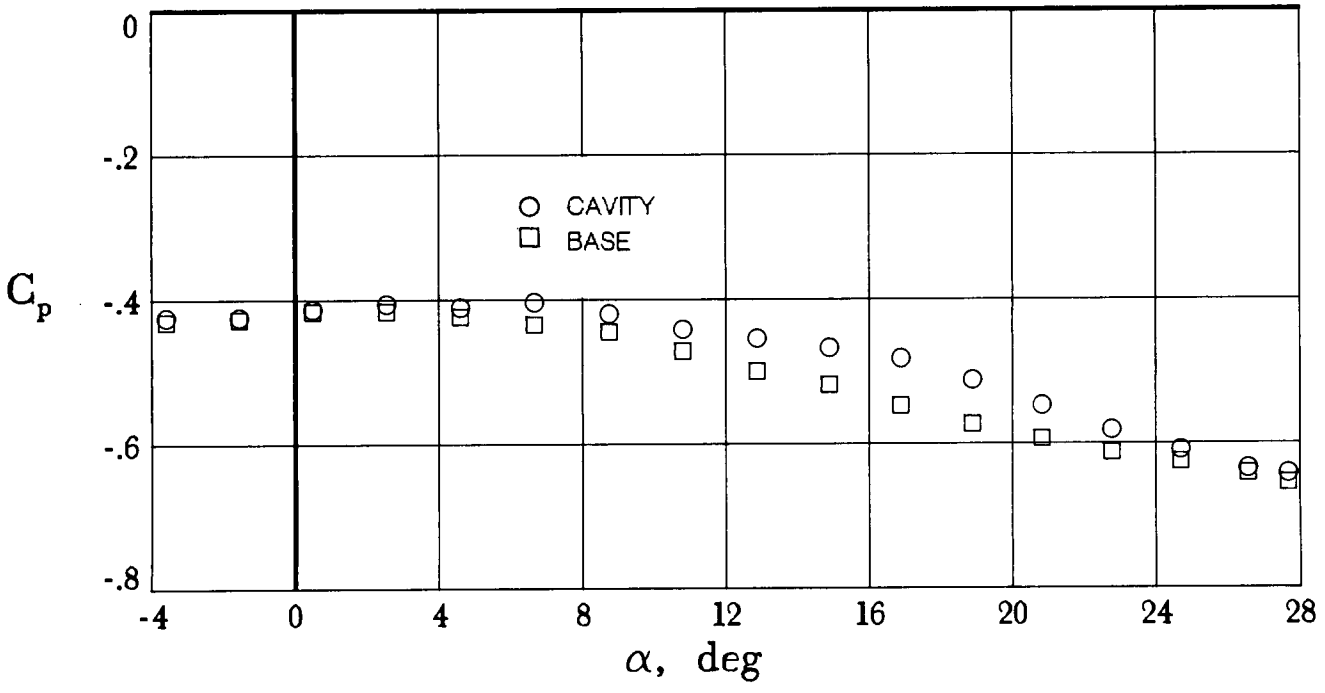

(e) $M = 1.1$.

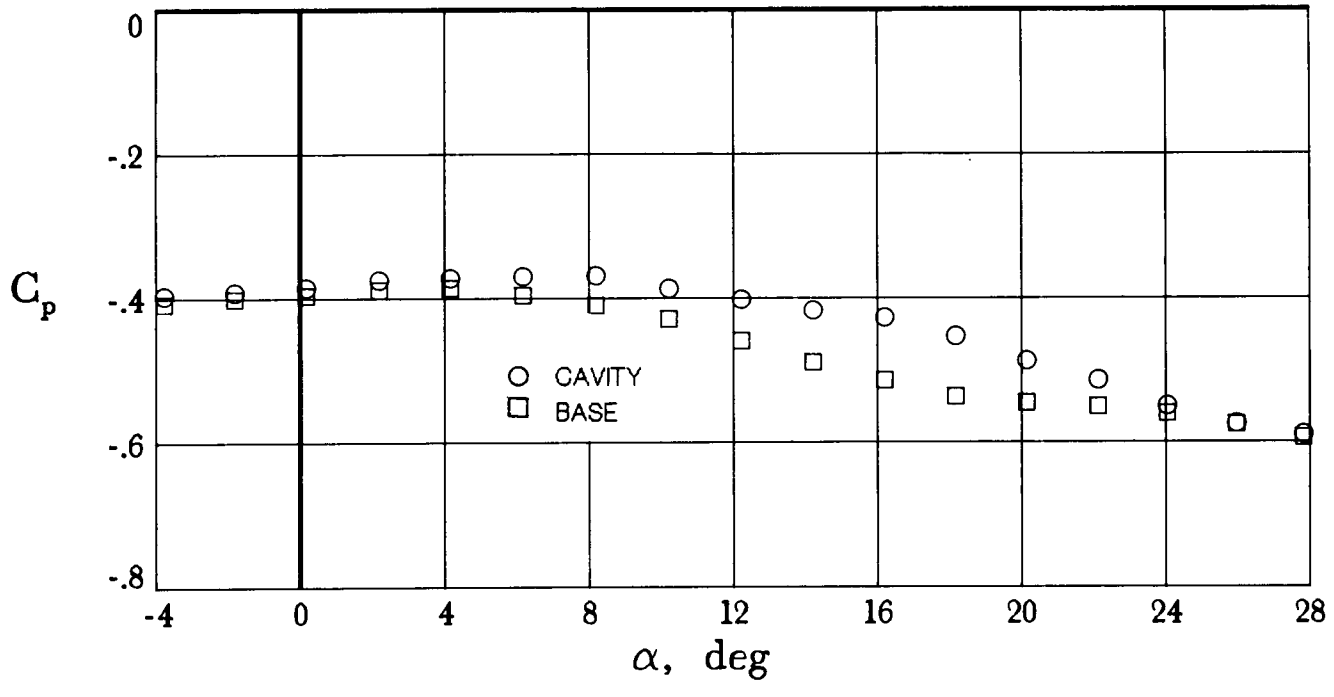

(f) $M = 1.2$.

Figure 6. Concluded.

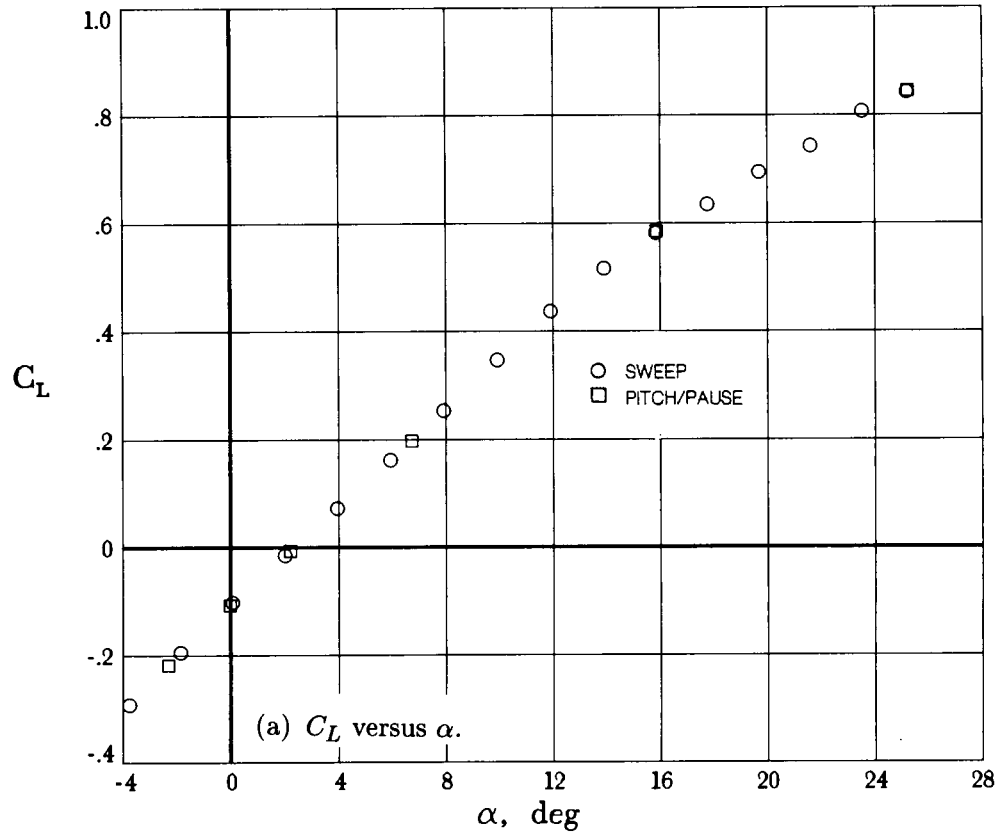

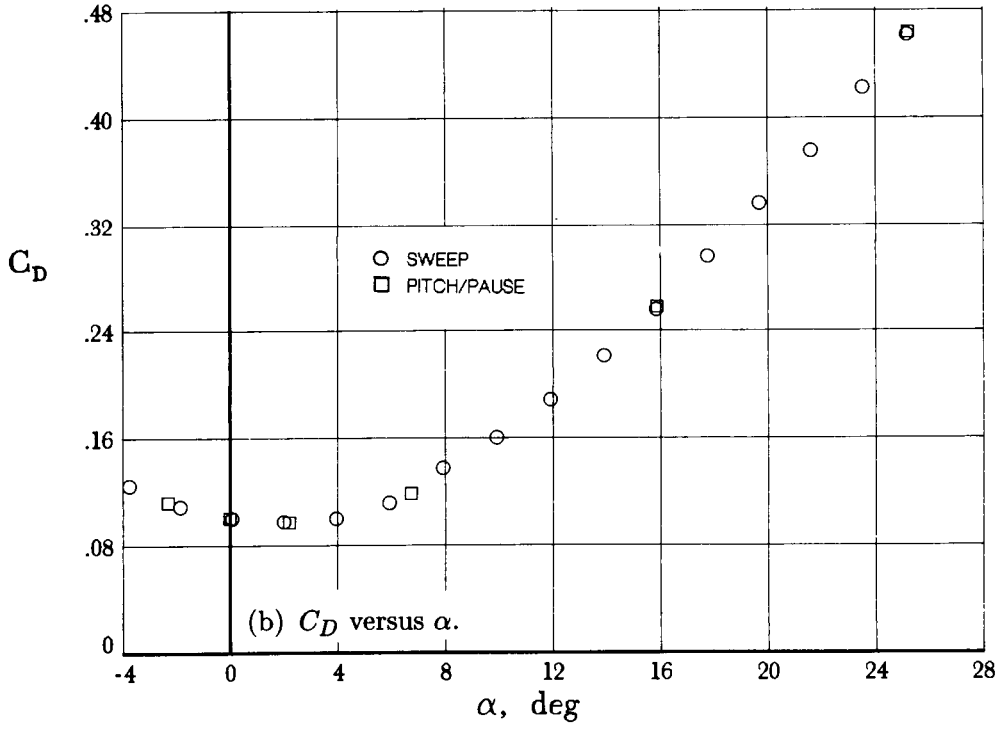

Figure 7. Comparison of data taken using sweep and pitch/pause methods. $M = 0.6$.

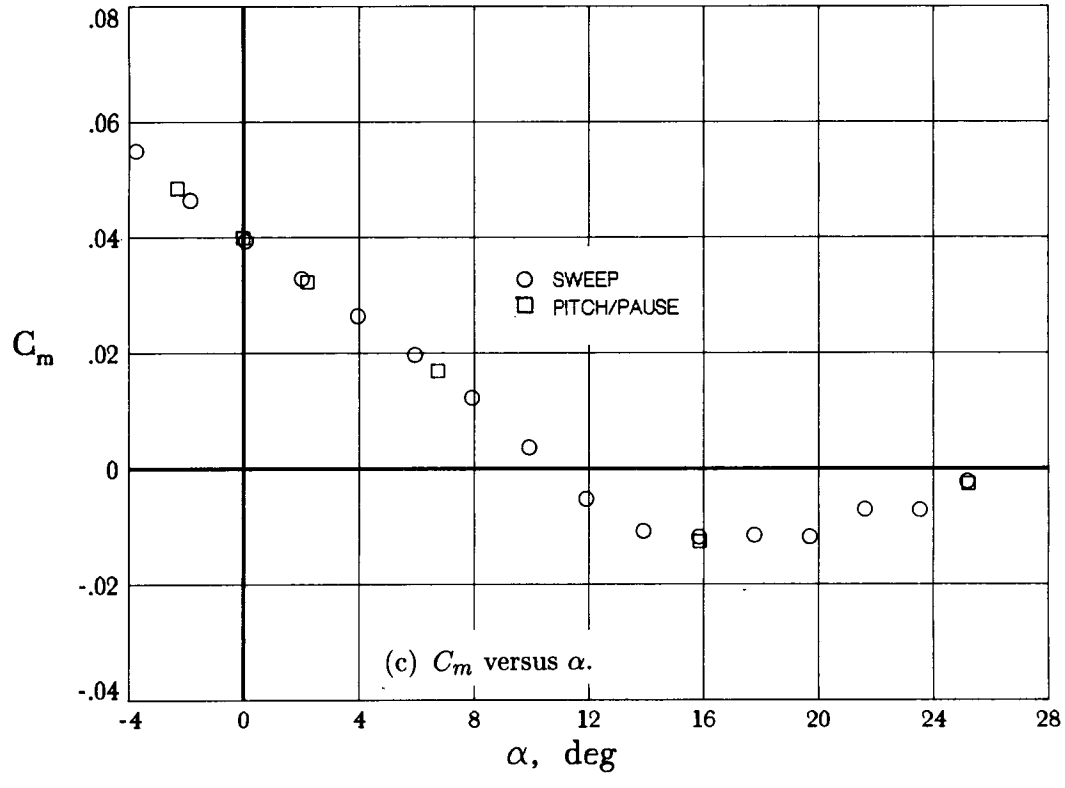

(c) C_m versus α.

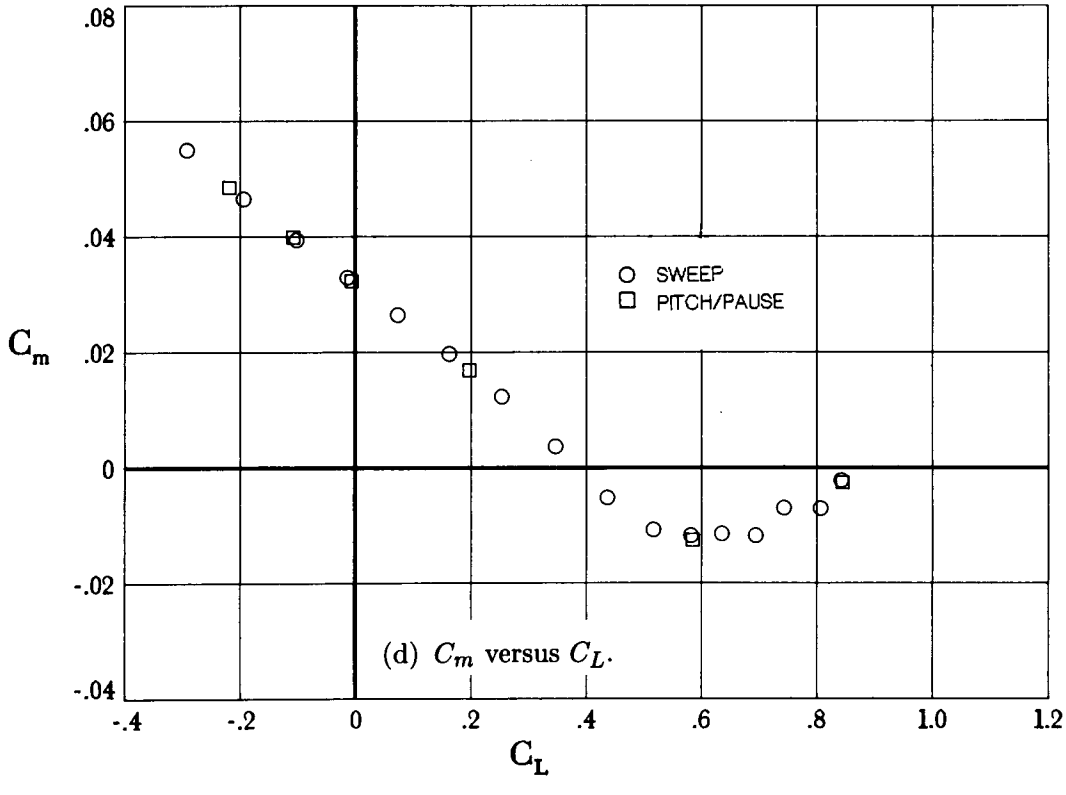

(d) C_m versus C_L.

Figure 7. Continued.

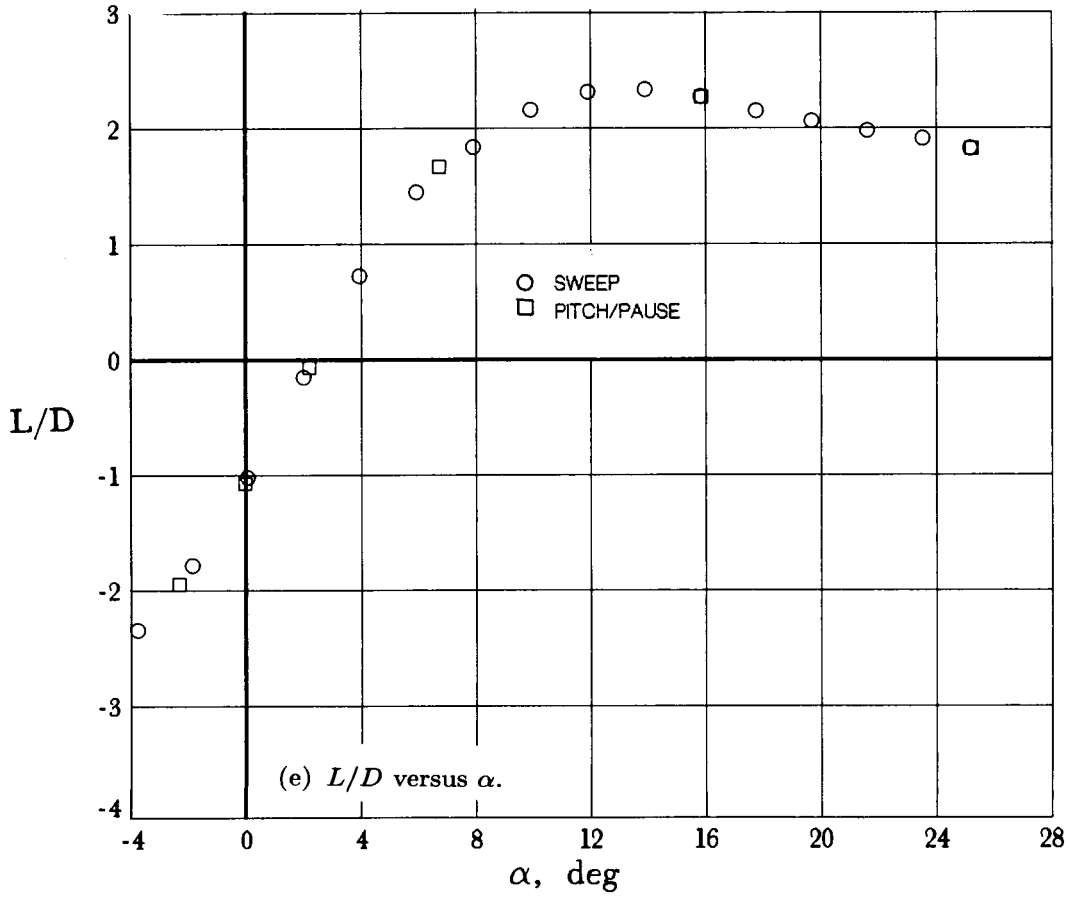

Figure 7. Concluded.

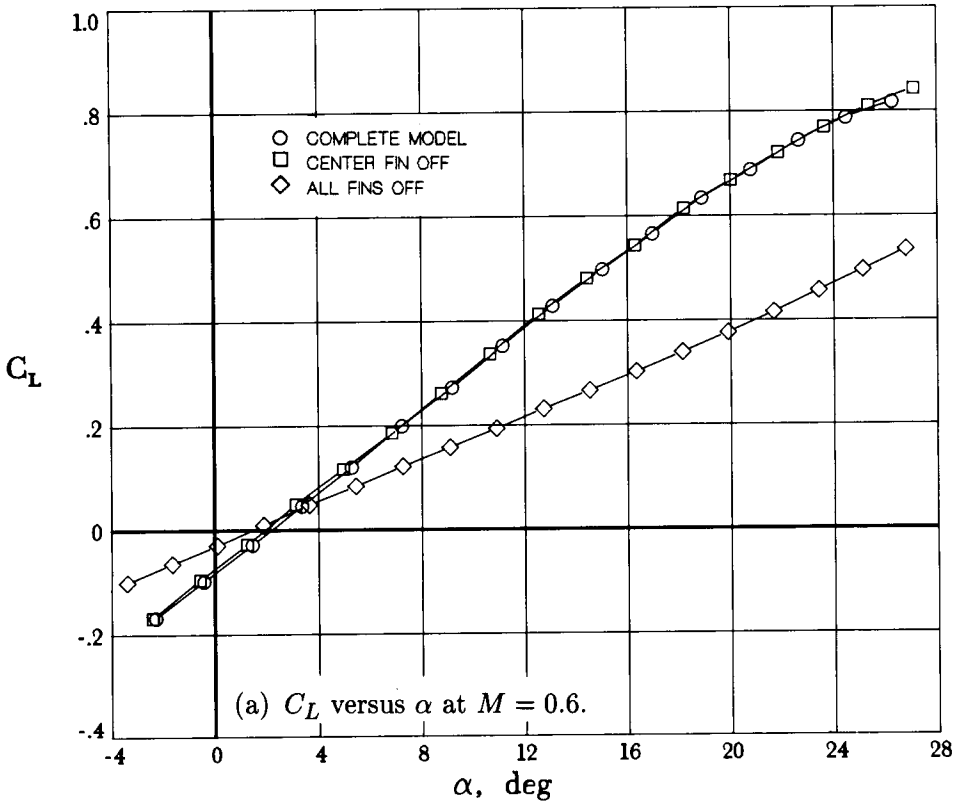

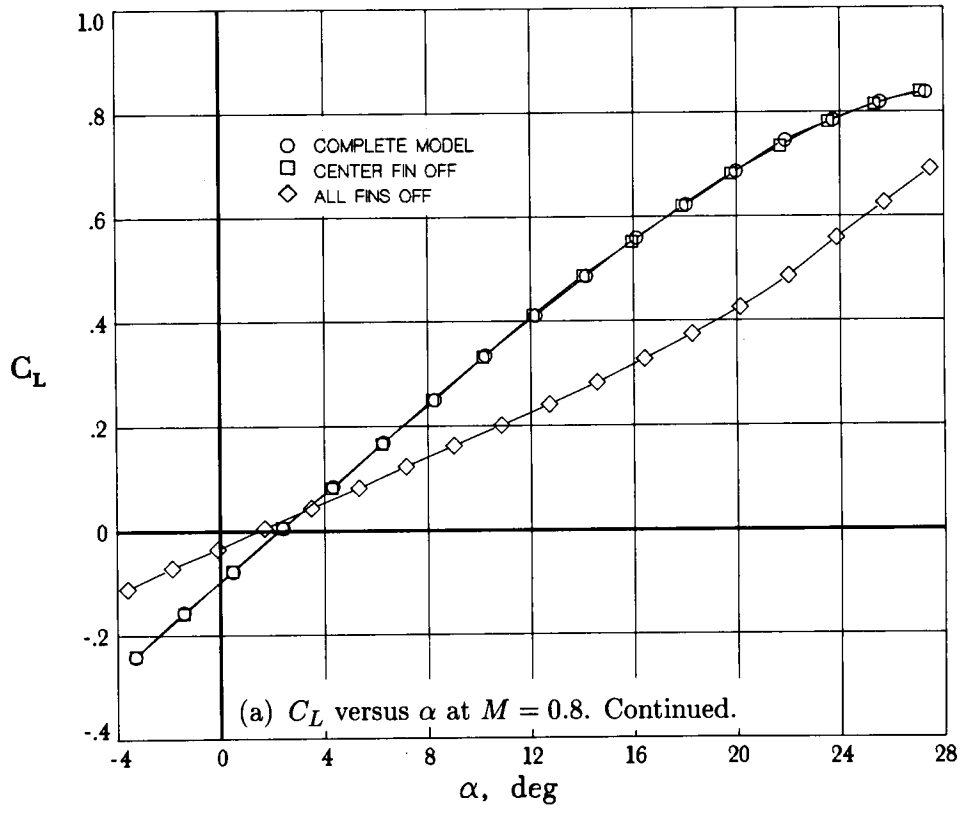

Figure 8. Effect of fins on longitudinal aerodynamic characteristics of model.

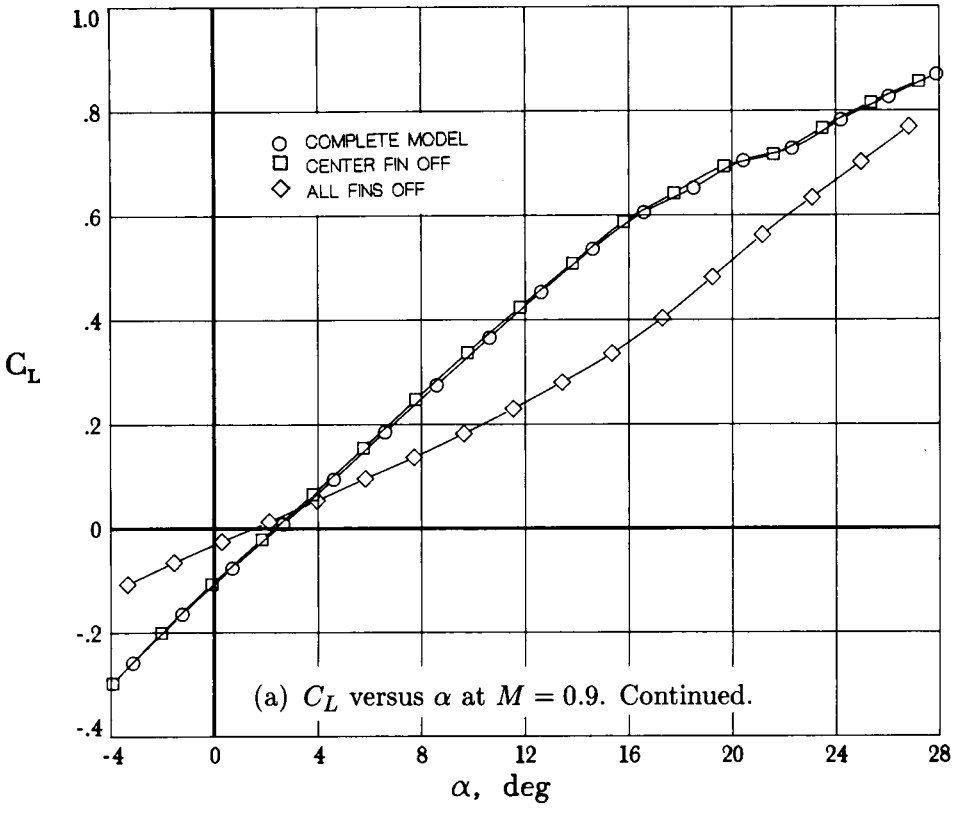

(a) C_L versus α at $M = 0.9$. Continued.

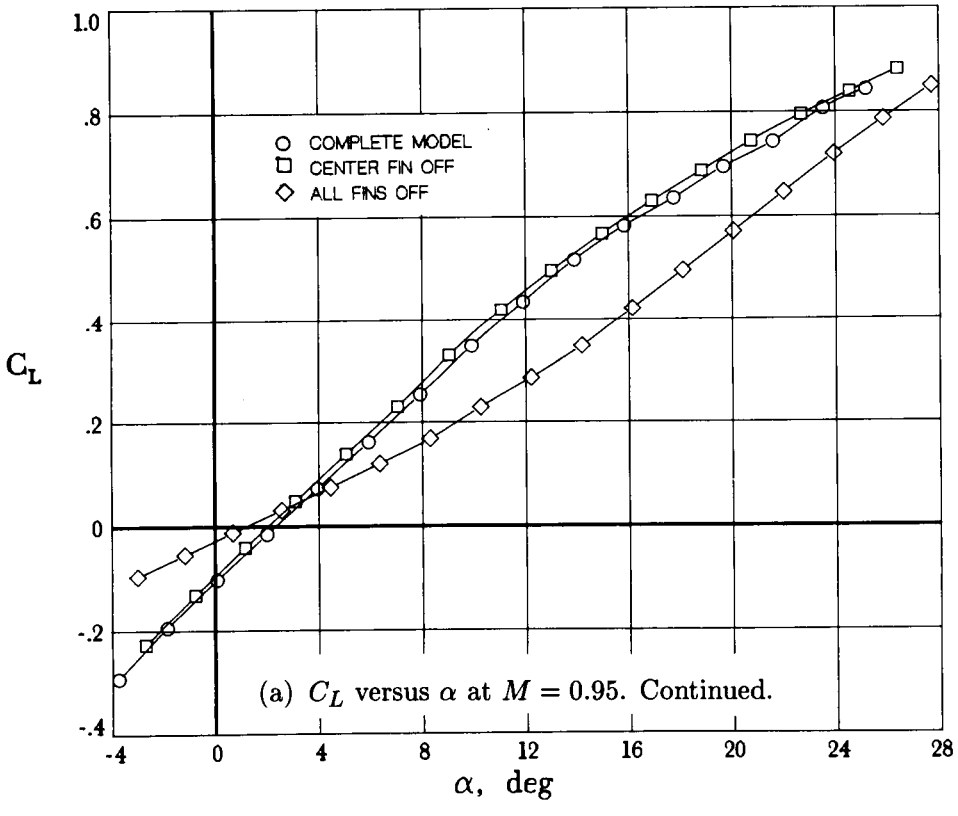

(a) C_L versus α at $M = 0.95$. Continued.

Figure 8. Continued.

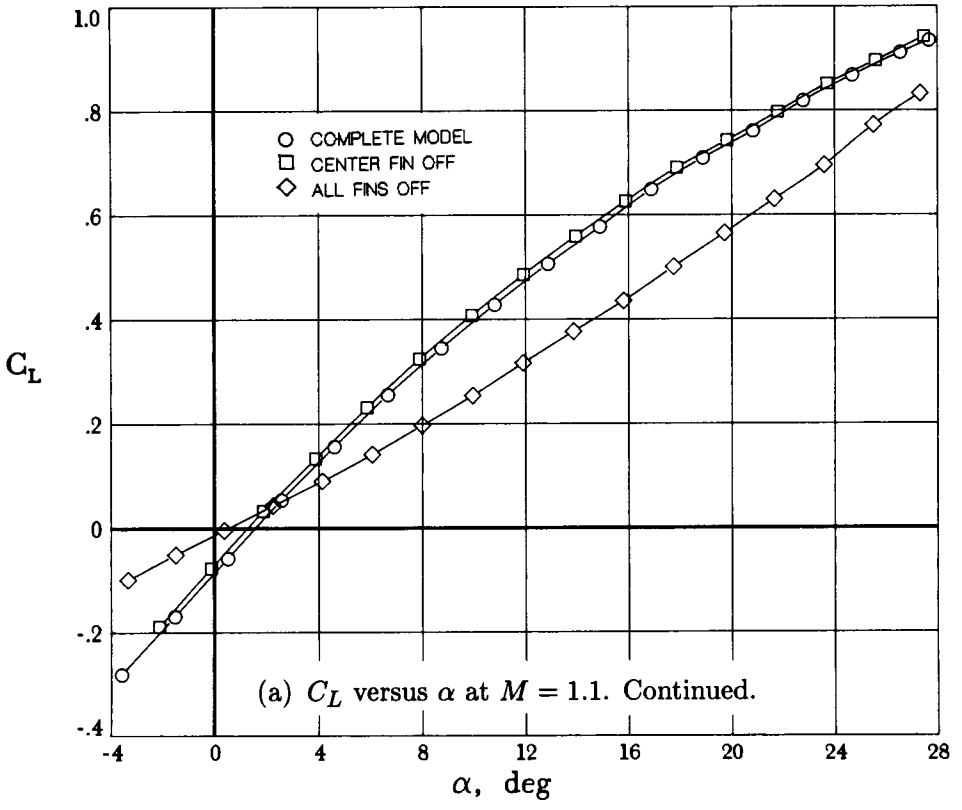

(a) C_L versus α at $M = 1.1$. Continued.

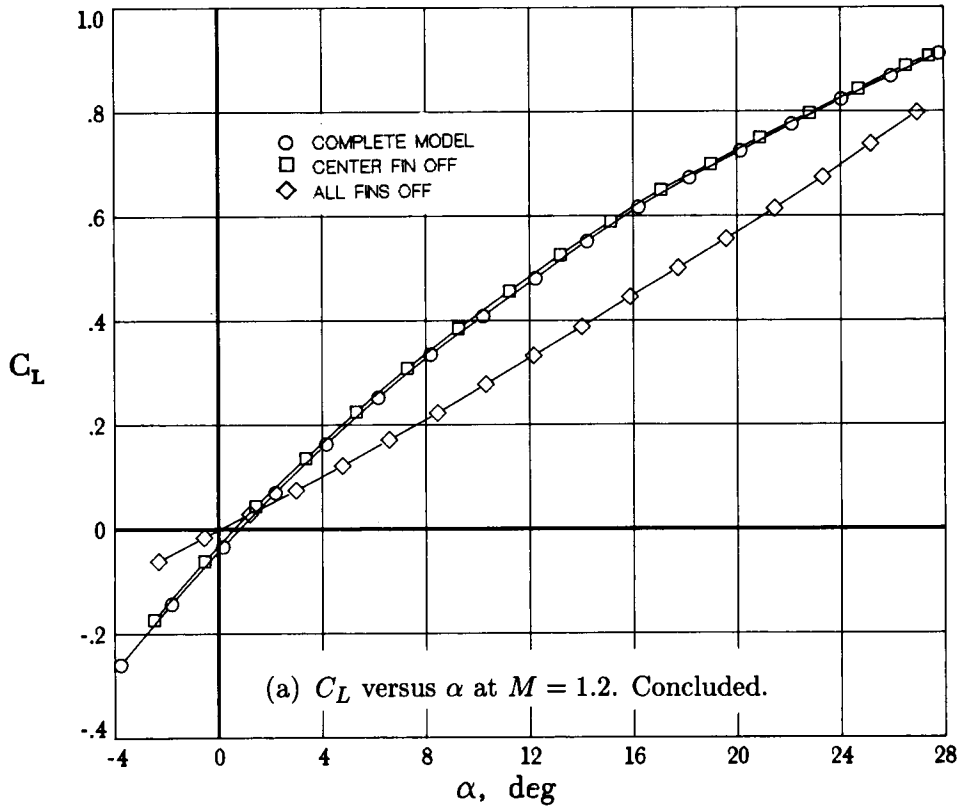

(a) C_L versus α at $M = 1.2$. Concluded.

Figure 8. Continued.

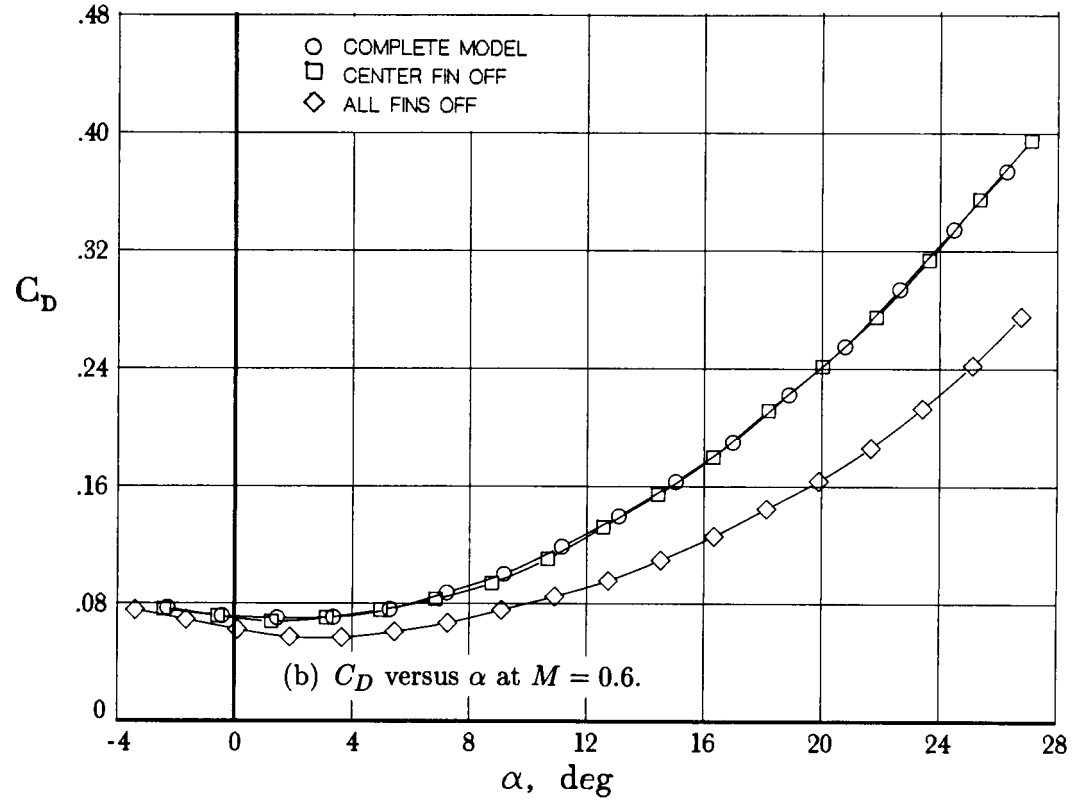

(b) C_D versus α at $M = 0.6$.

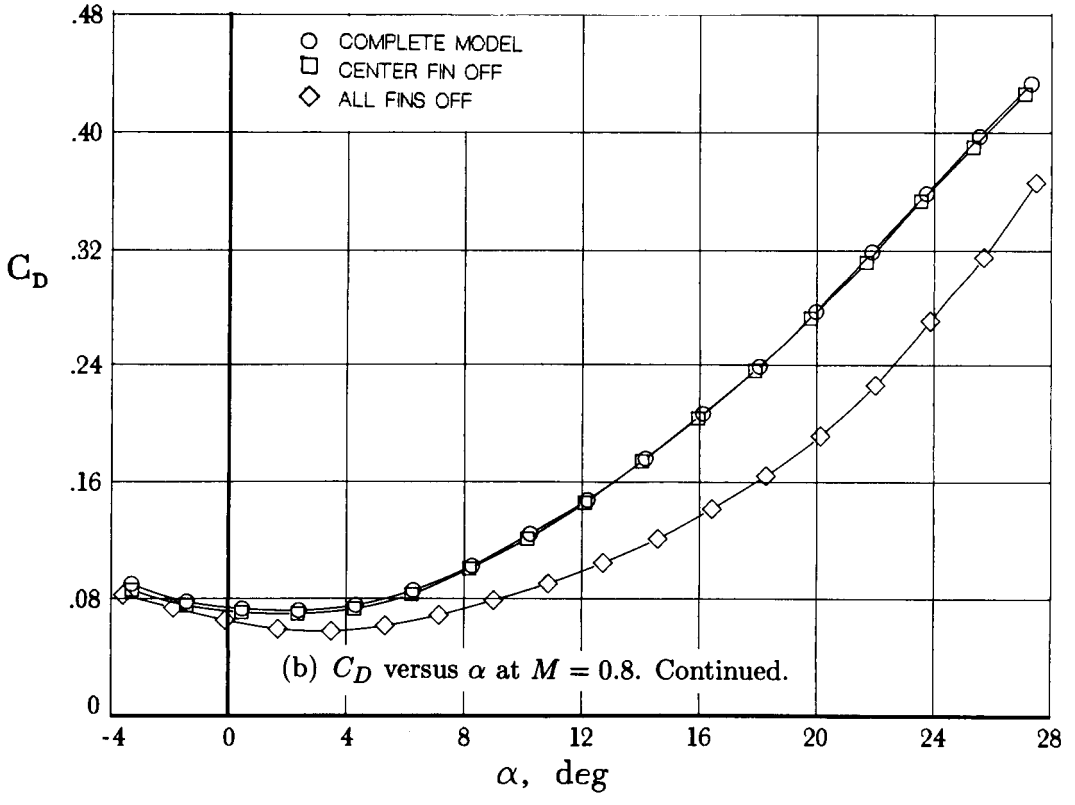

(b) C_D versus α at $M = 0.8$. Continued.

Figure 8. Continued.

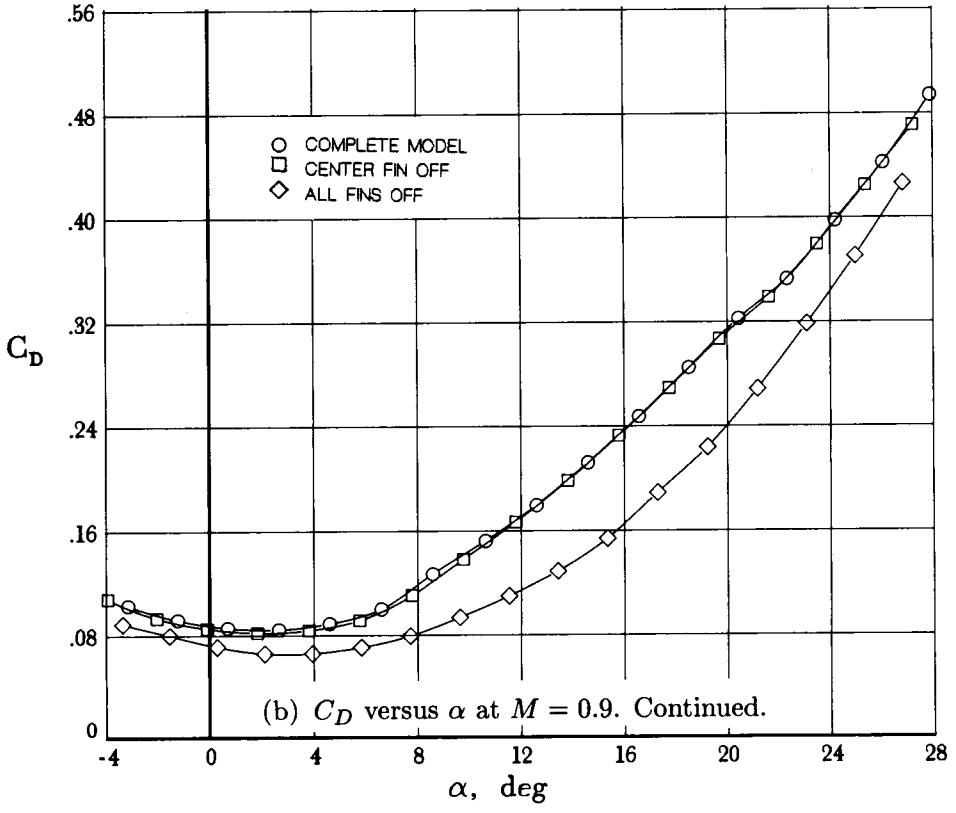

(b) C_D versus α at $M = 0.9$. Continued.

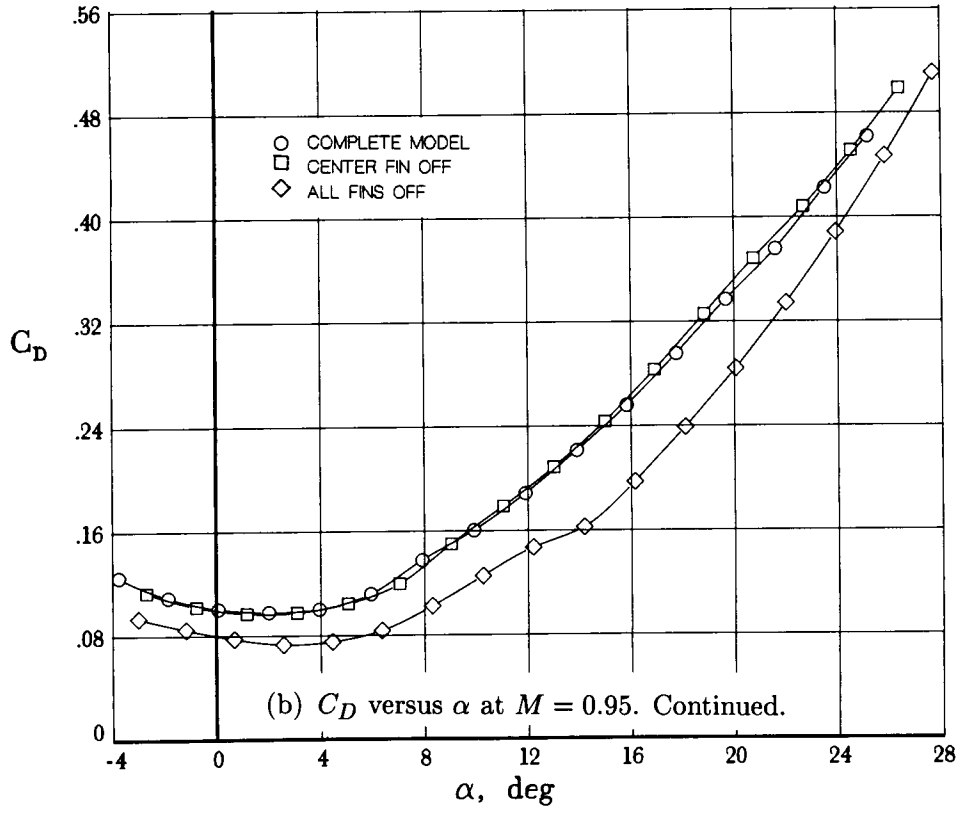

(b) C_D versus α at $M = 0.95$. Continued.

Figure 8. Continued.

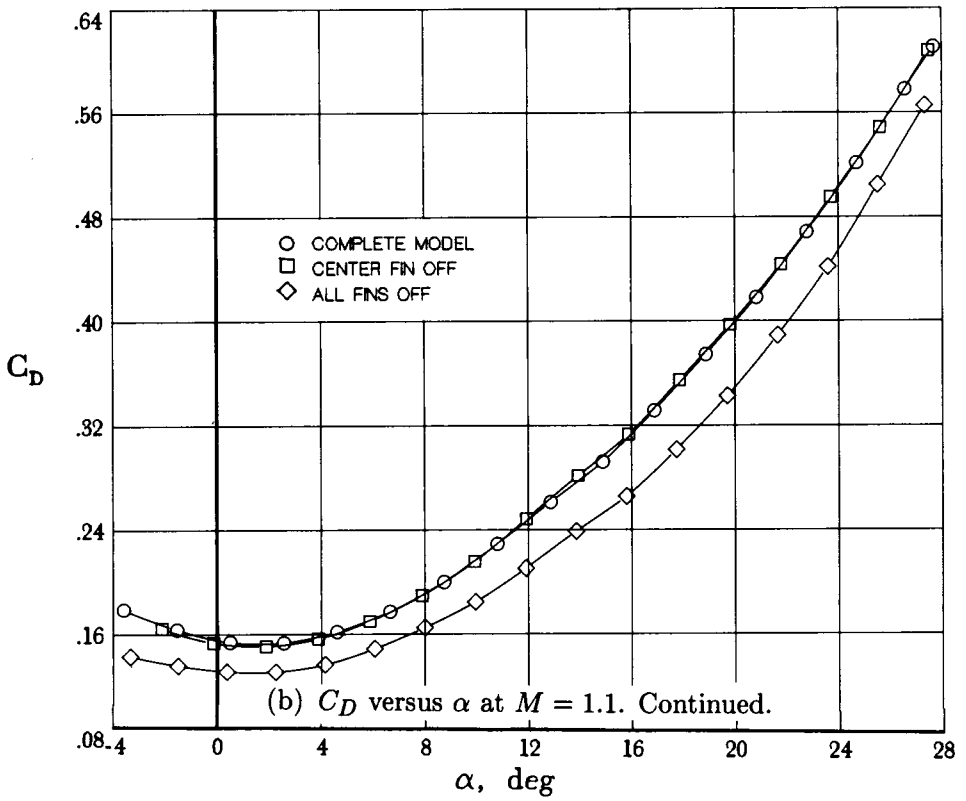

(b) C_D versus α at $M = 1.1$. Continued.

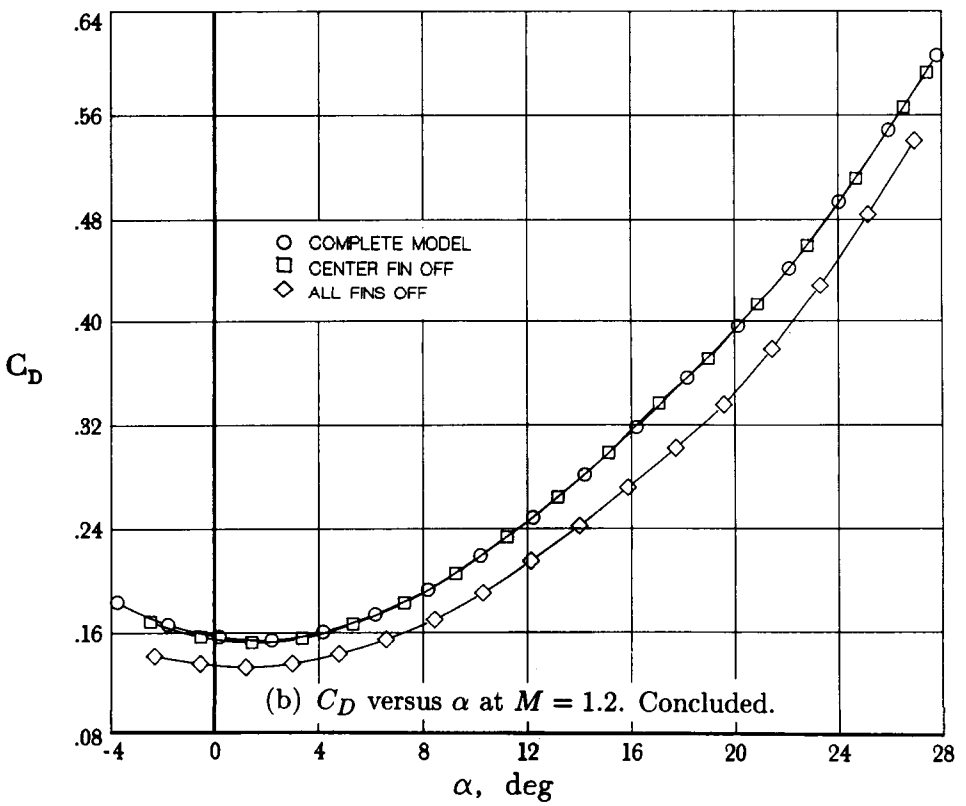

(b) C_D versus α at $M = 1.2$. Concluded.

Figure 8. Continued.

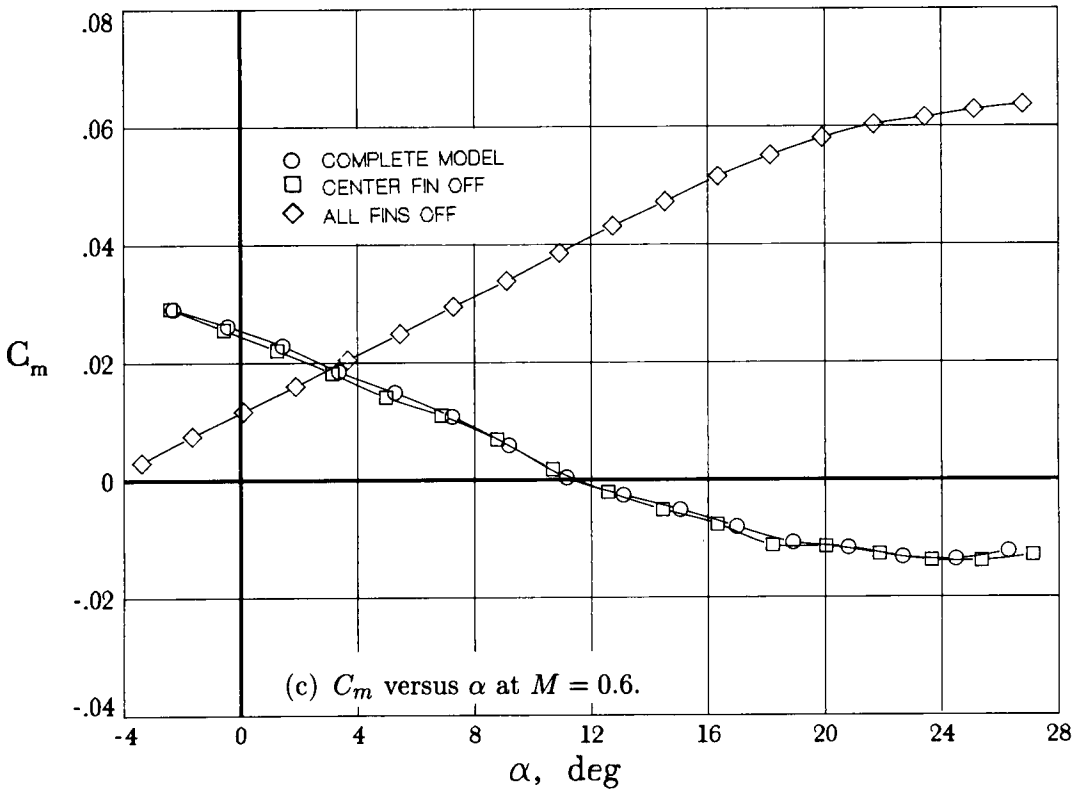

(c) C_m versus α at $M = 0.6$.

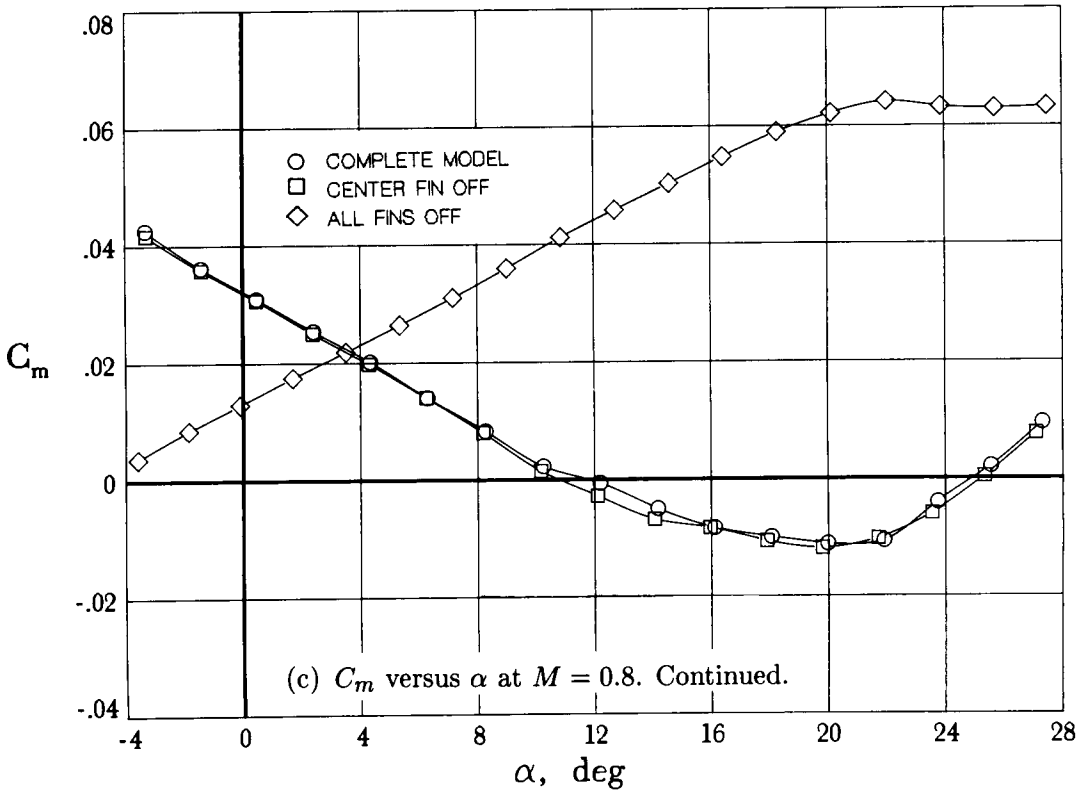

(c) C_m versus α at $M = 0.8$. Continued.

Figure 8. Continued.

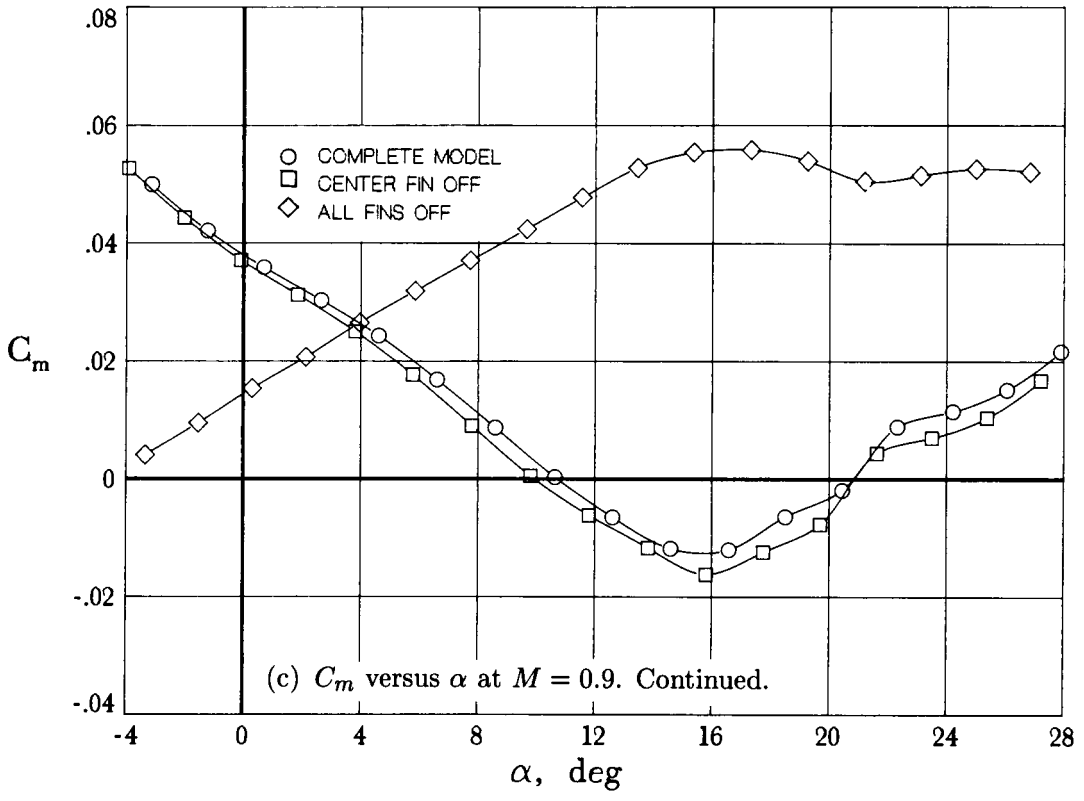

(c) C_m versus α at $M = 0.9$. Continued.

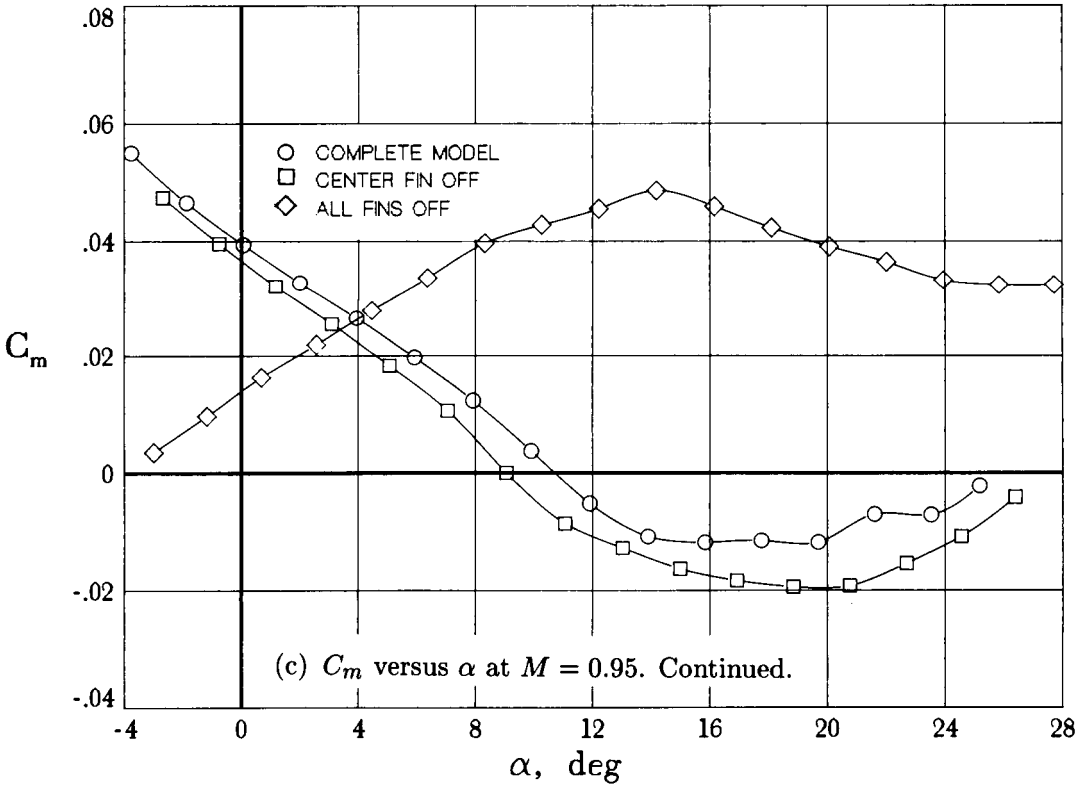

(c) C_m versus α at $M = 0.95$. Continued.

Figure 8. Continued.

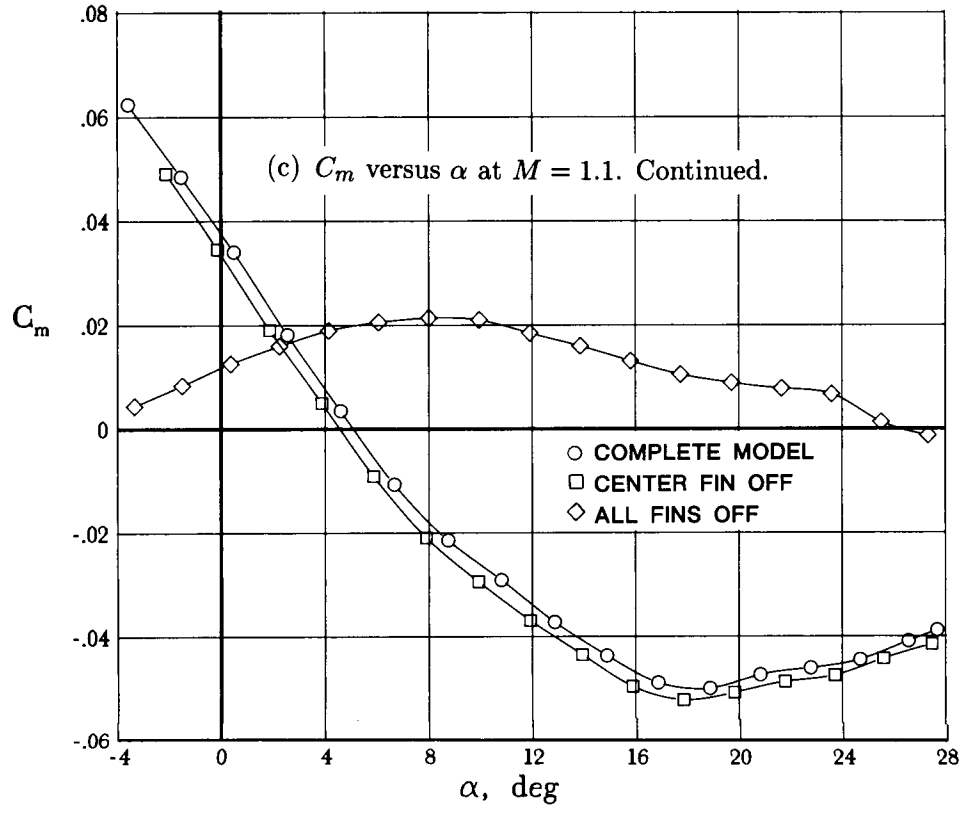

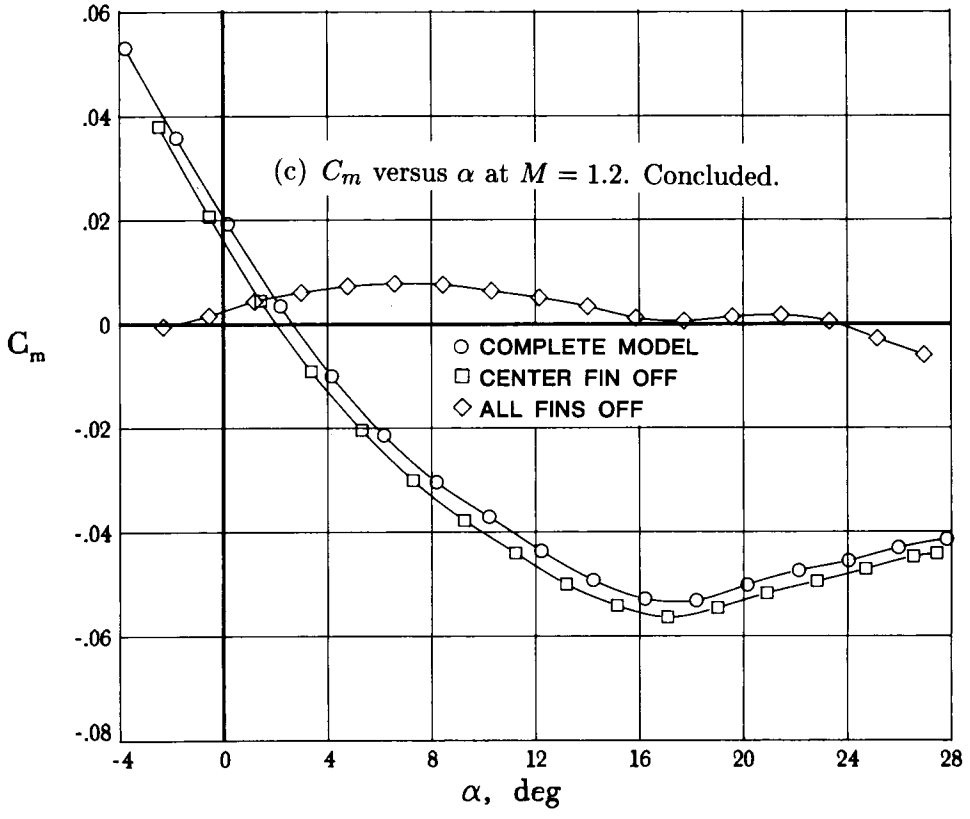

Figure 8. Continued.

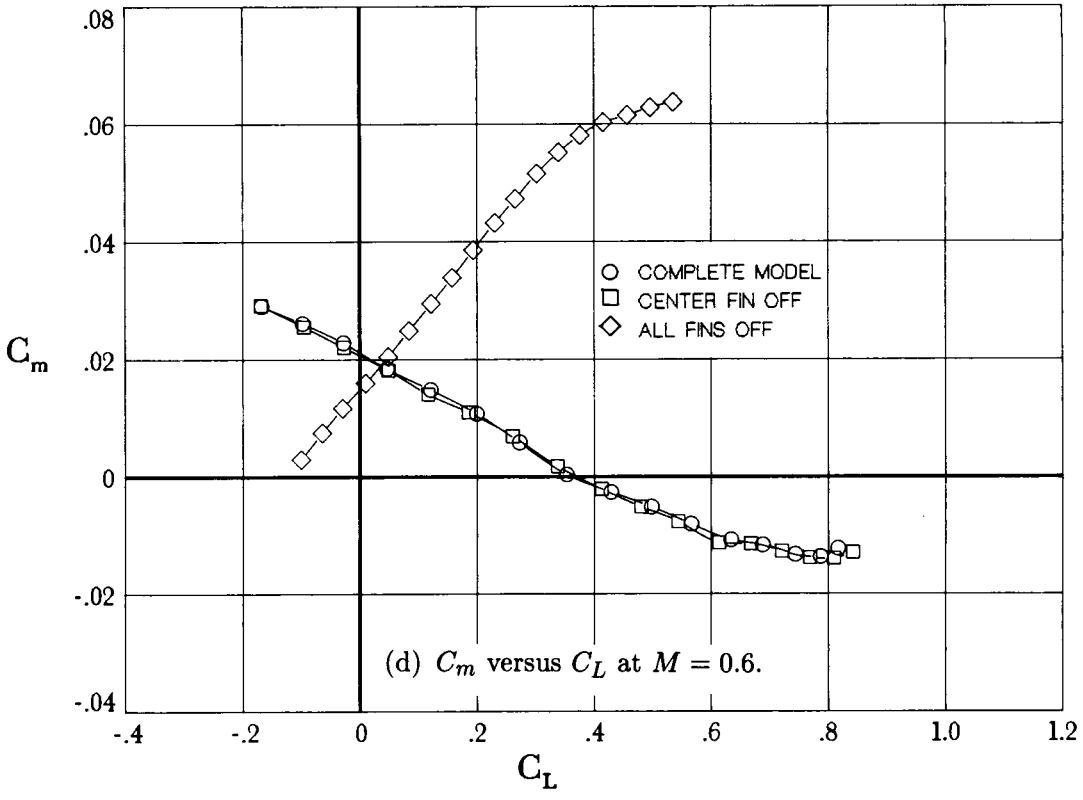

(d) C_m versus C_L at $M = 0.6$.

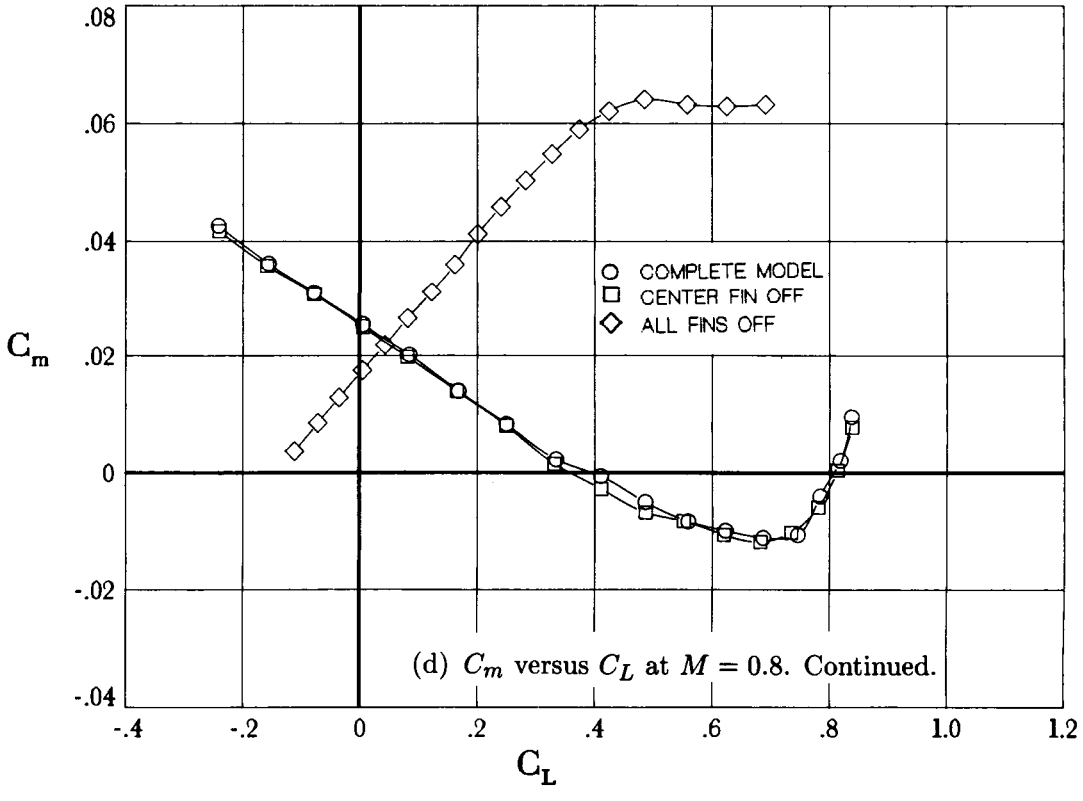

(d) C_m versus C_L at $M = 0.8$. Continued.

Figure 8. Continued.

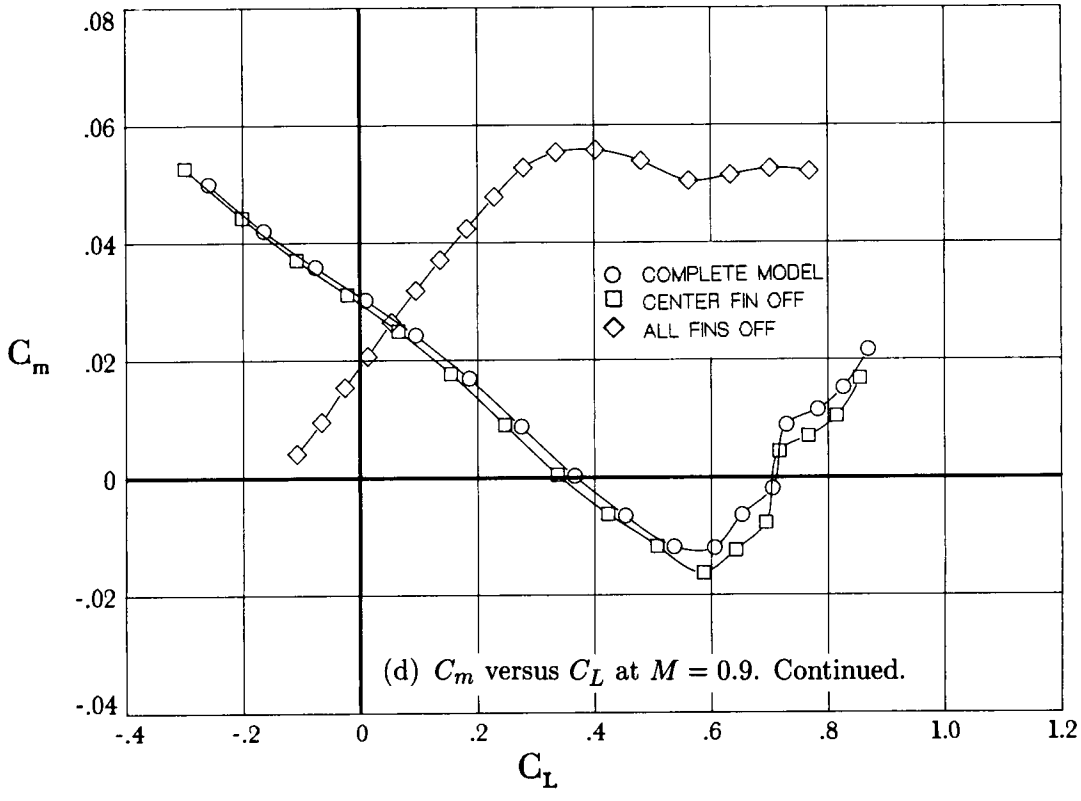

(d) C_m versus C_L at $M = 0.9$. Continued.

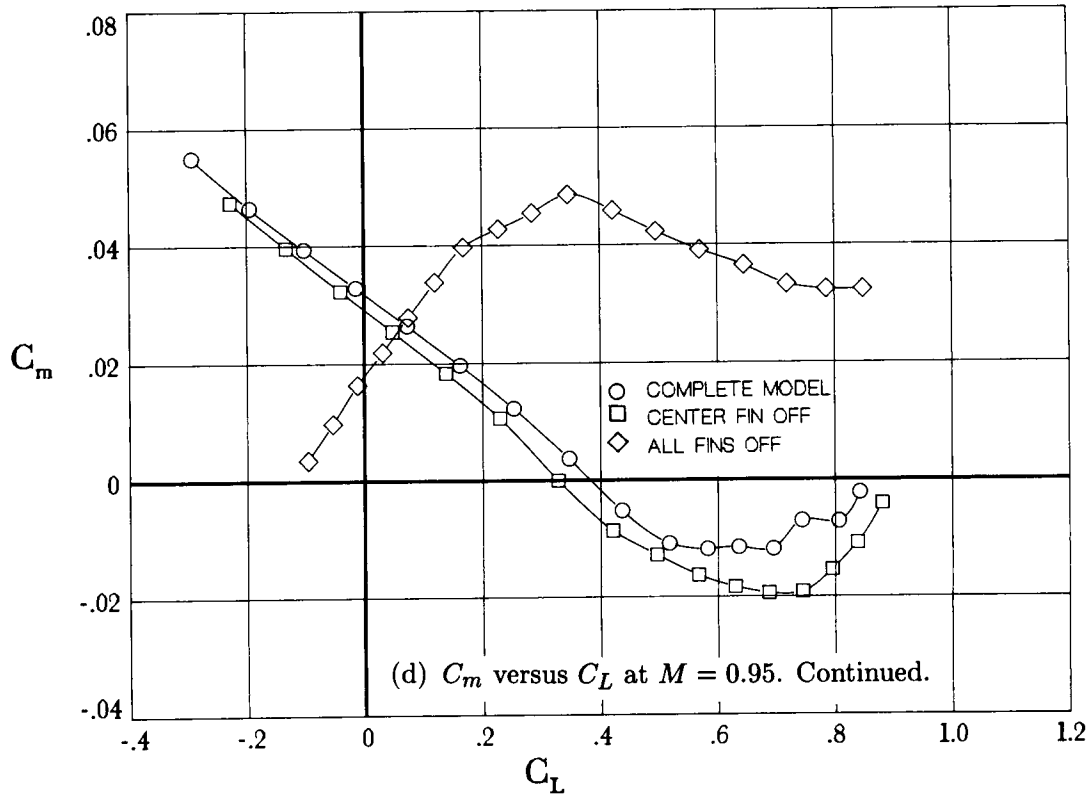

(d) C_m versus C_L at $M = 0.95$. Continued.

Figure 8. Continued.

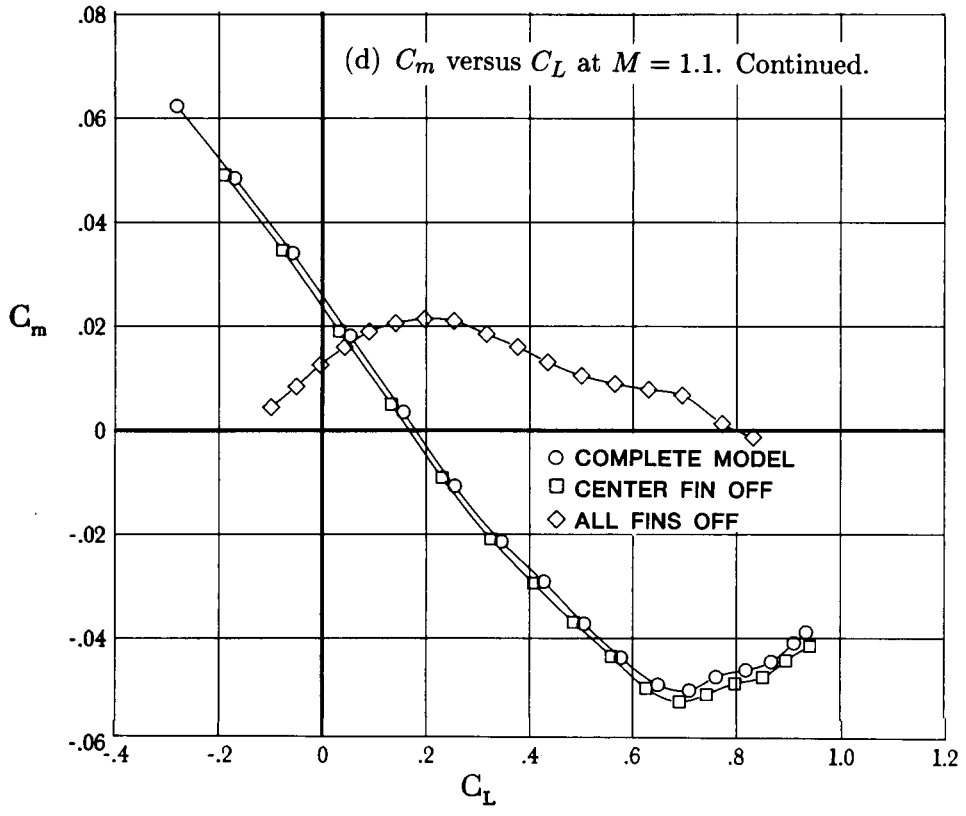

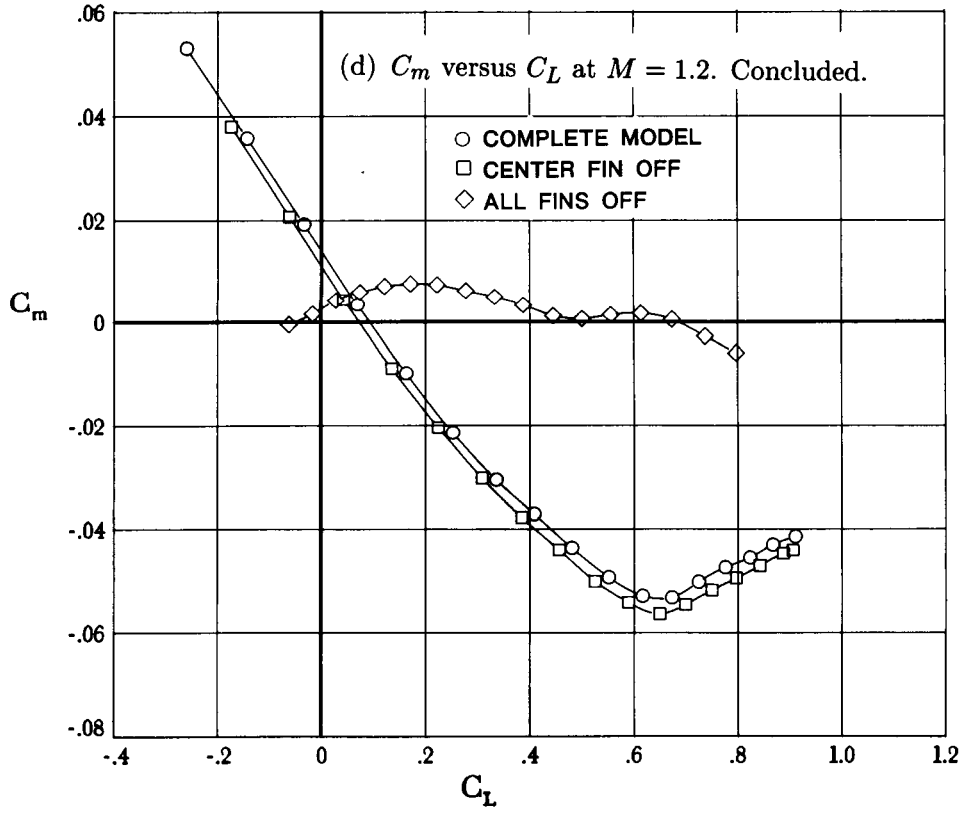

Figure 8. Continued.

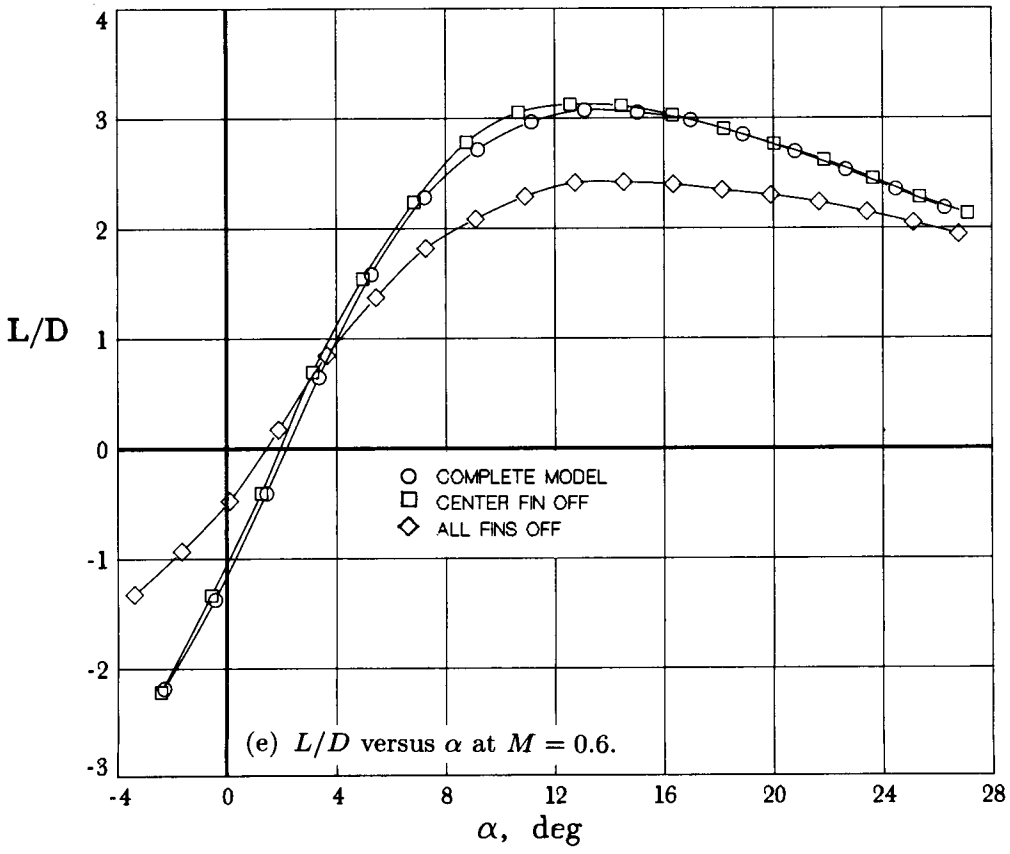

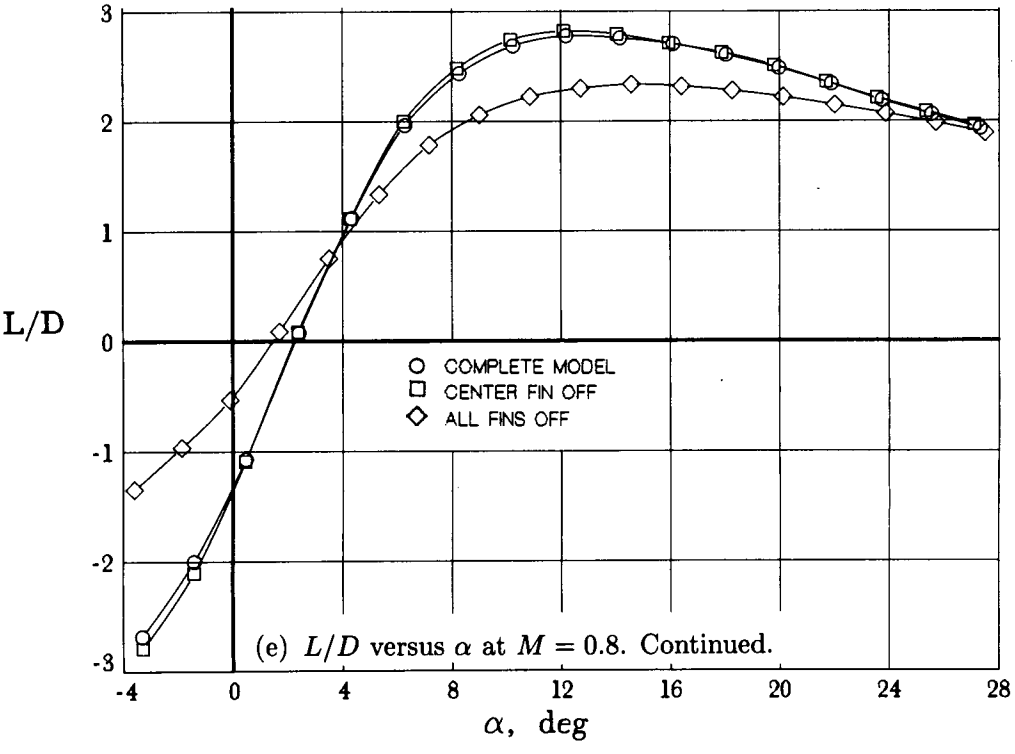

Figure 8. Continued.

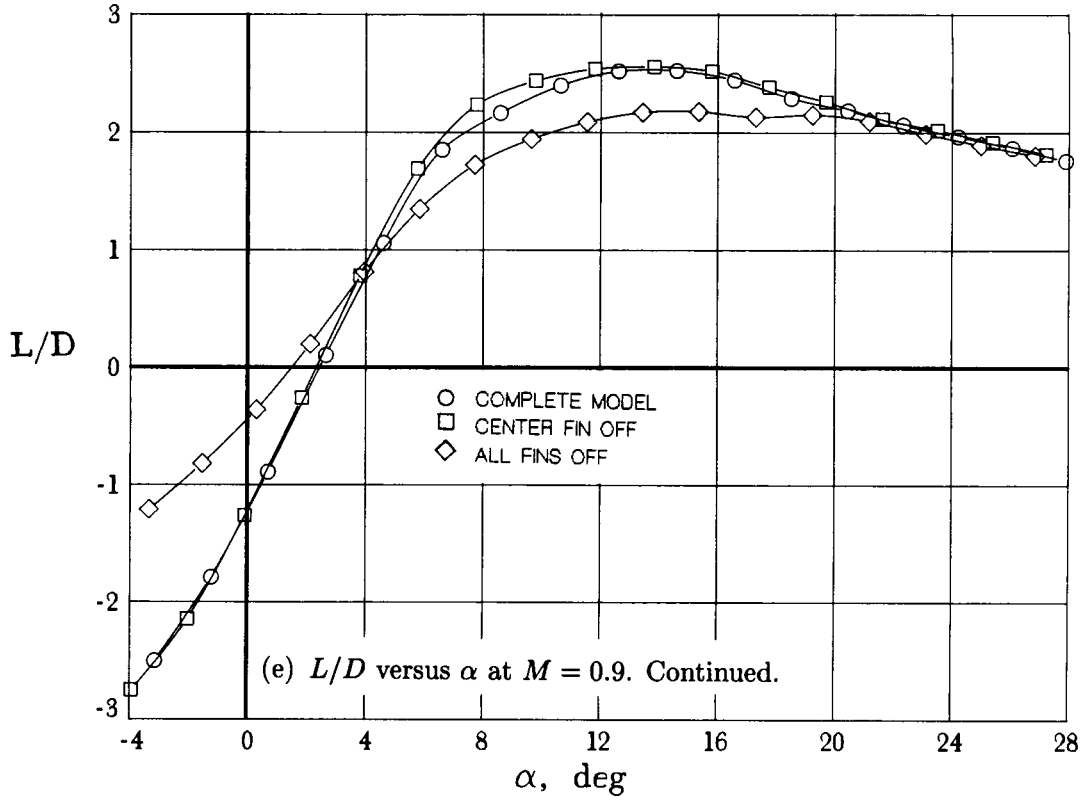

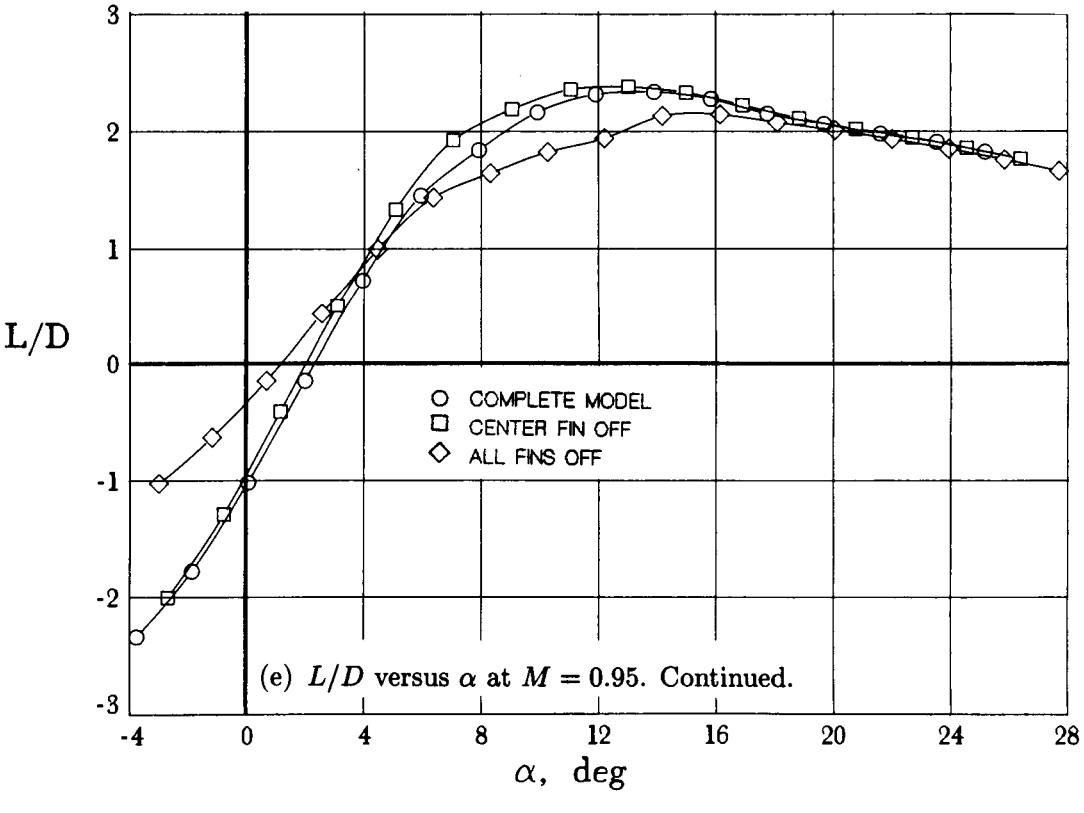

Figure 8. Continued.

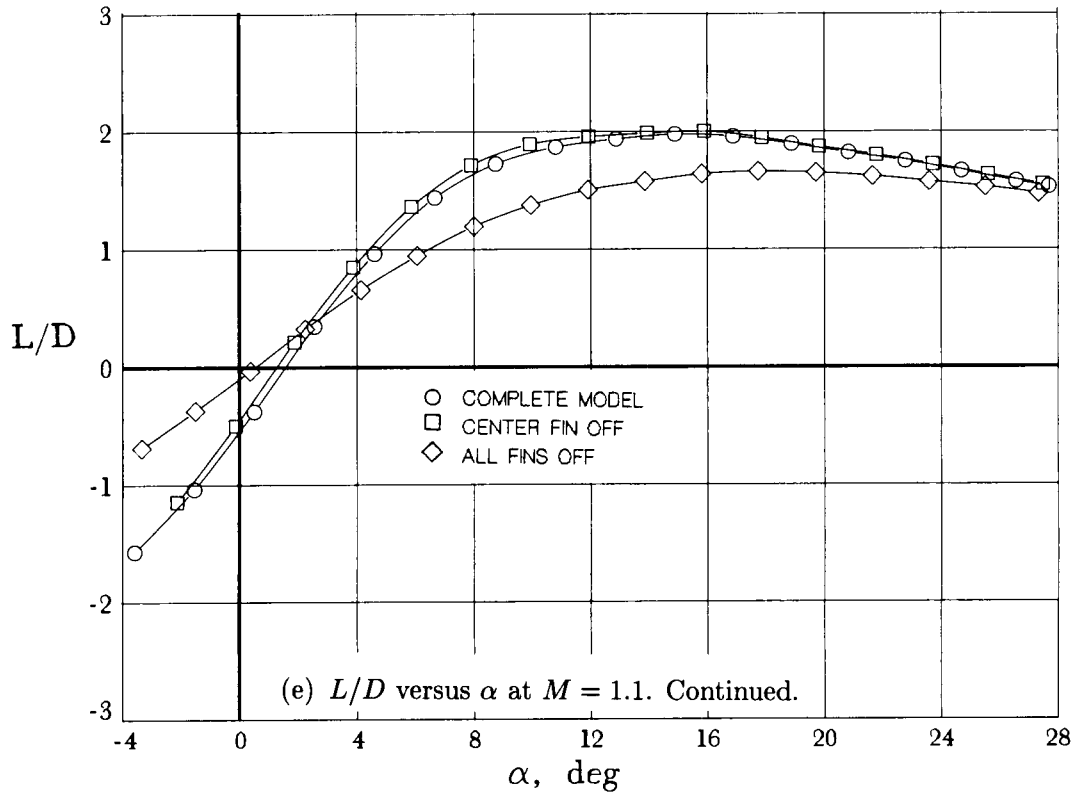

(e) L/D versus α at $M = 1.1$. Continued.

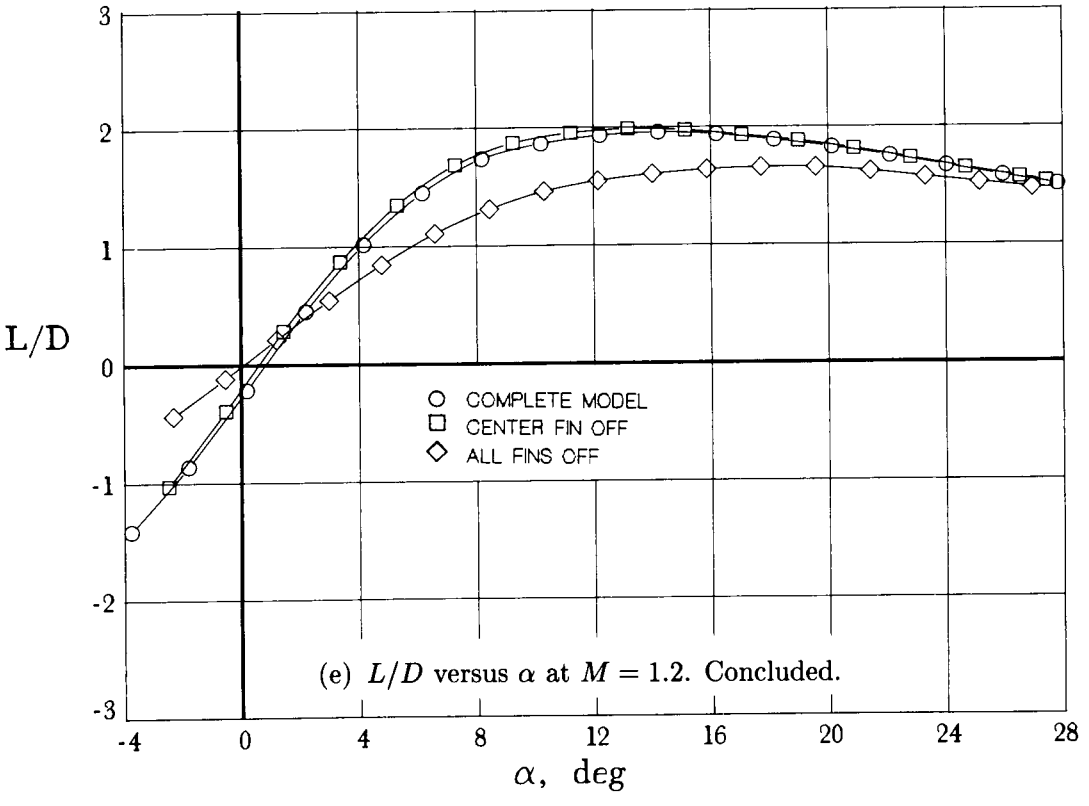

(e) L/D versus α at $M = 1.2$. Concluded.

Figure 8. Concluded.

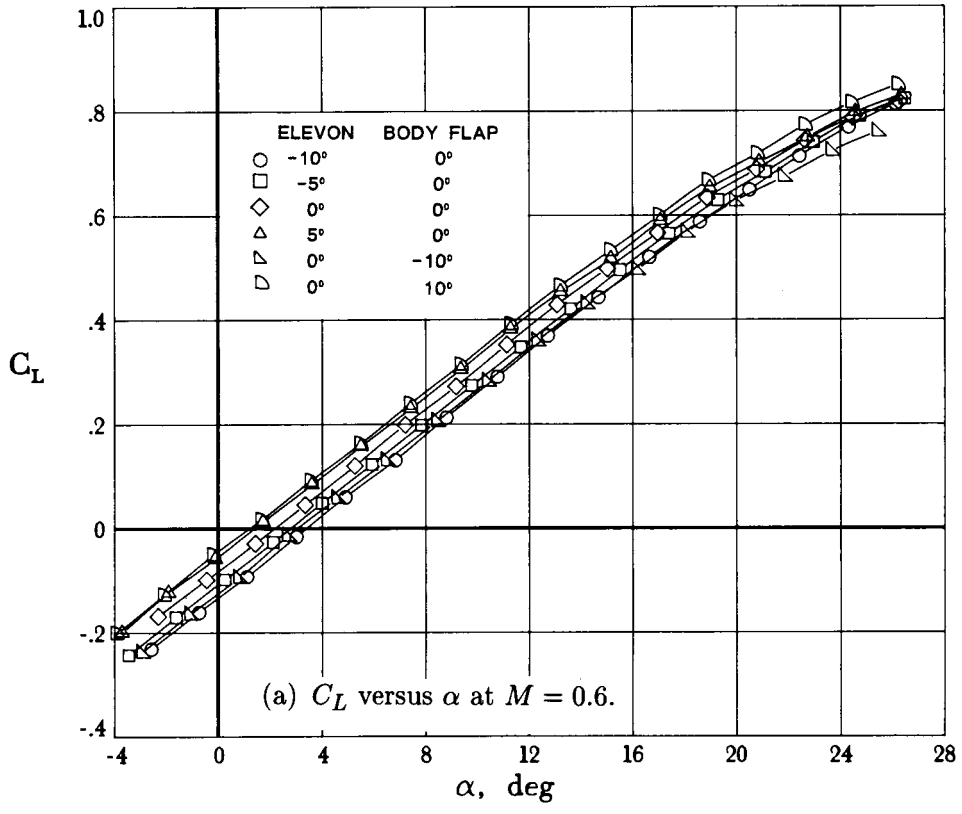

(a) C_L versus α at $M = 0.6$.

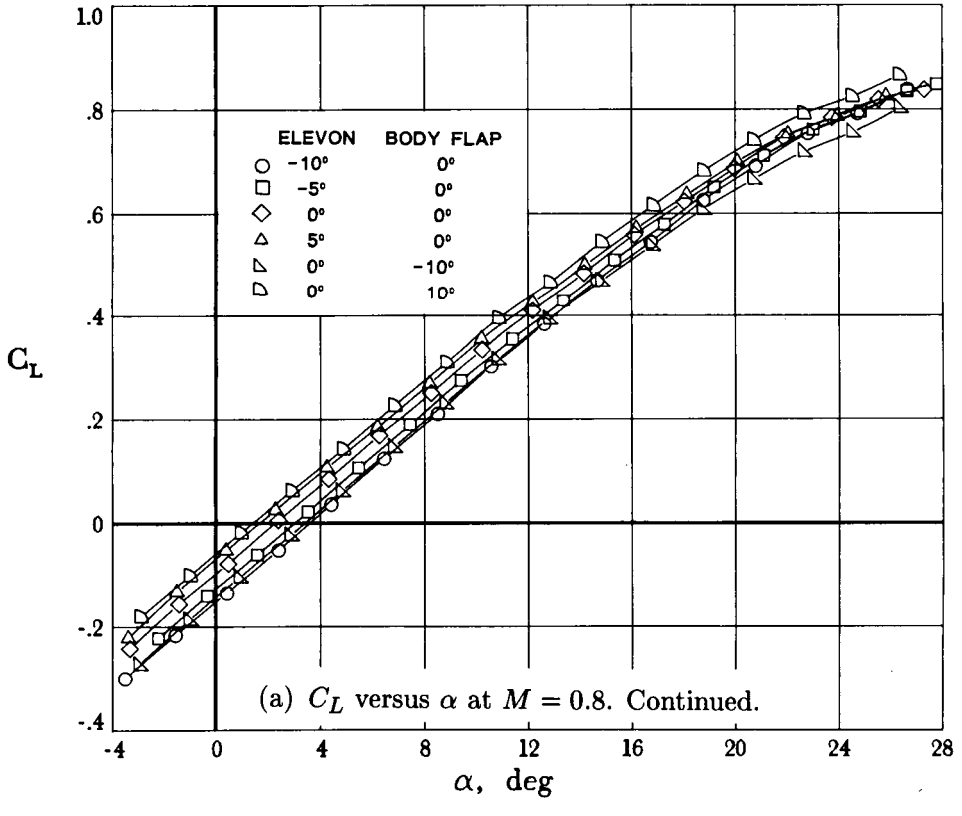

(a) C_L versus α at $M = 0.8$. Continued.

Figure 9. Effect of pitch control on longitudinal aerodynamic characteristics of model.

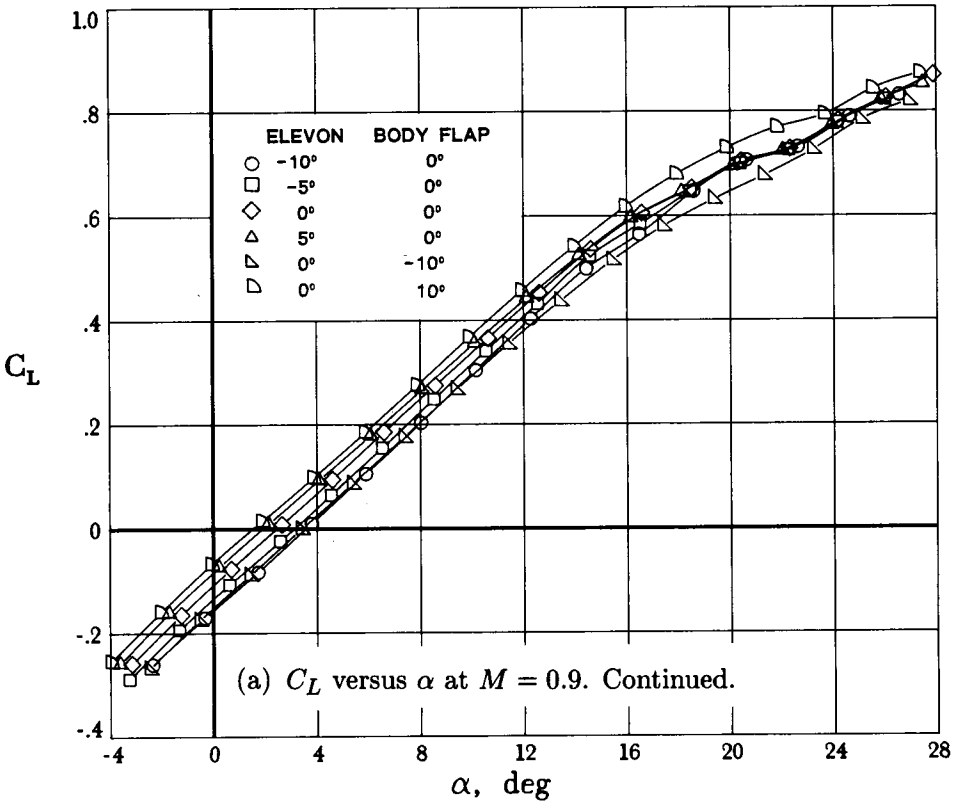

(a) C_L versus α at $M = 0.9$. Continued.

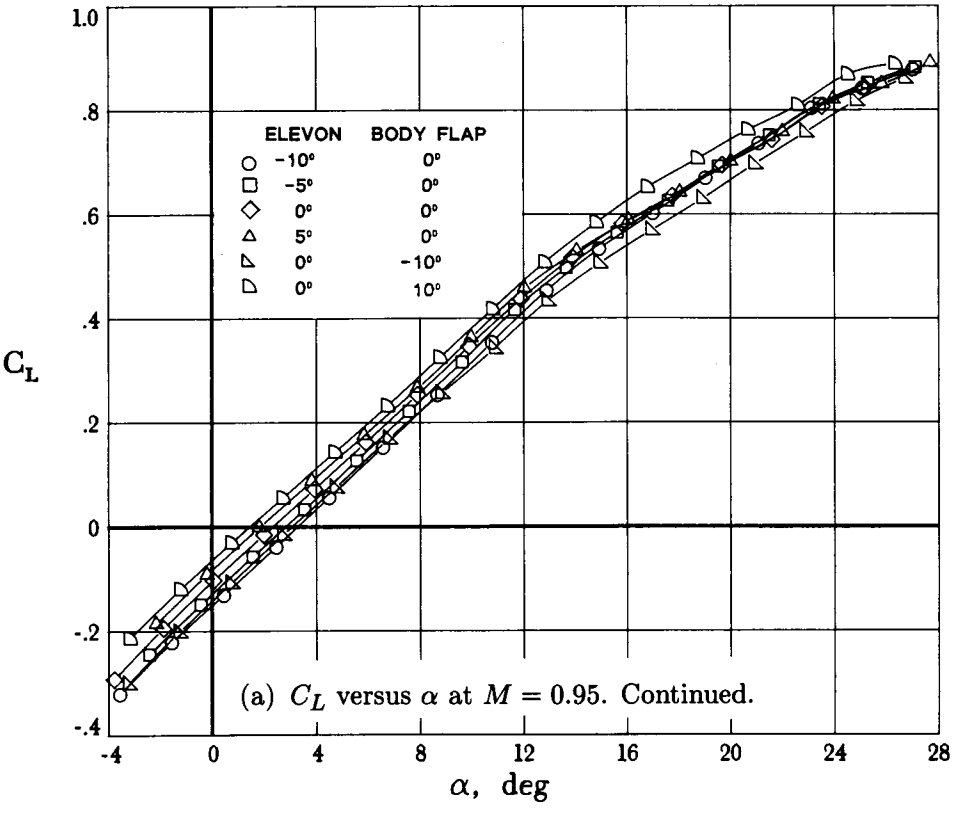

(a) C_L versus α at $M = 0.95$. Continued.

Figure 9. Continued.

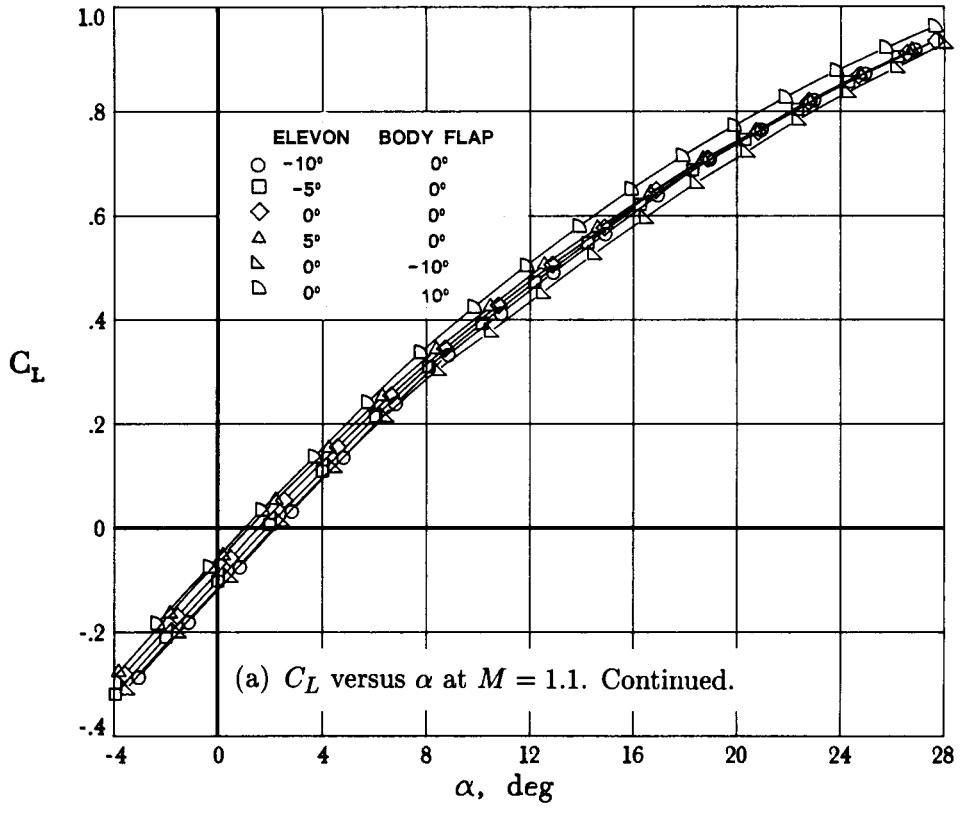

(a) C_L versus α at $M = 1.1$. Continued.

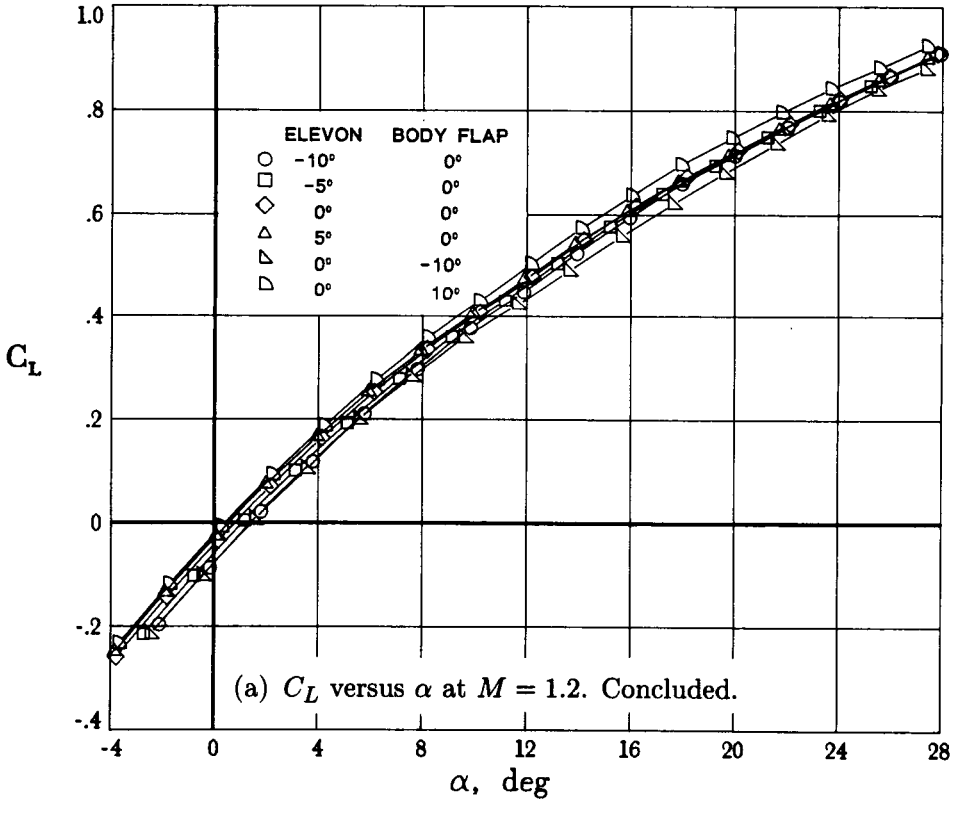

(a) C_L versus α at $M = 1.2$. Concluded.

Figure 9. Continued.

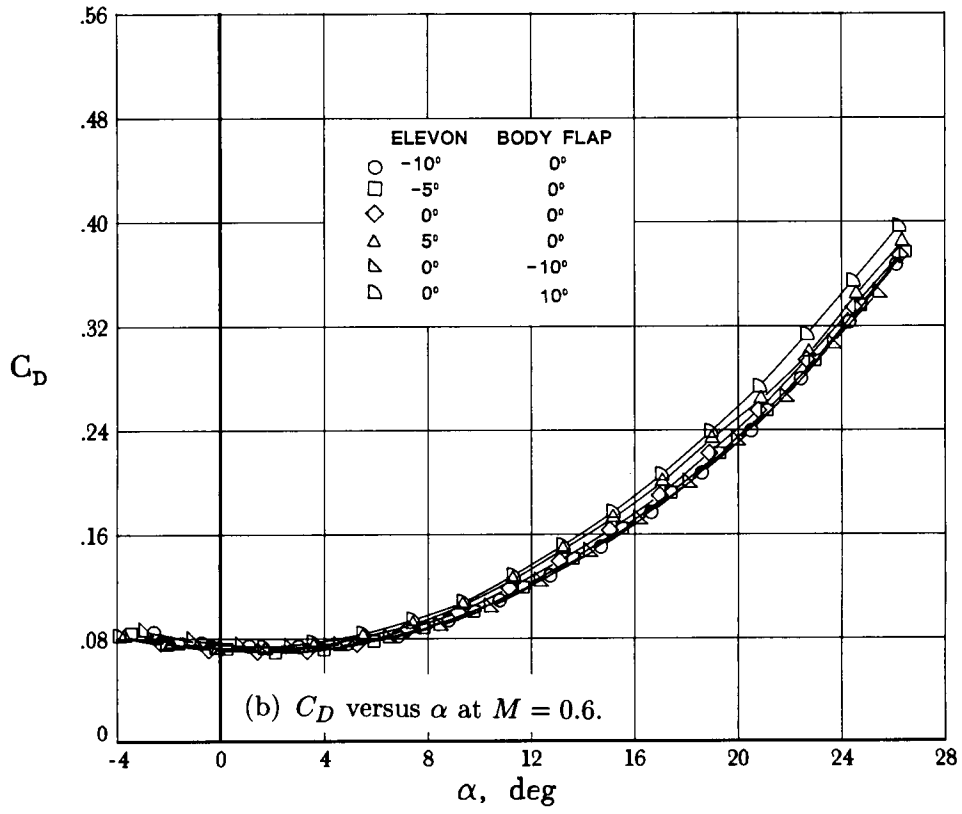

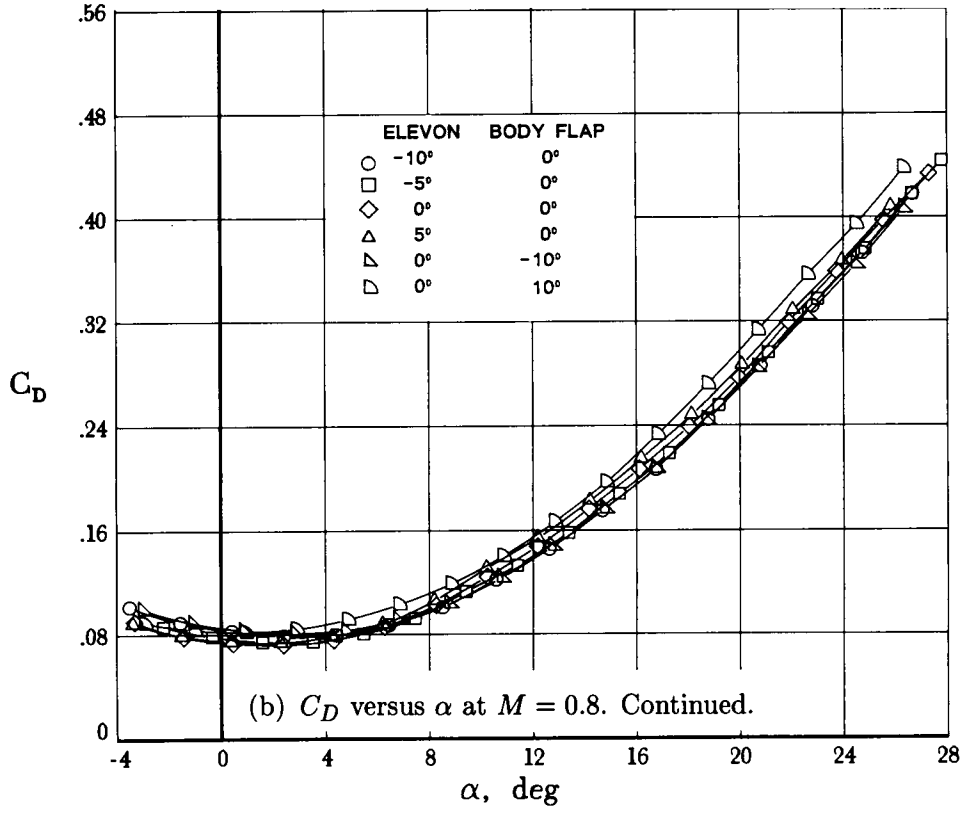

Figure 9. Continued.

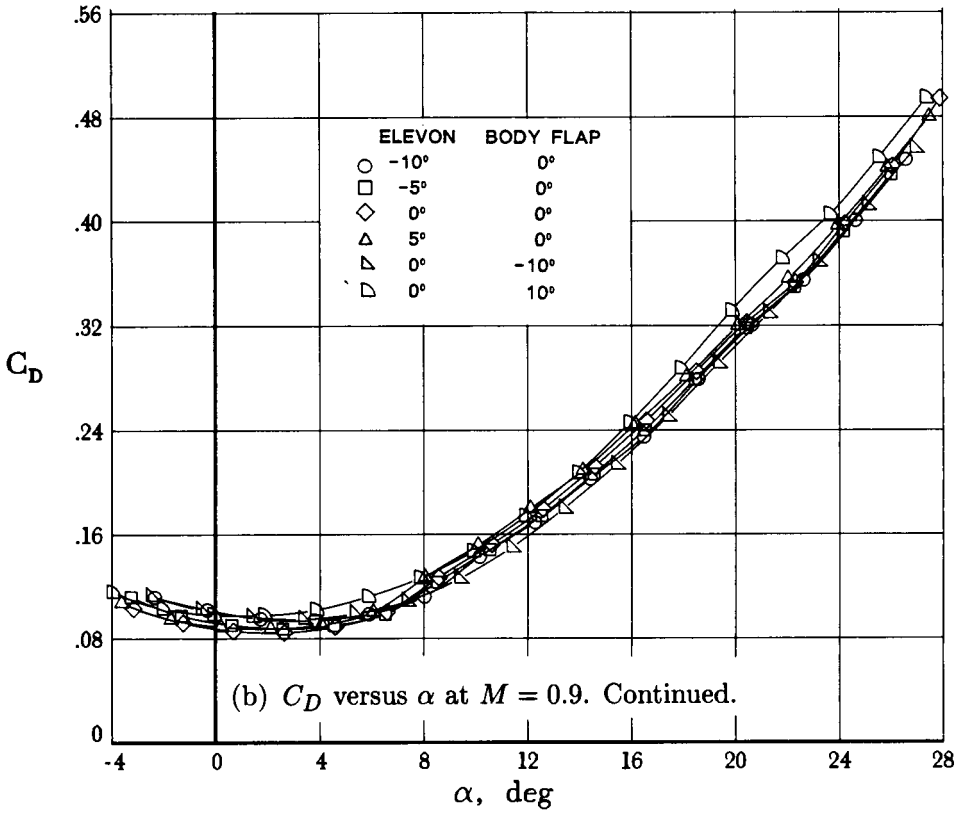

(b) C_D versus α at $M = 0.9$. Continued.

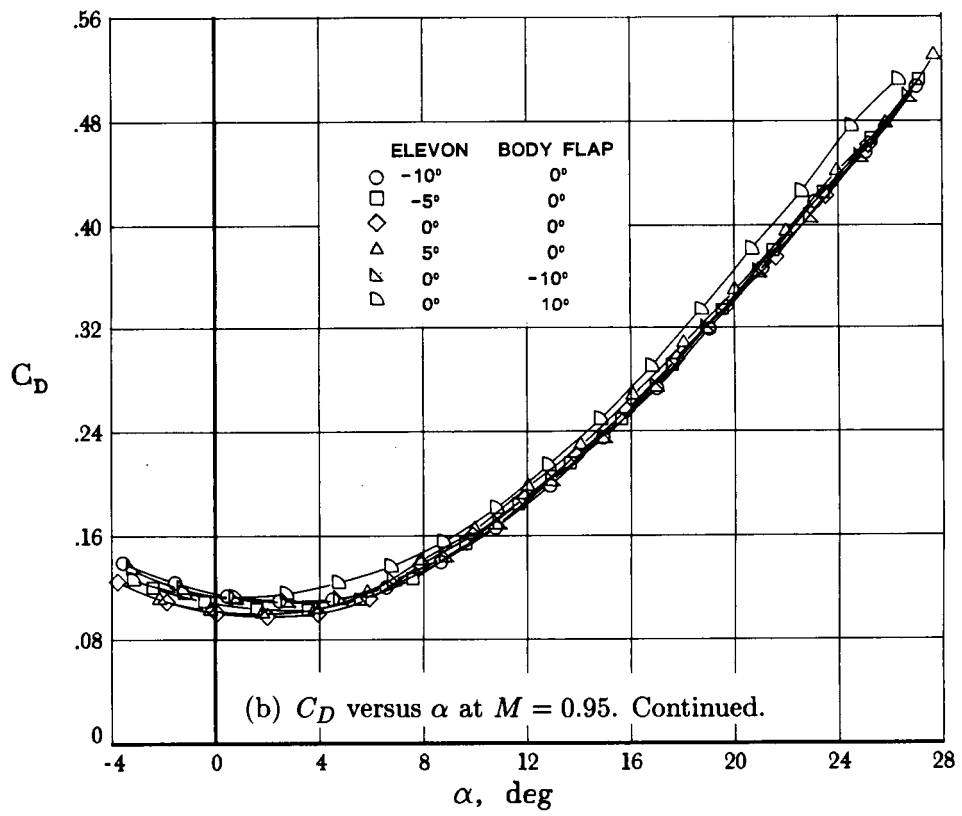

(b) C_D versus α at $M = 0.95$. Continued.

Figure 9. Continued.

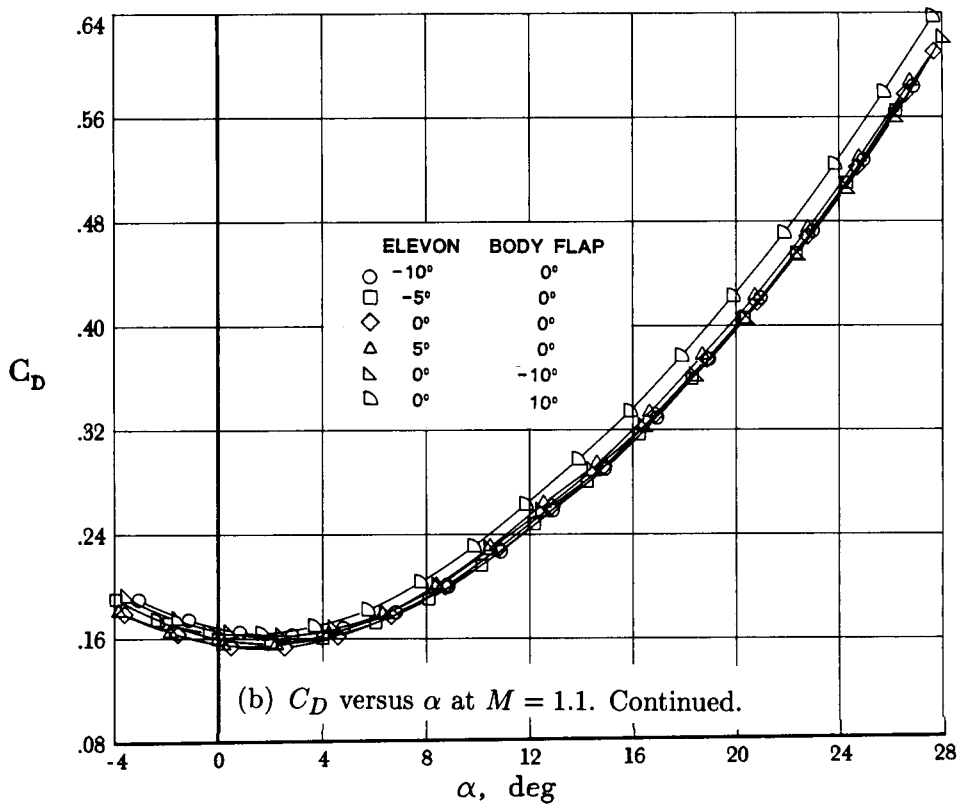

(b) C_D versus α at $M = 1.1$. Continued.

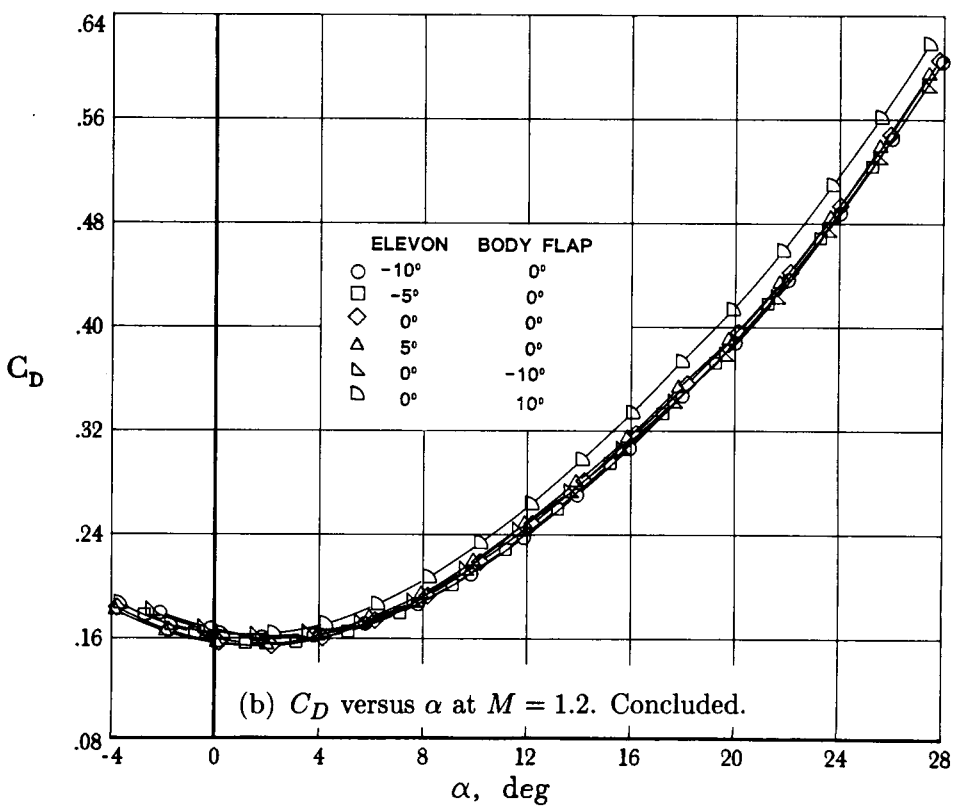

(b) C_D versus α at $M = 1.2$. Concluded.

Figure 9. Continued.

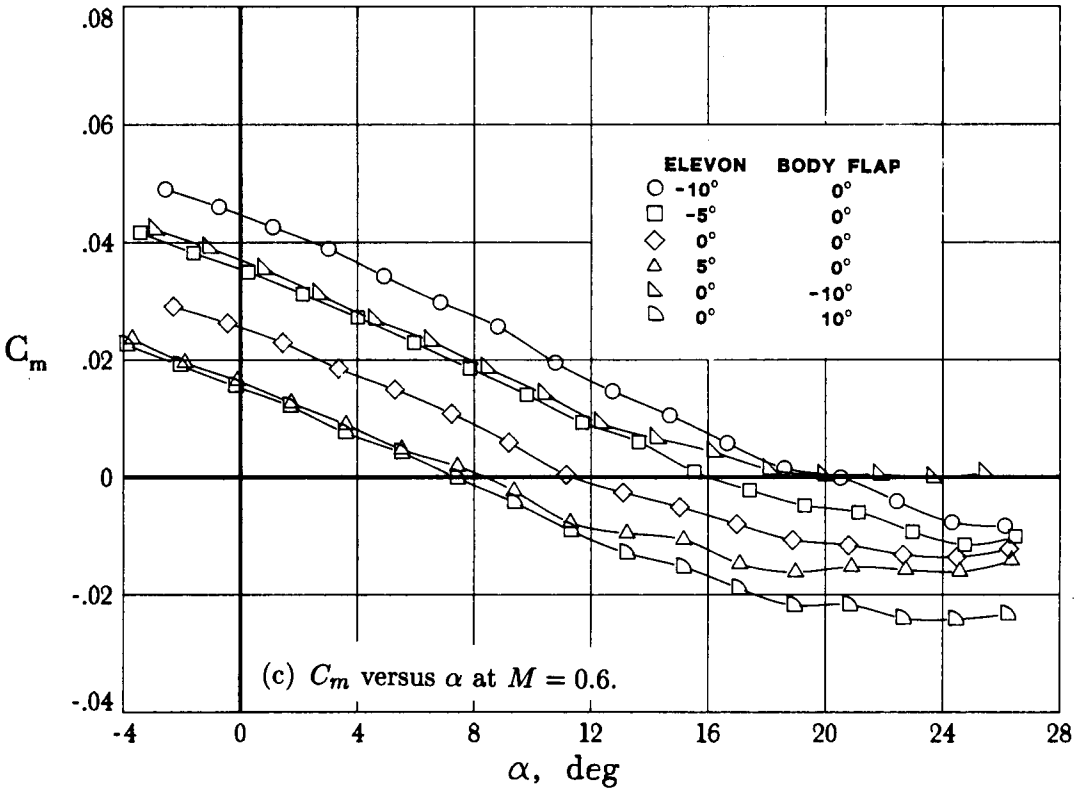

(c) C_m versus α at $M = 0.6$.

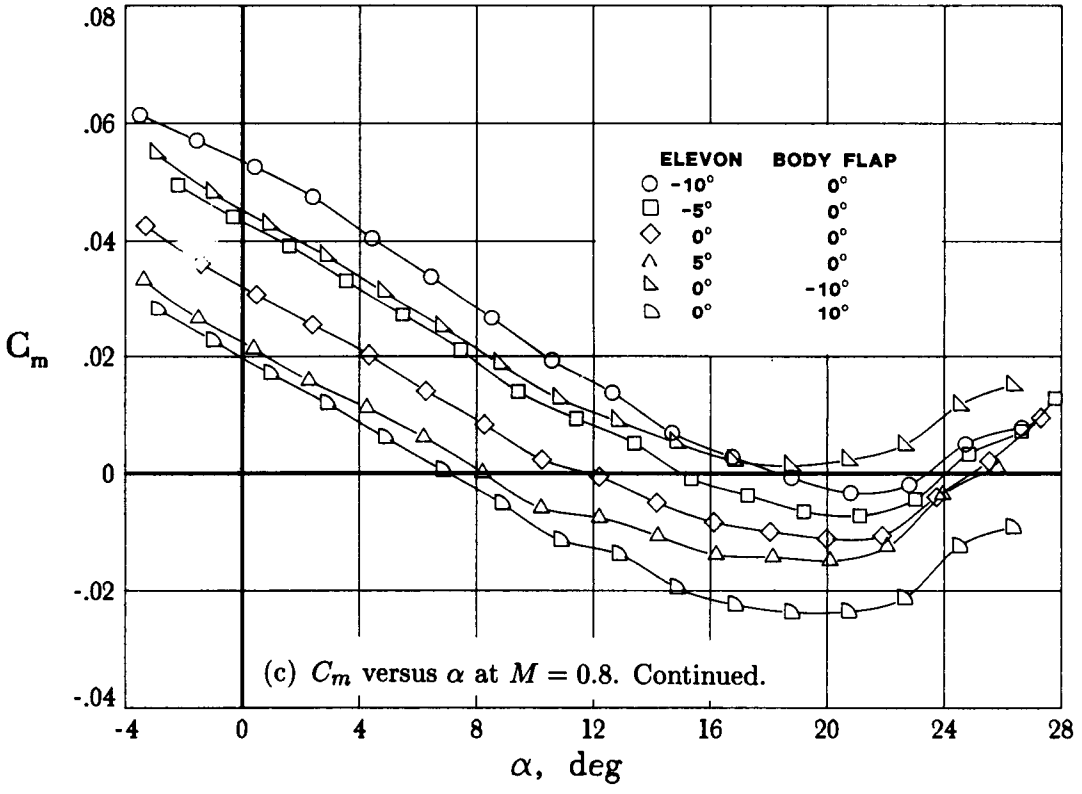

(c) C_m versus α at $M = 0.8$. Continued.

Figure 9. Continued.

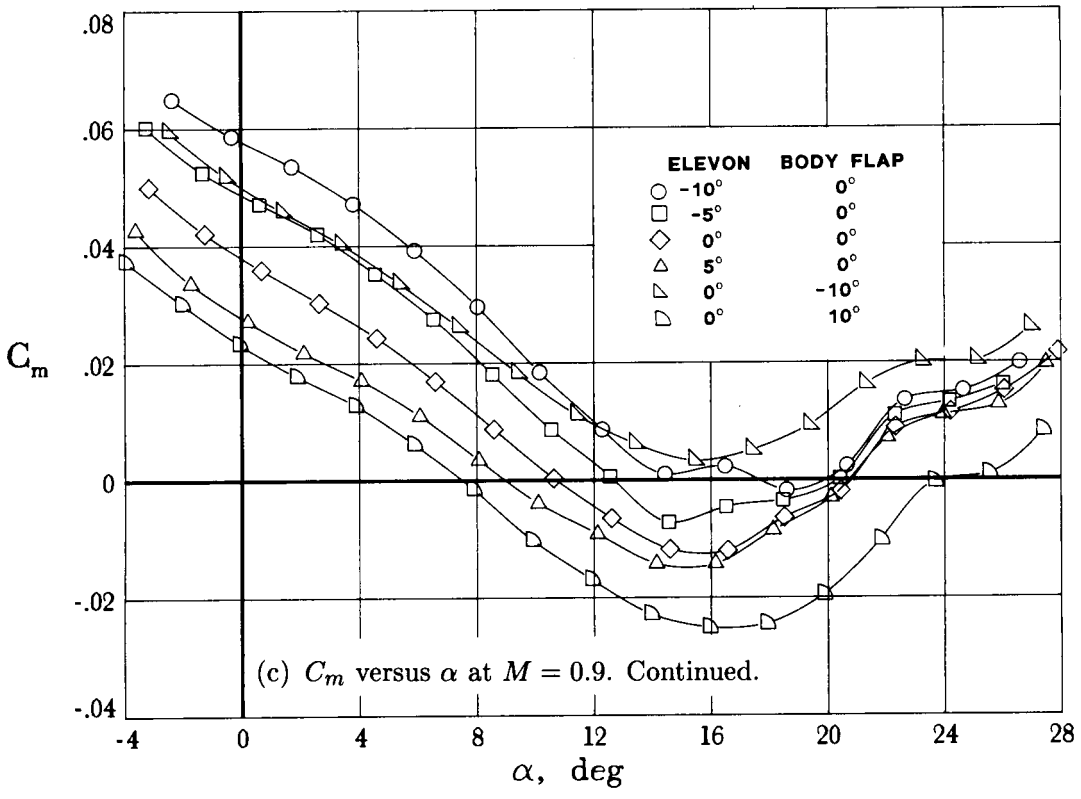

(c) C_m versus α at $M = 0.9$. Continued.

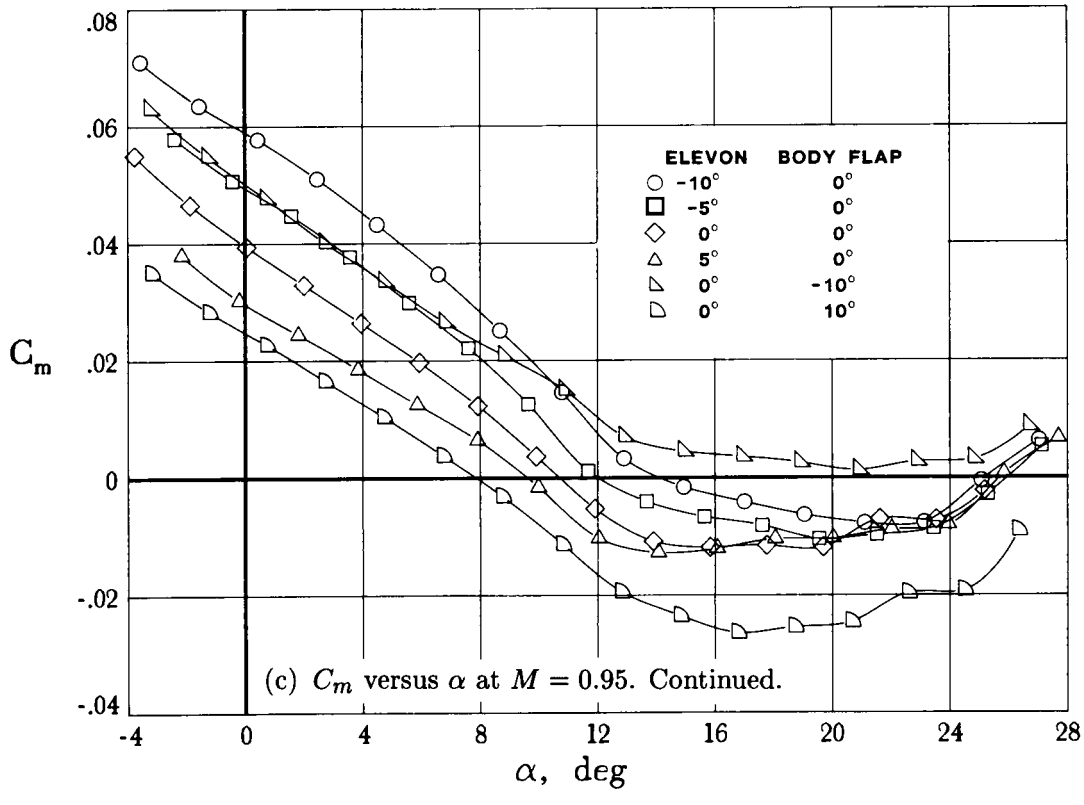

(c) C_m versus α at $M = 0.95$. Continued.

Figure 9. Continued.

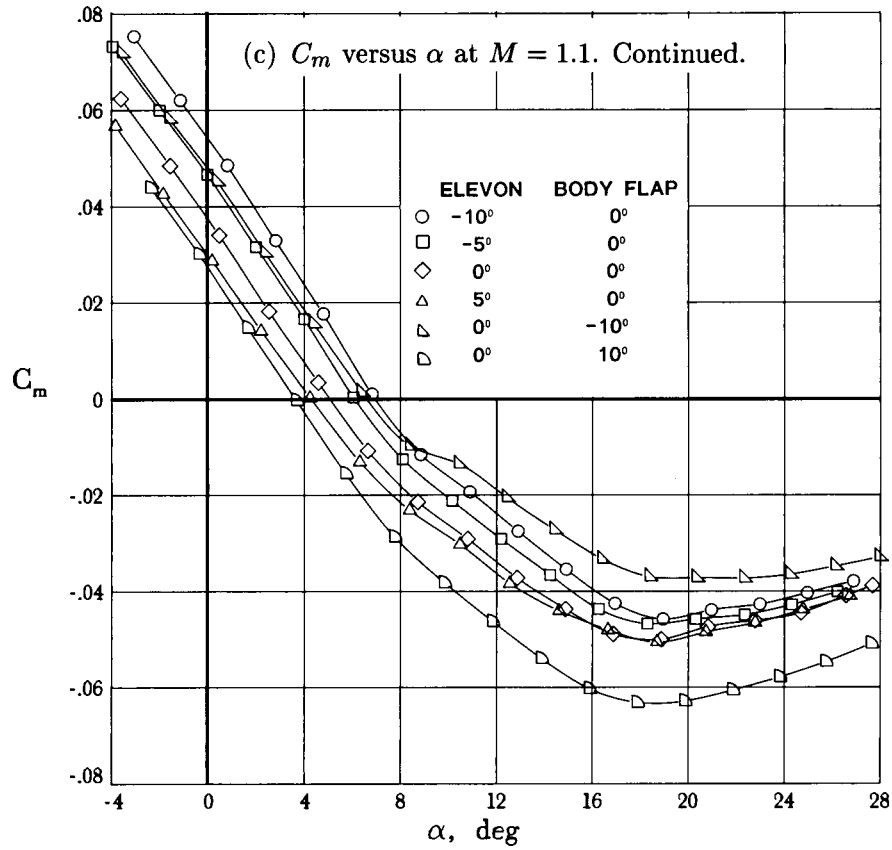

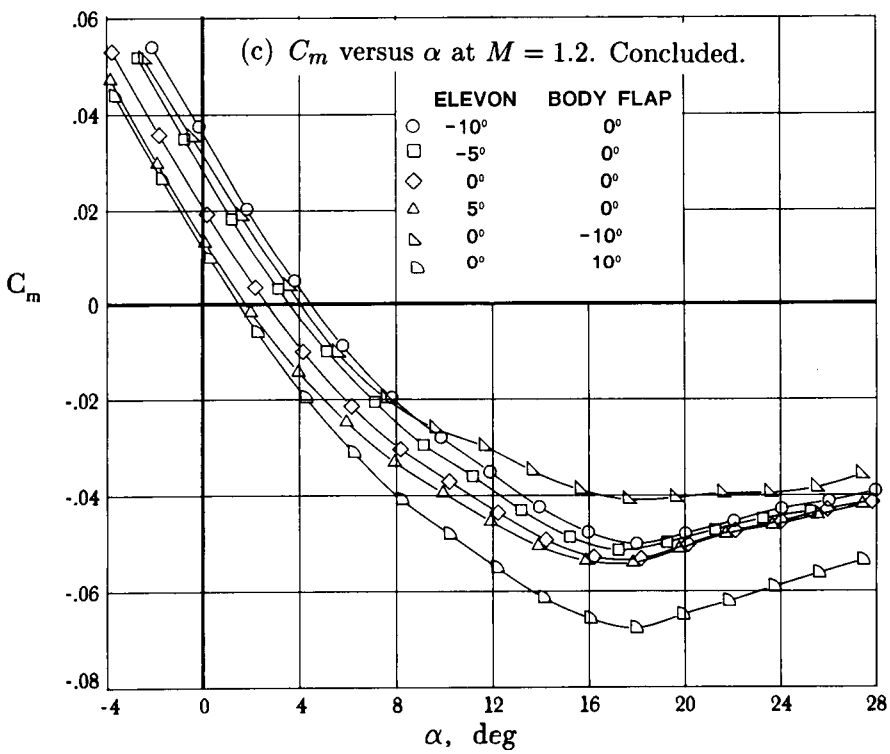

Figure 9. Continued.

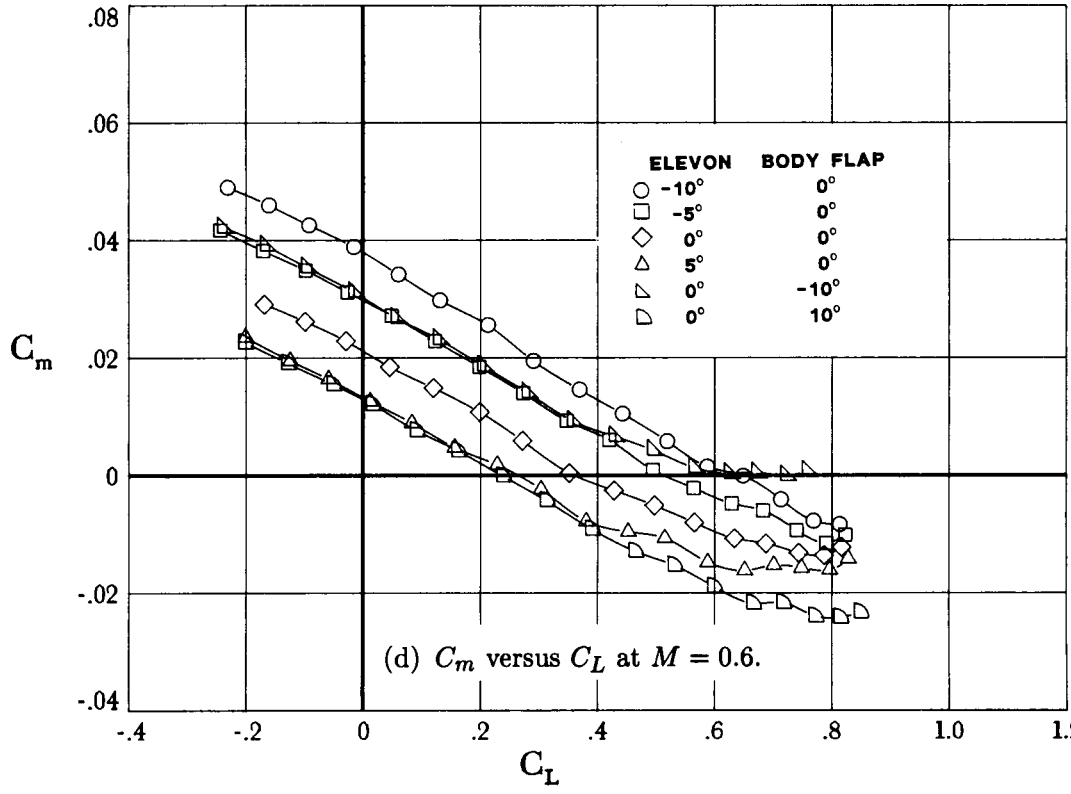

(d) C_m versus C_L at $M = 0.6$.

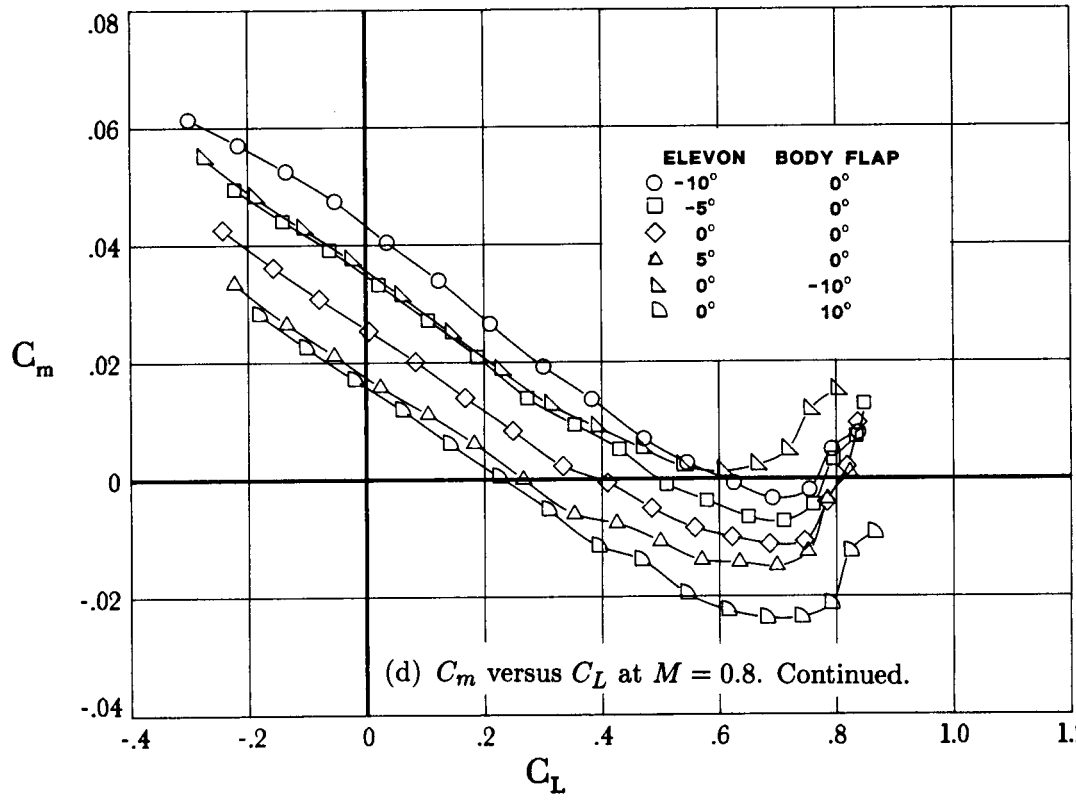

(d) C_m versus C_L at $M = 0.8$. Continued.

Figure 9. Continued.

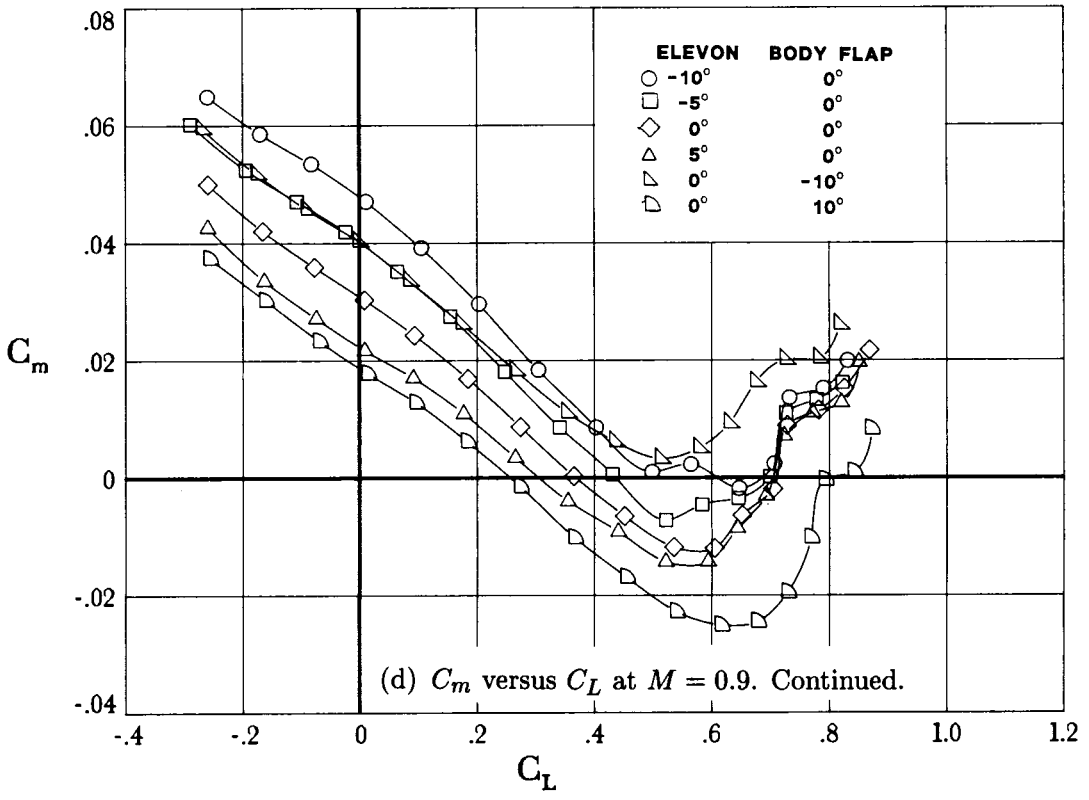

(d) C_m versus C_L at $M = 0.9$. Continued.

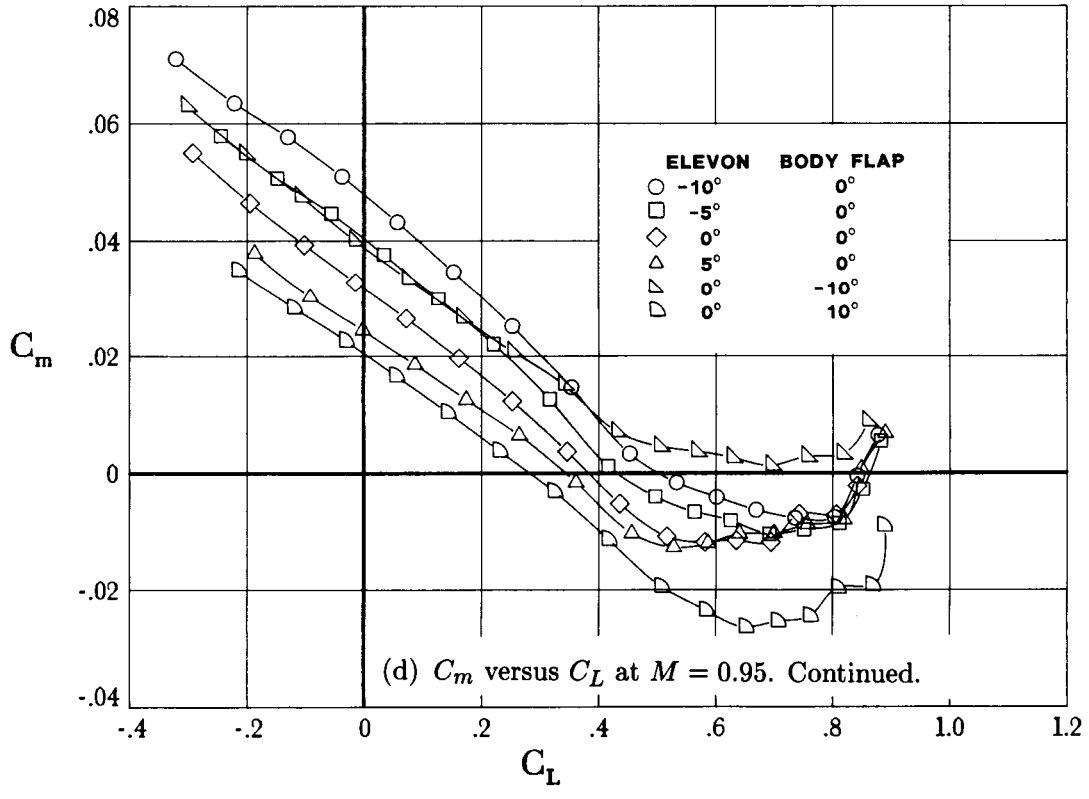

(d) C_m versus C_L at $M = 0.95$. Continued.

Figure 9. Continued.

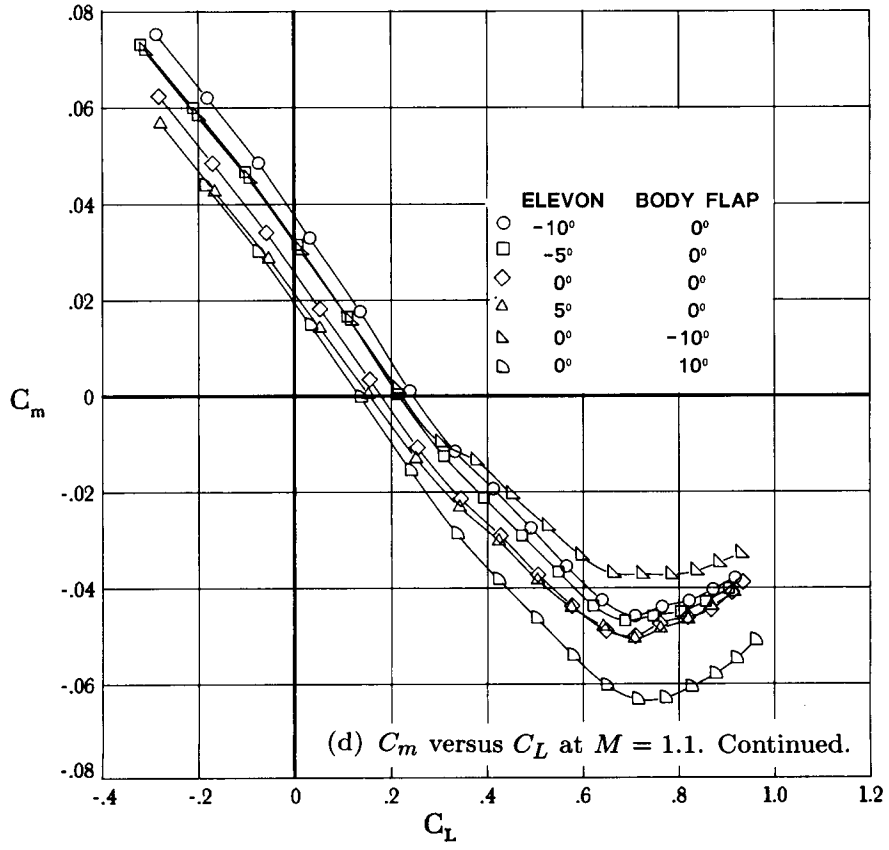

(d) C_m versus C_L at $M = 1.1$. Continued.

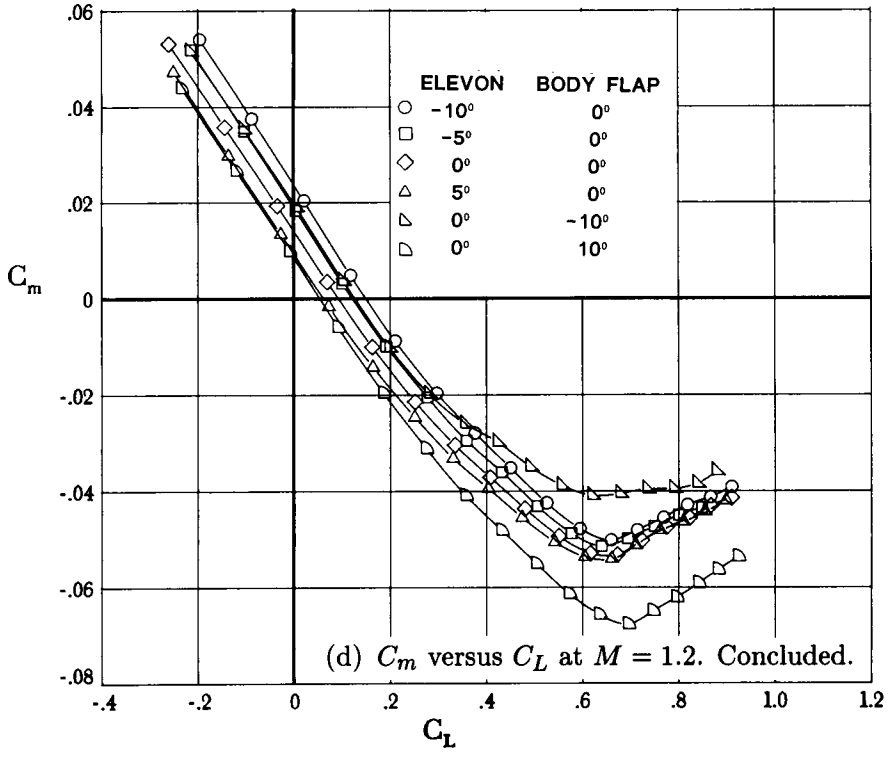

(d) C_m versus C_L at $M = 1.2$. Concluded.

Figure 9. Continued.

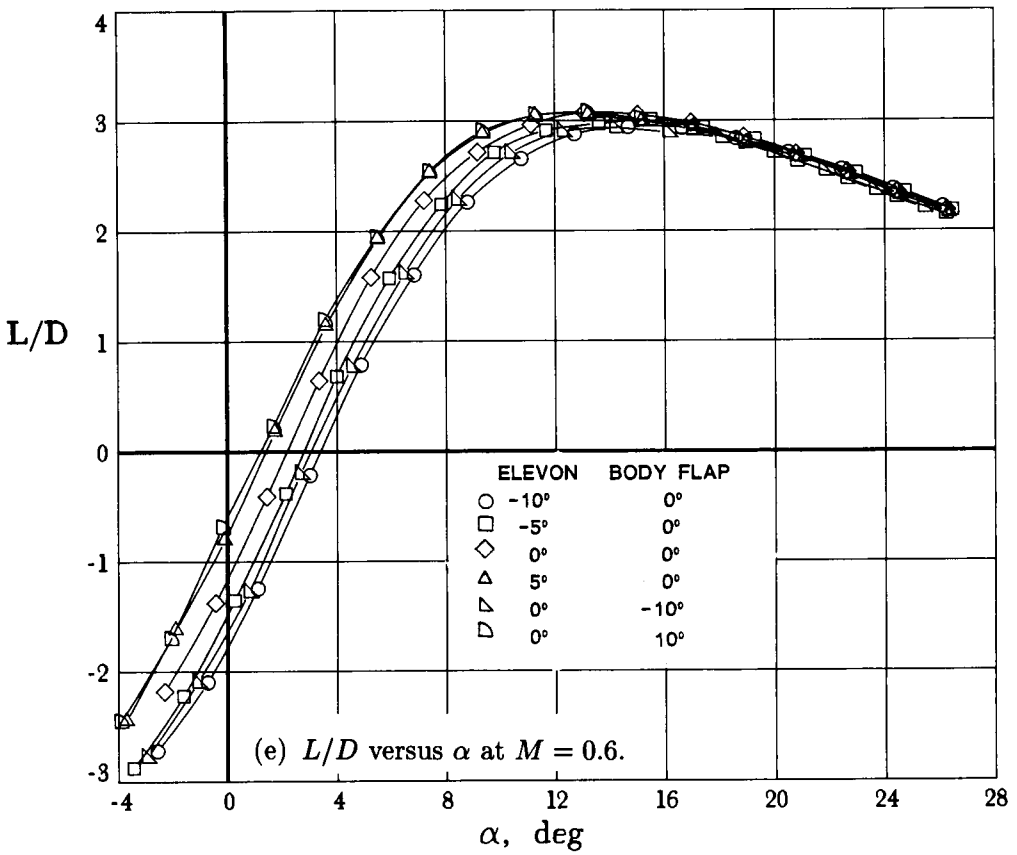

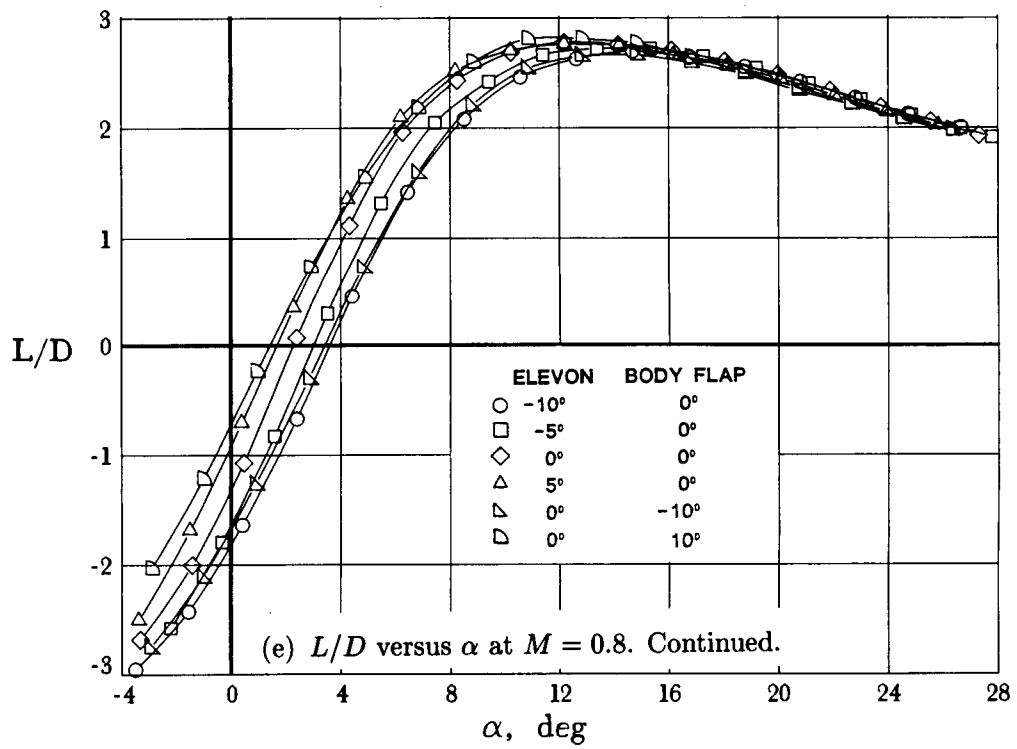

Figure 9. Continued.

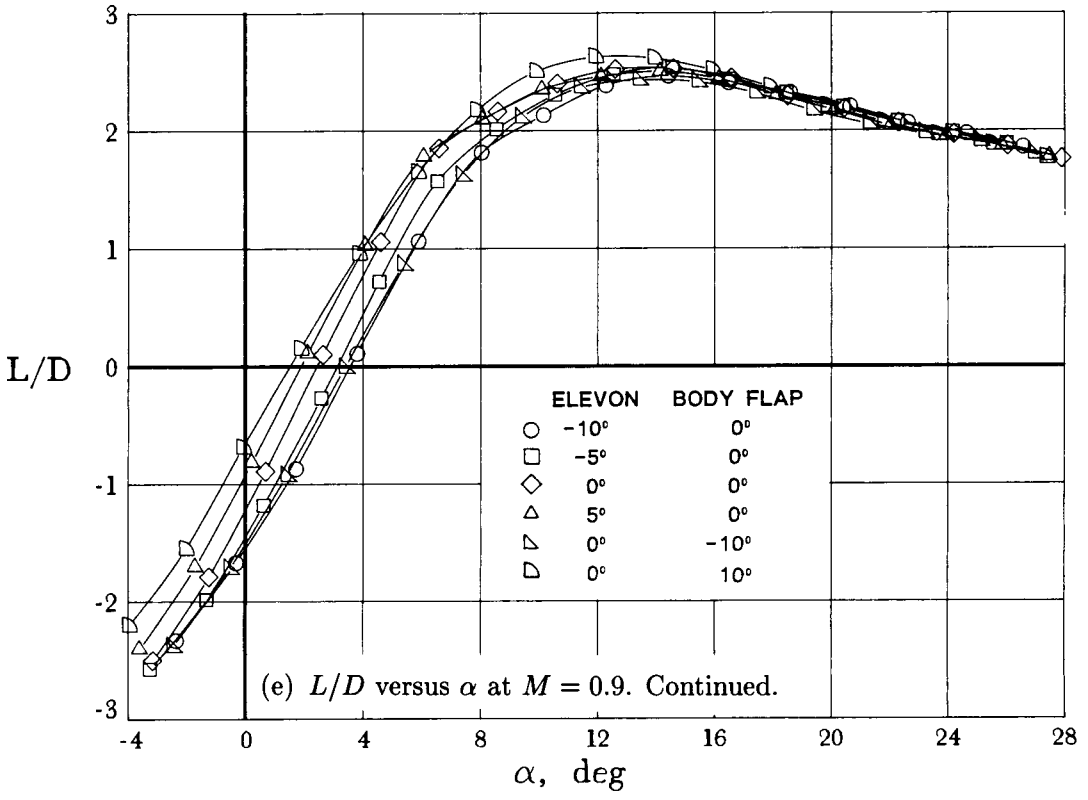

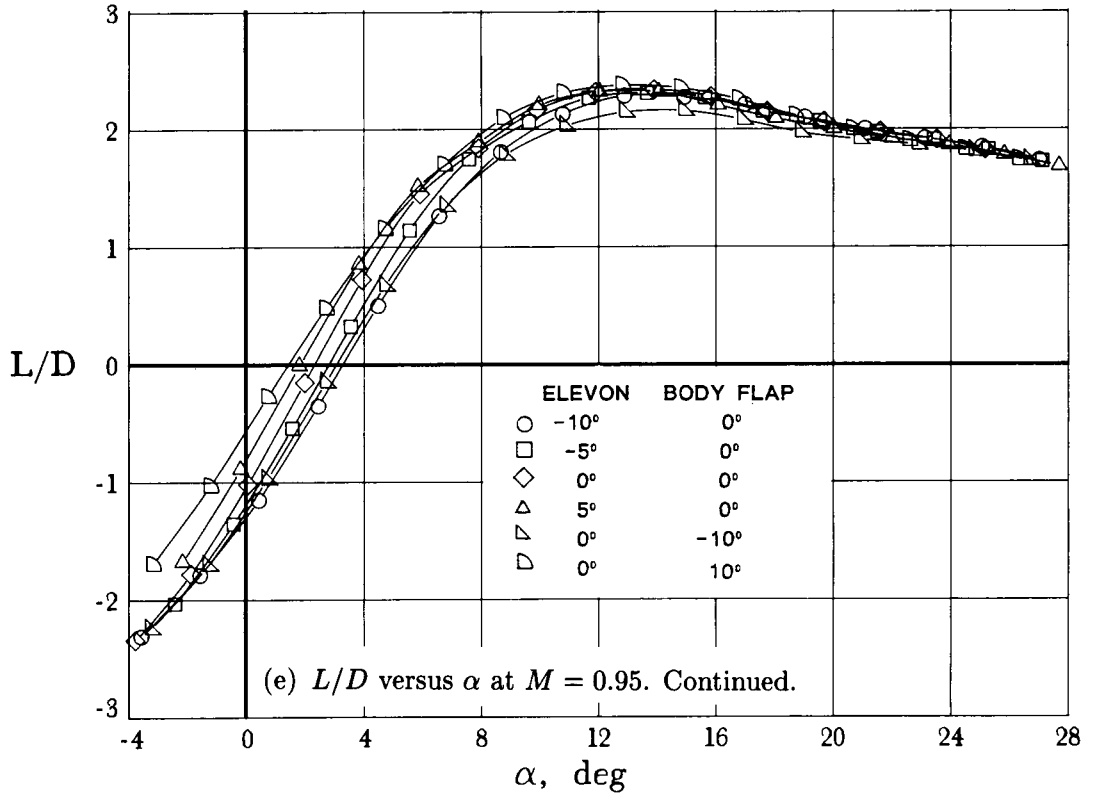

Figure 9. Continued.

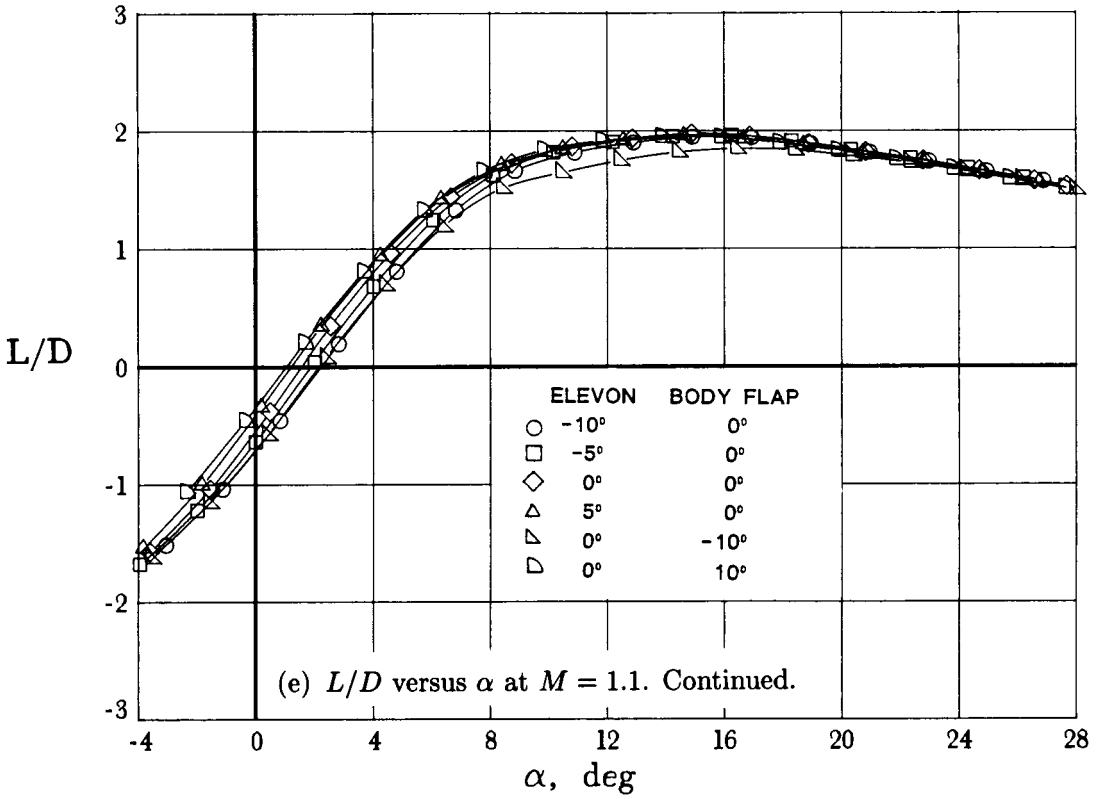

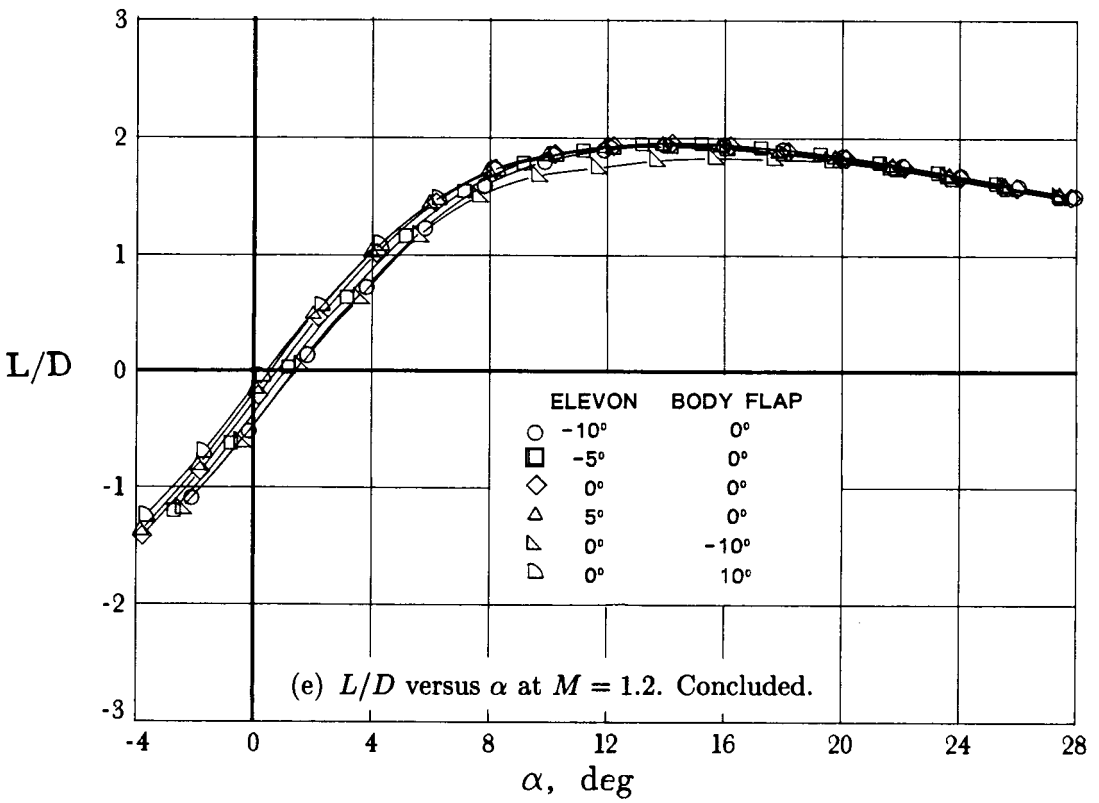

Figure 9. Concluded.

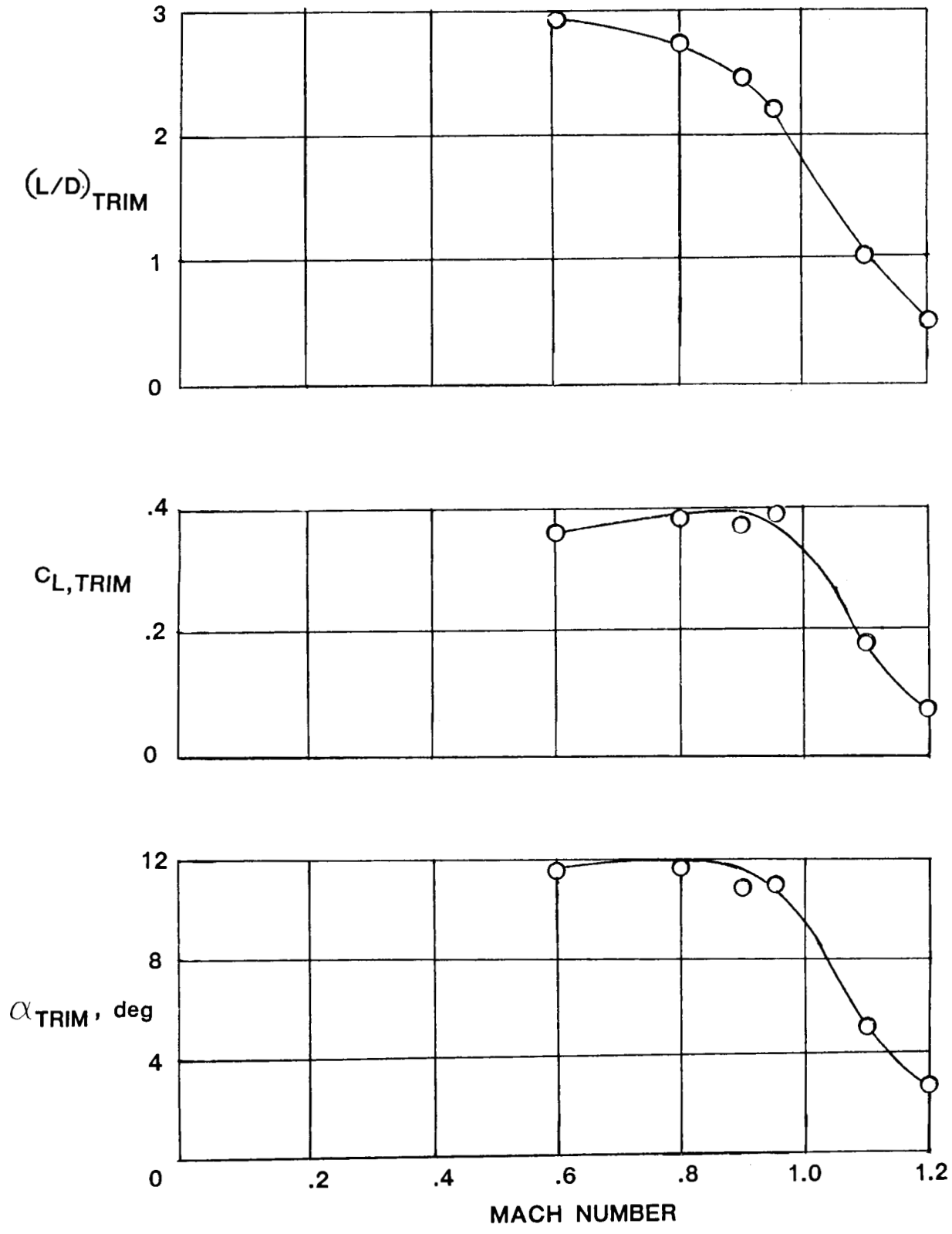

Figure 10. Variation of longitudinal trim characteristics of baseline configuration with Mach number. No controls deflected.

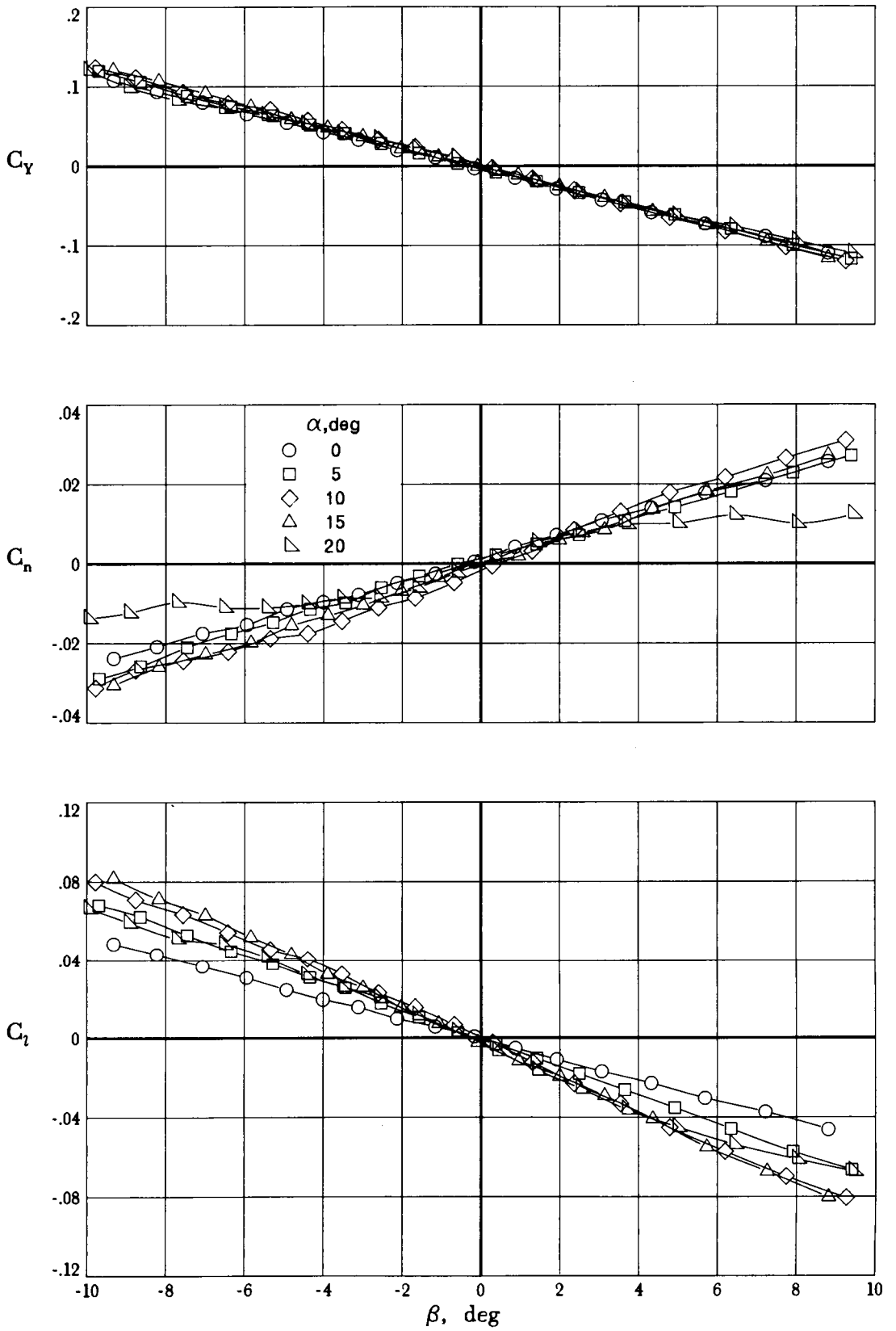

(a) $M = 0.6$.

Figure 11. Variation of lateral aerodynamic characteristics with sideslip. Complete model.

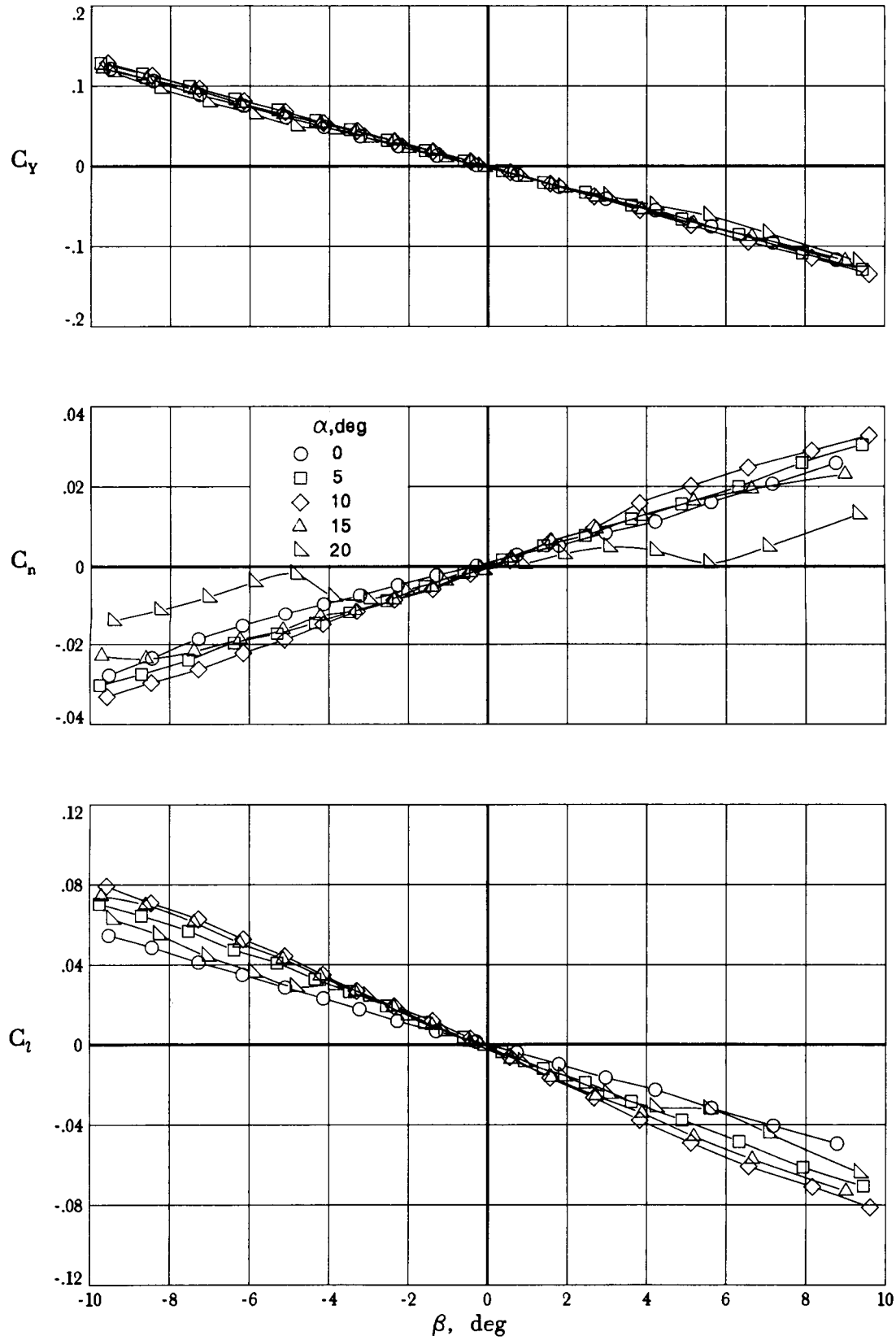

(b) $M = 0.8$.

Figure 11. Continued.

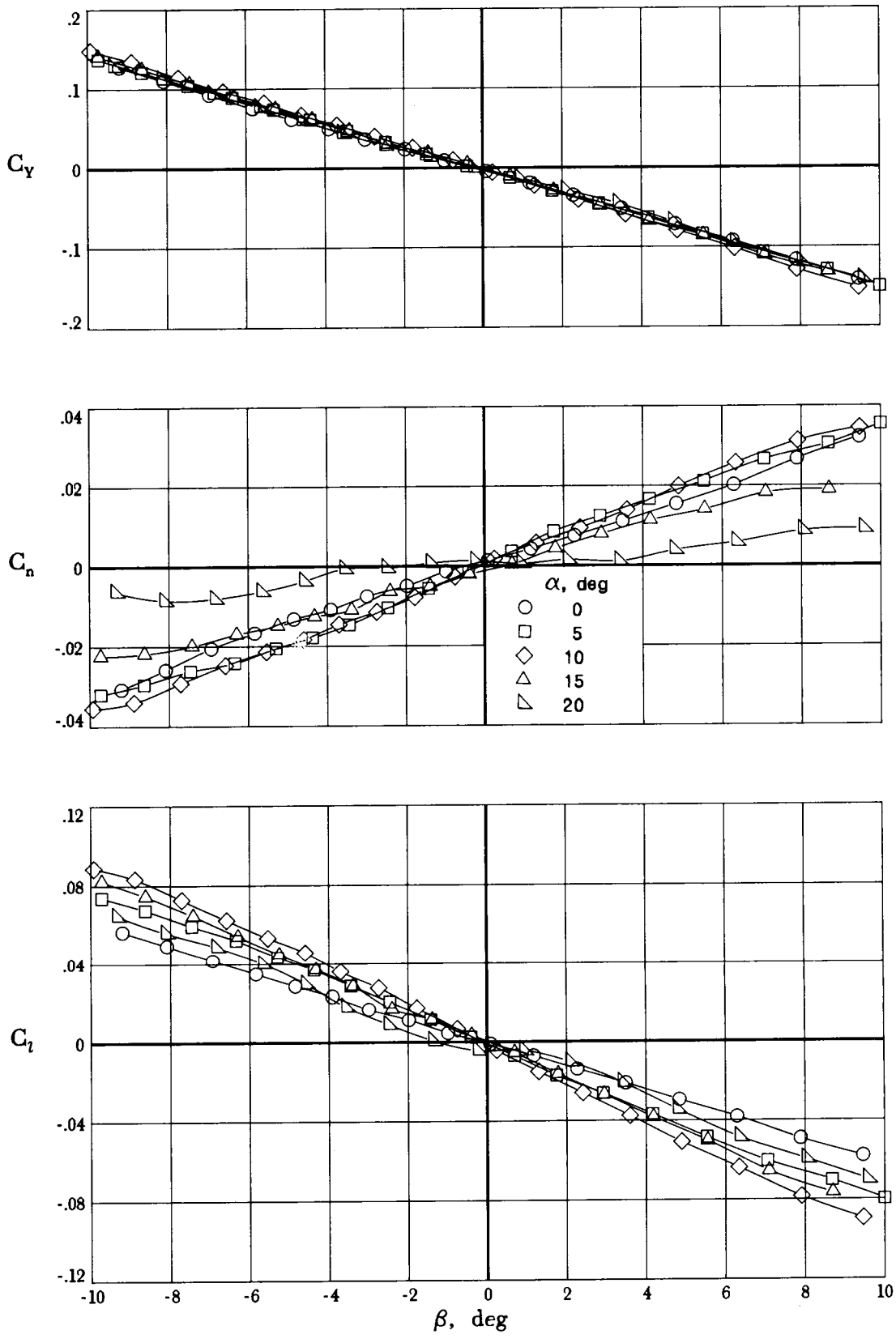

(c) $M = 0.9$.

Figure 11. Continued.

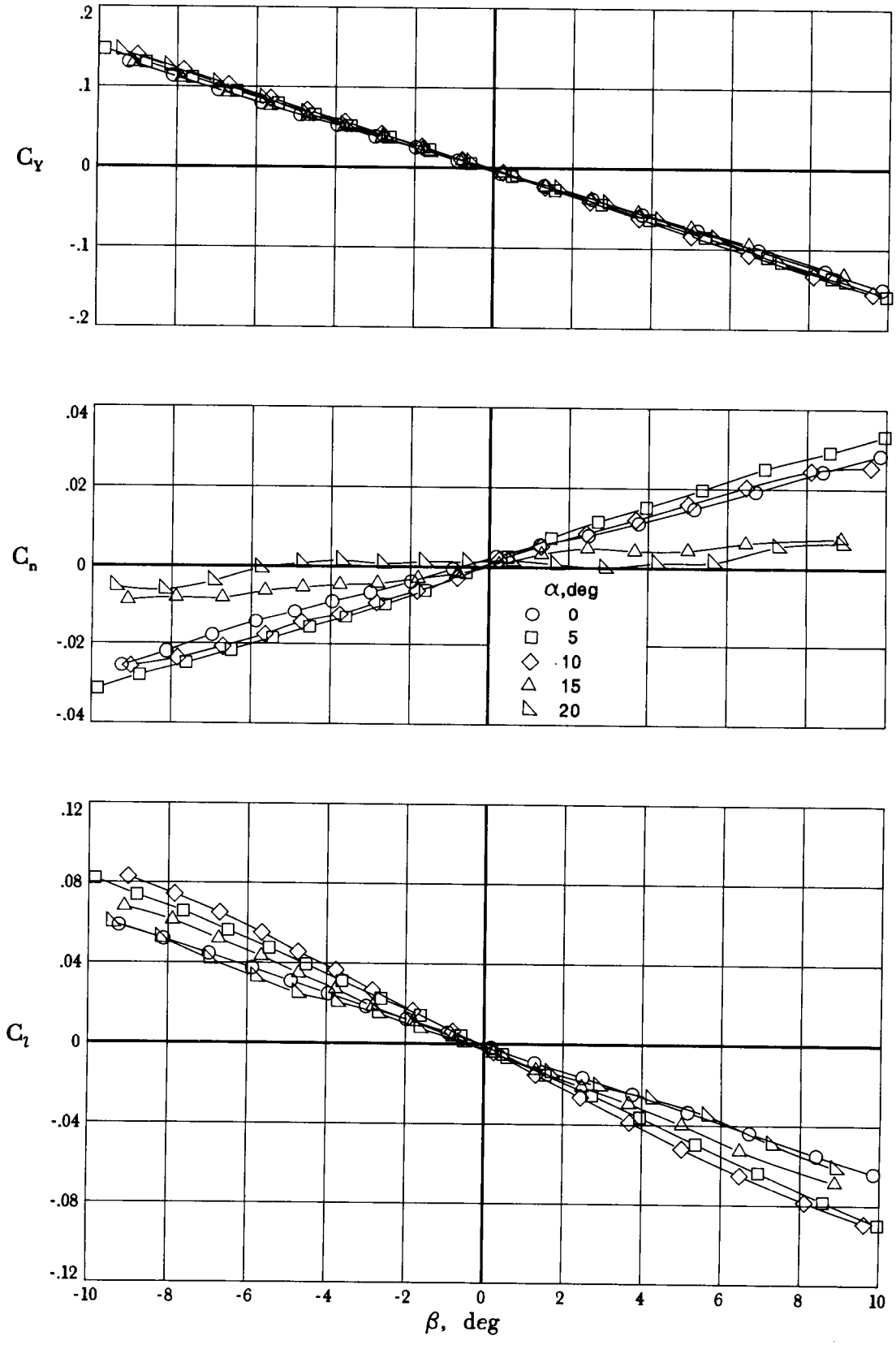

(d) $M = 0.95$.

Figure 11. Continued.

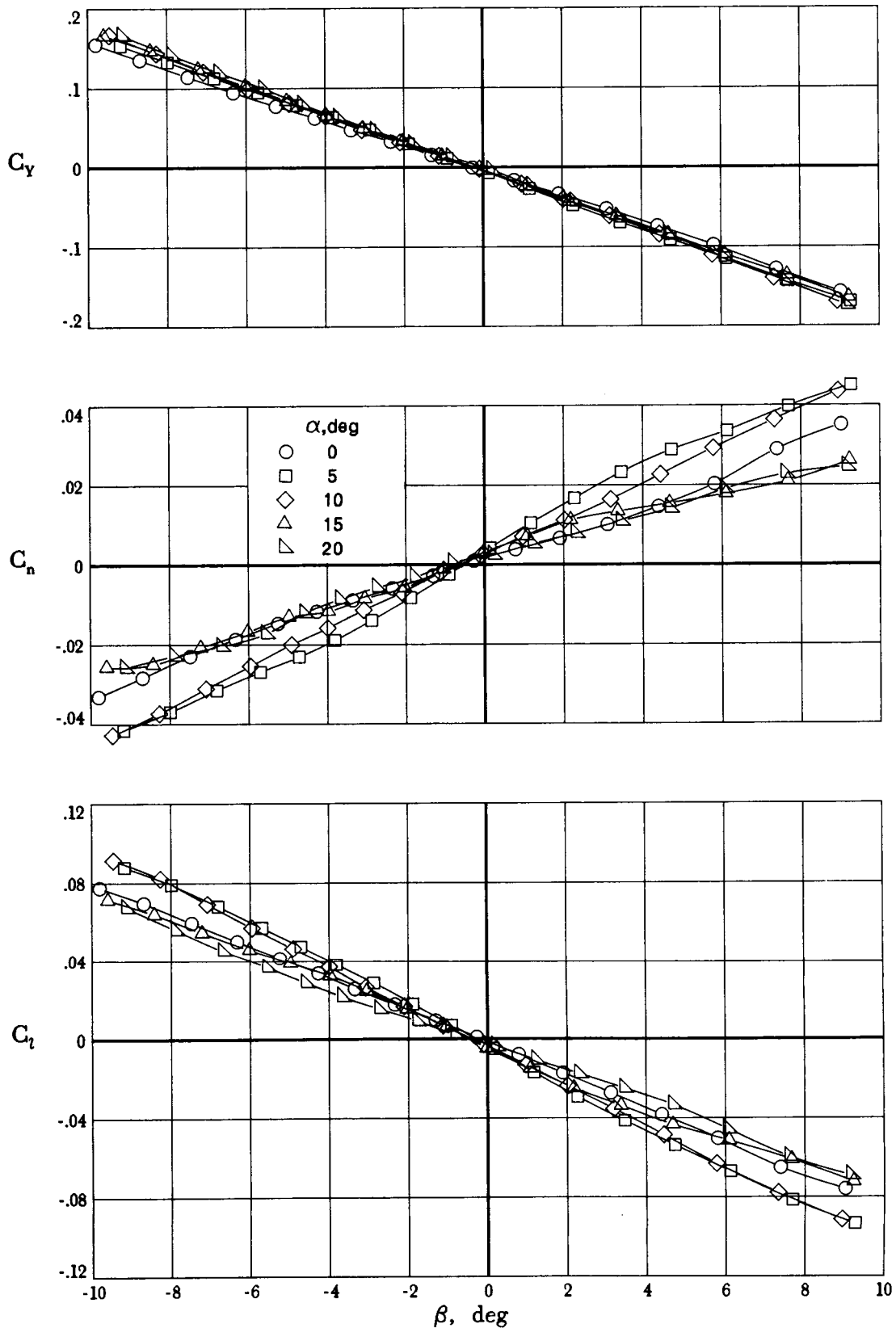

(e) $M = 1.1$.

Figure 11. Continued.

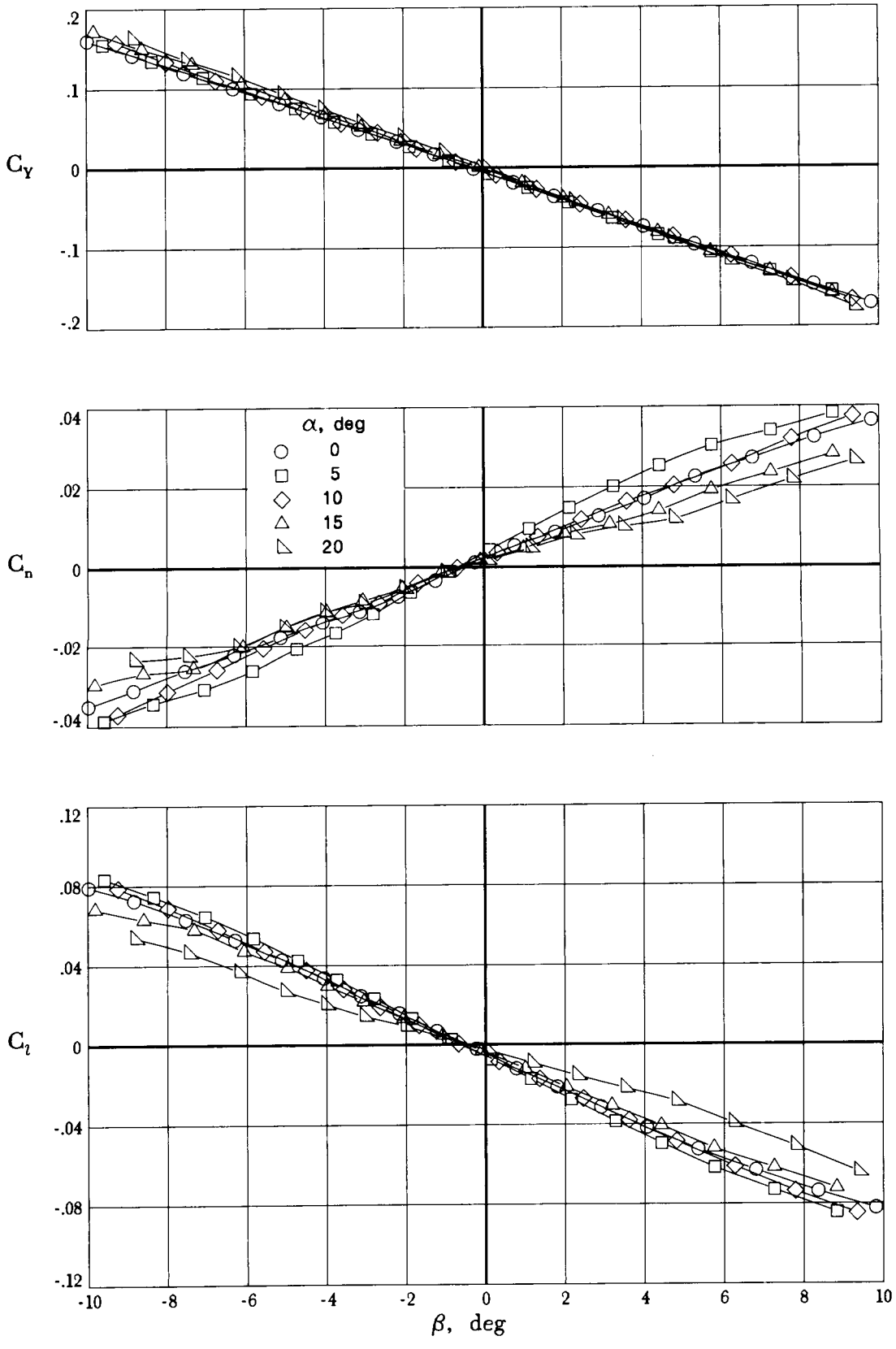

(f) $M = 1.2$.

Figure 11. Concluded.

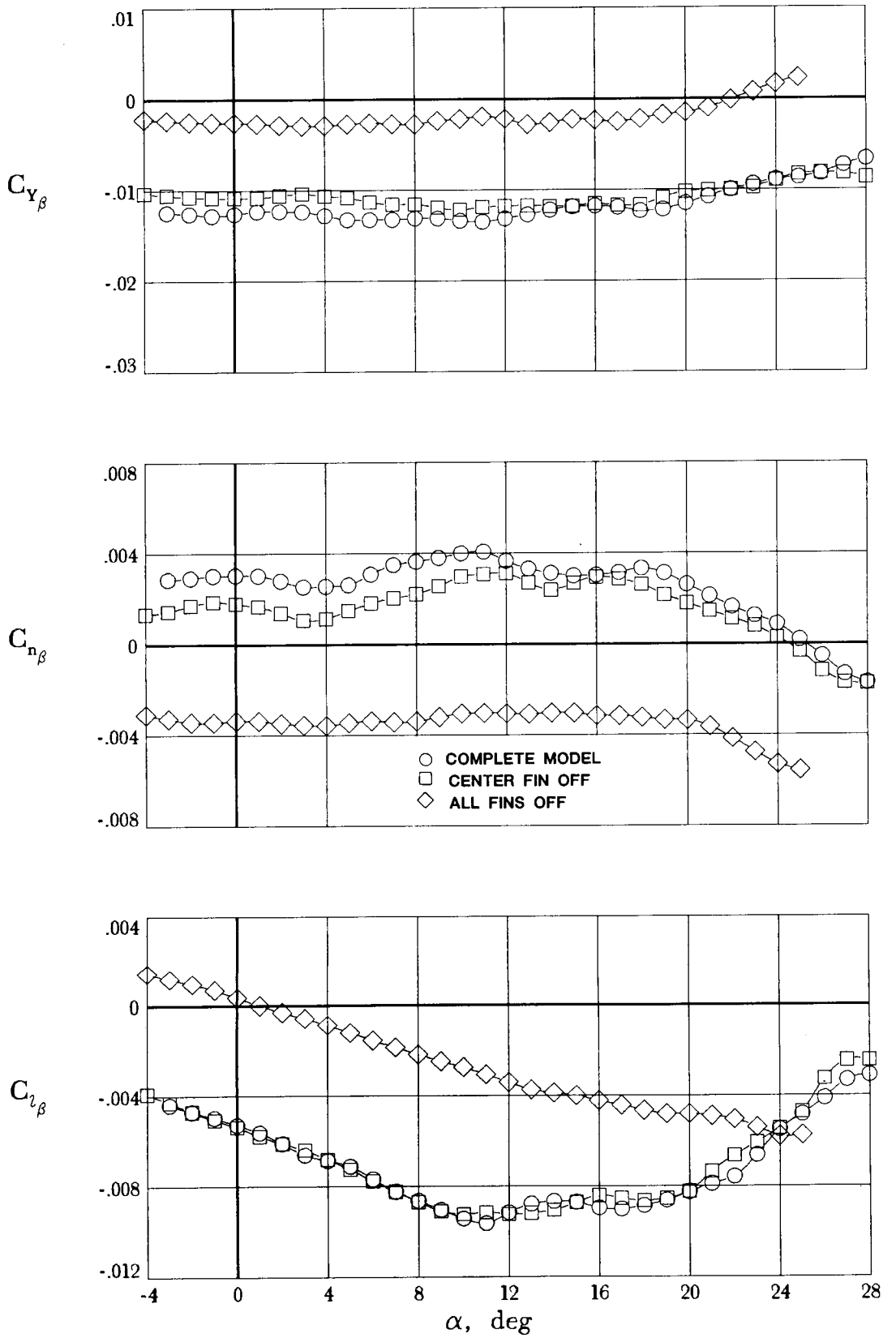

(a) $M = 0.6$.

Figure 12. Effect of fins on lateral-directional stability characteristics.

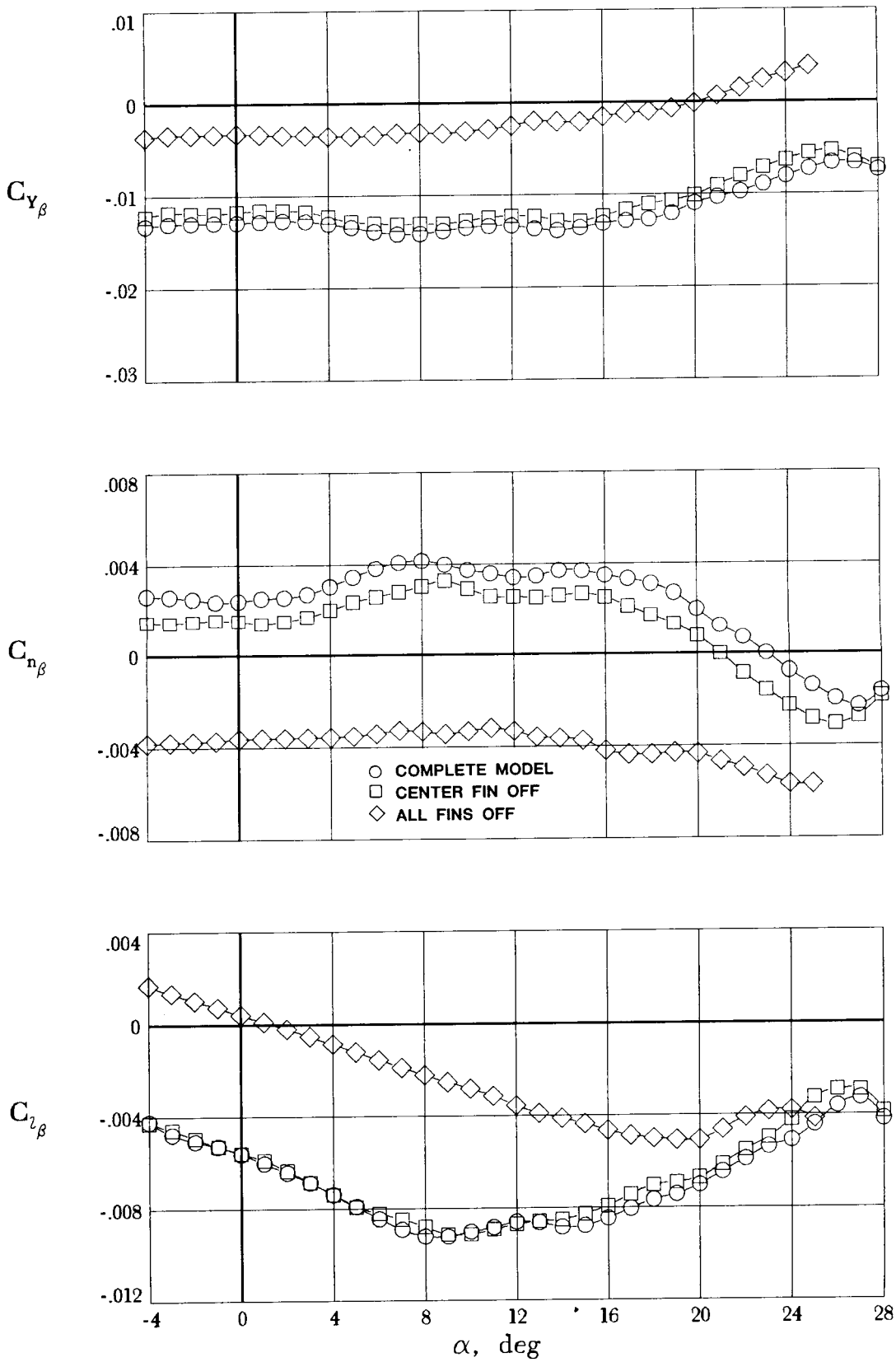

(b) $M = 0.8$.

Figure 12. Continued.

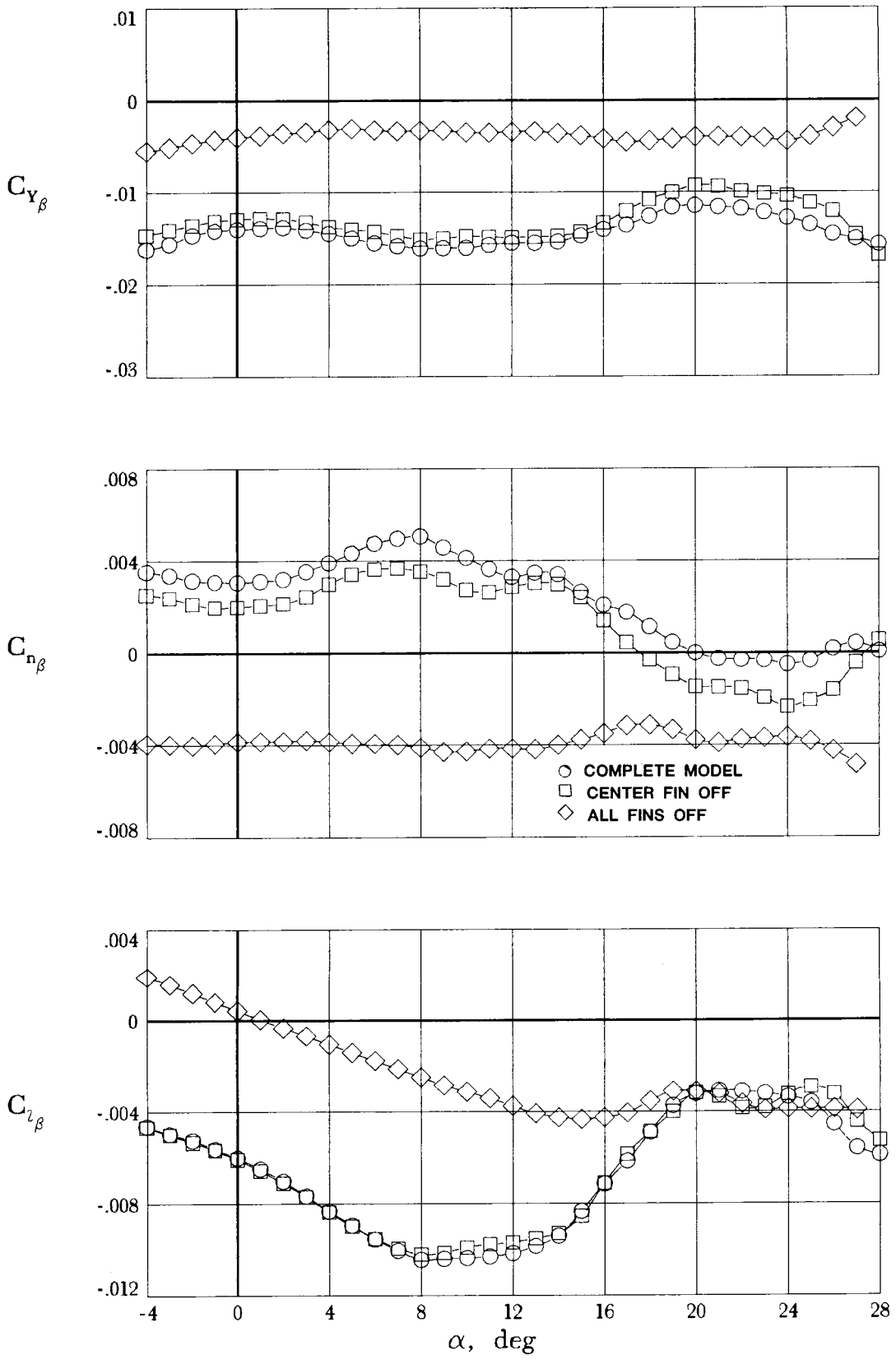

(c) $M = 0.9$.

Figure 12. Continued.

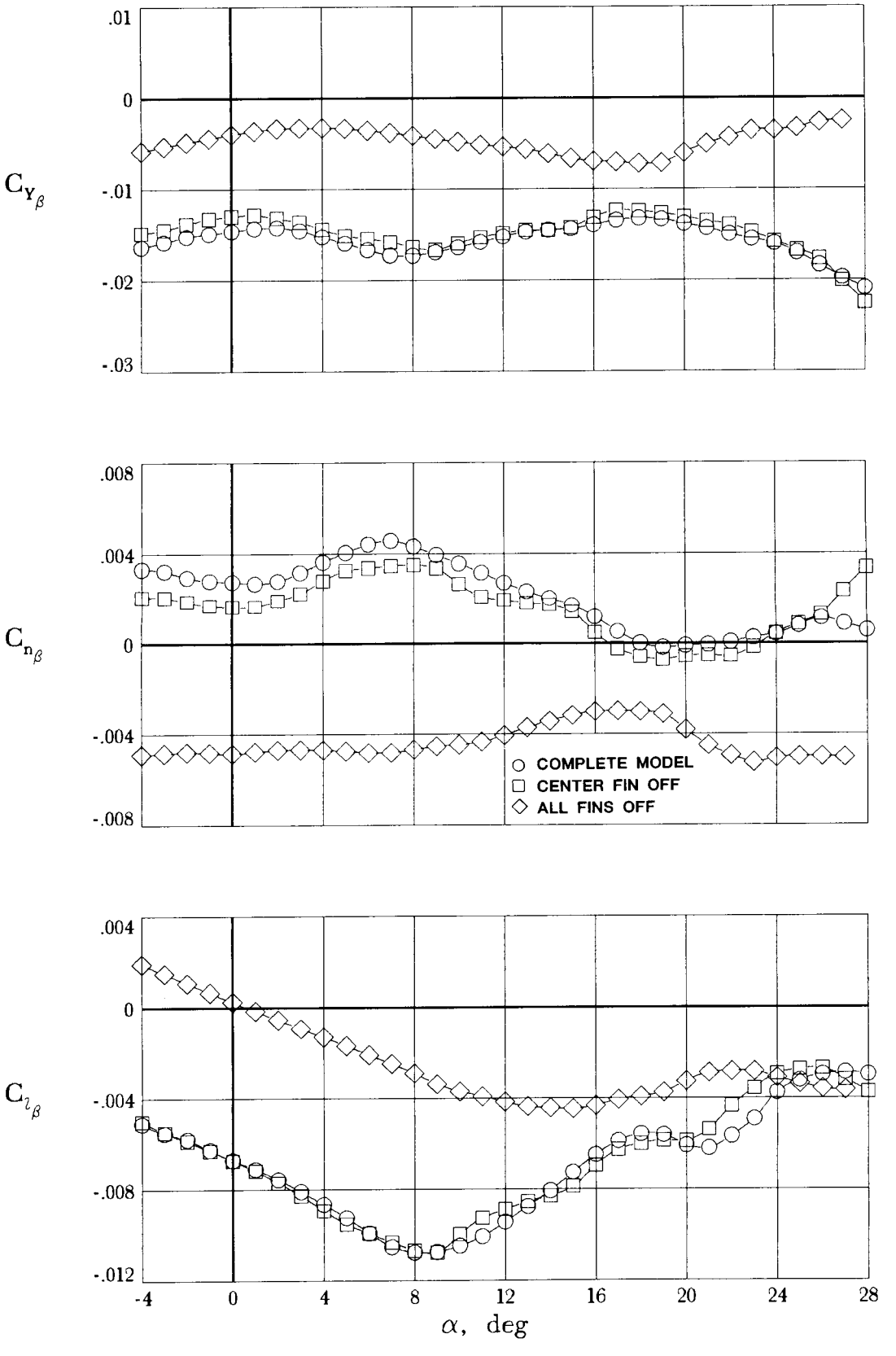

(d) $M = 0.95$.

Figure 12. Continued.

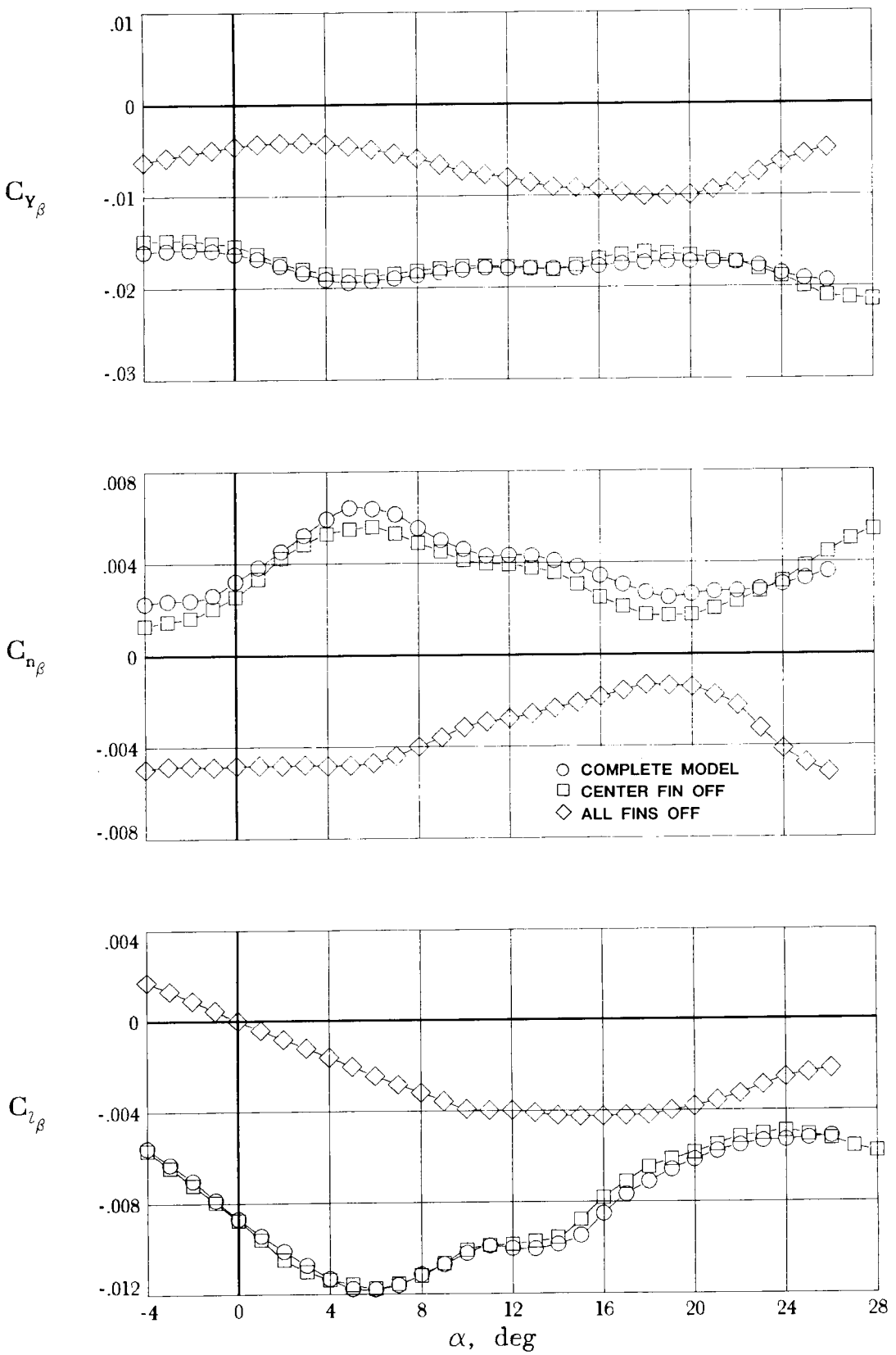

(e) $M = 1.1$.

Figure 12. Continued.

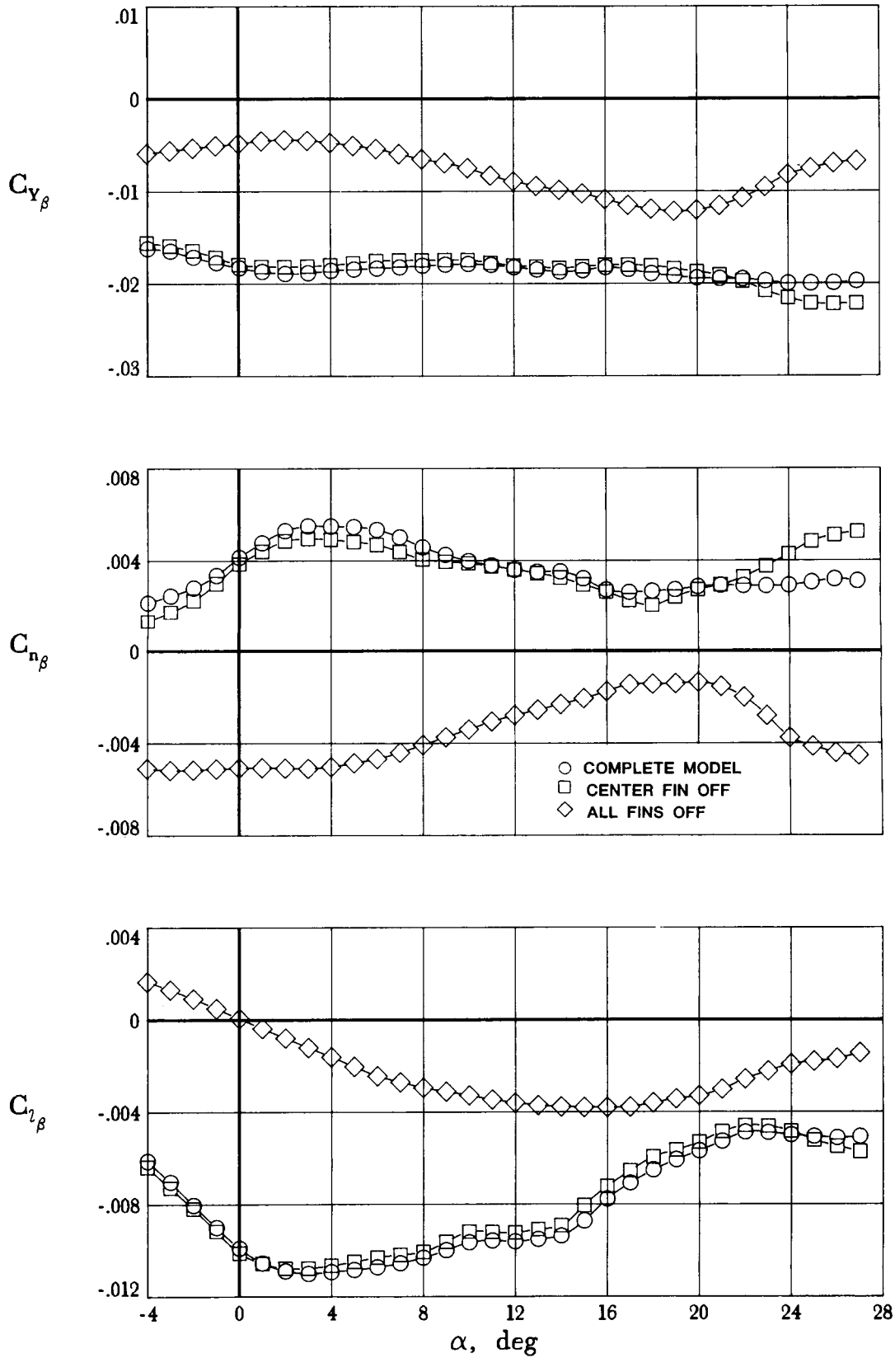

(f) $M = 1.2$.

Figure 12. Concluded.

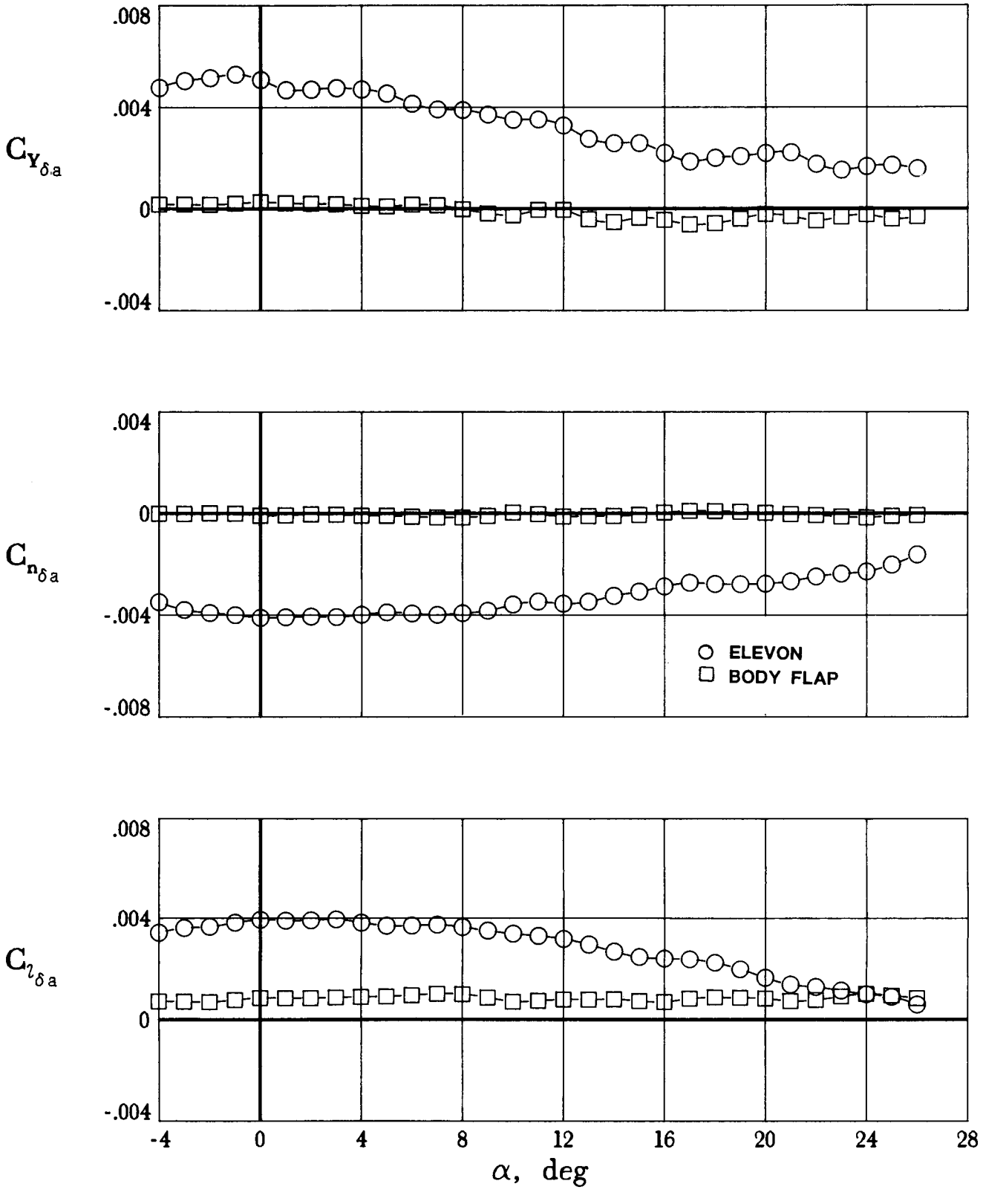

(a) $M = 0.6$.

Figure 13. Roll control effectiveness.

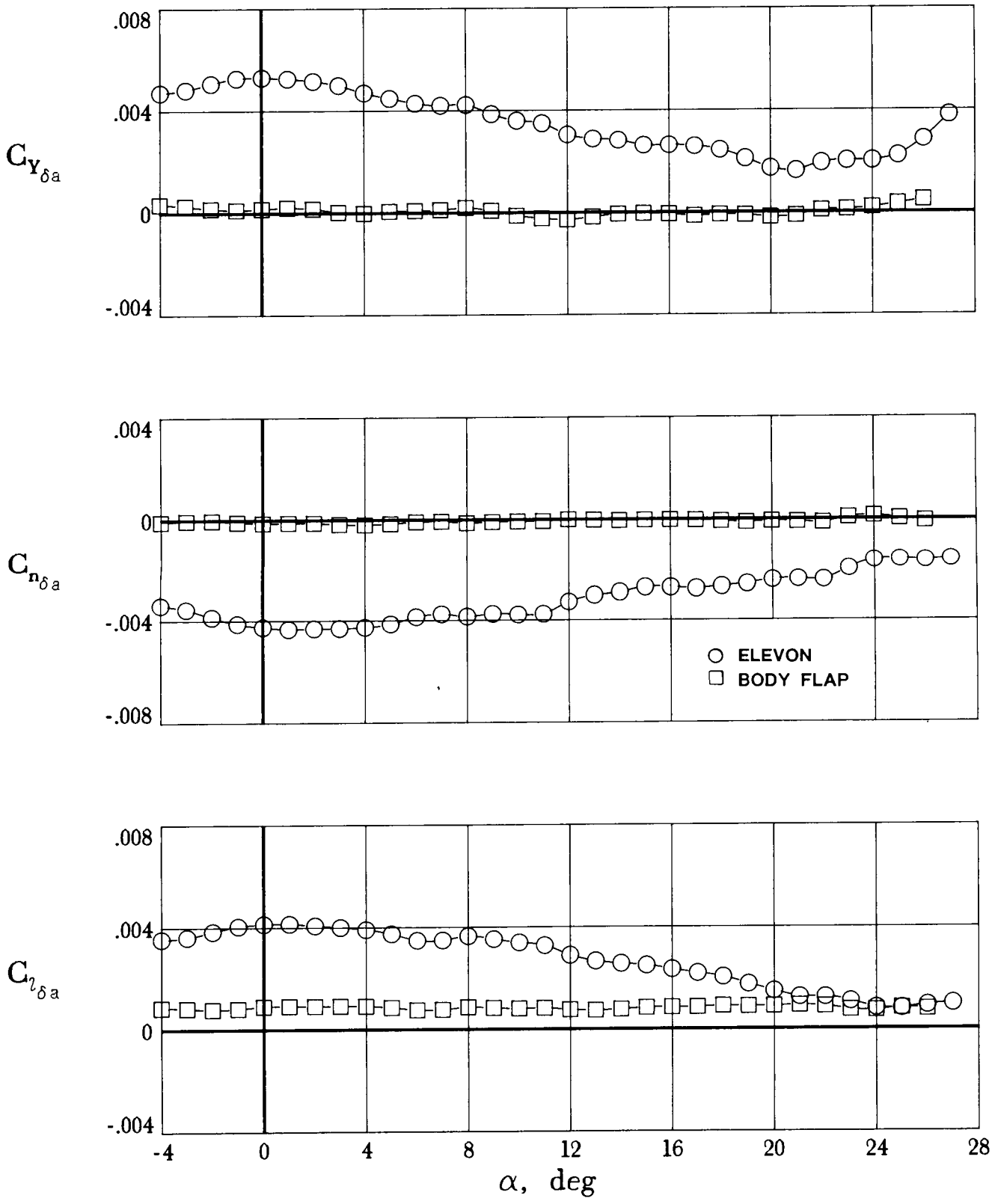

(b) $M = 0.8$.

Figure 13. Continued.

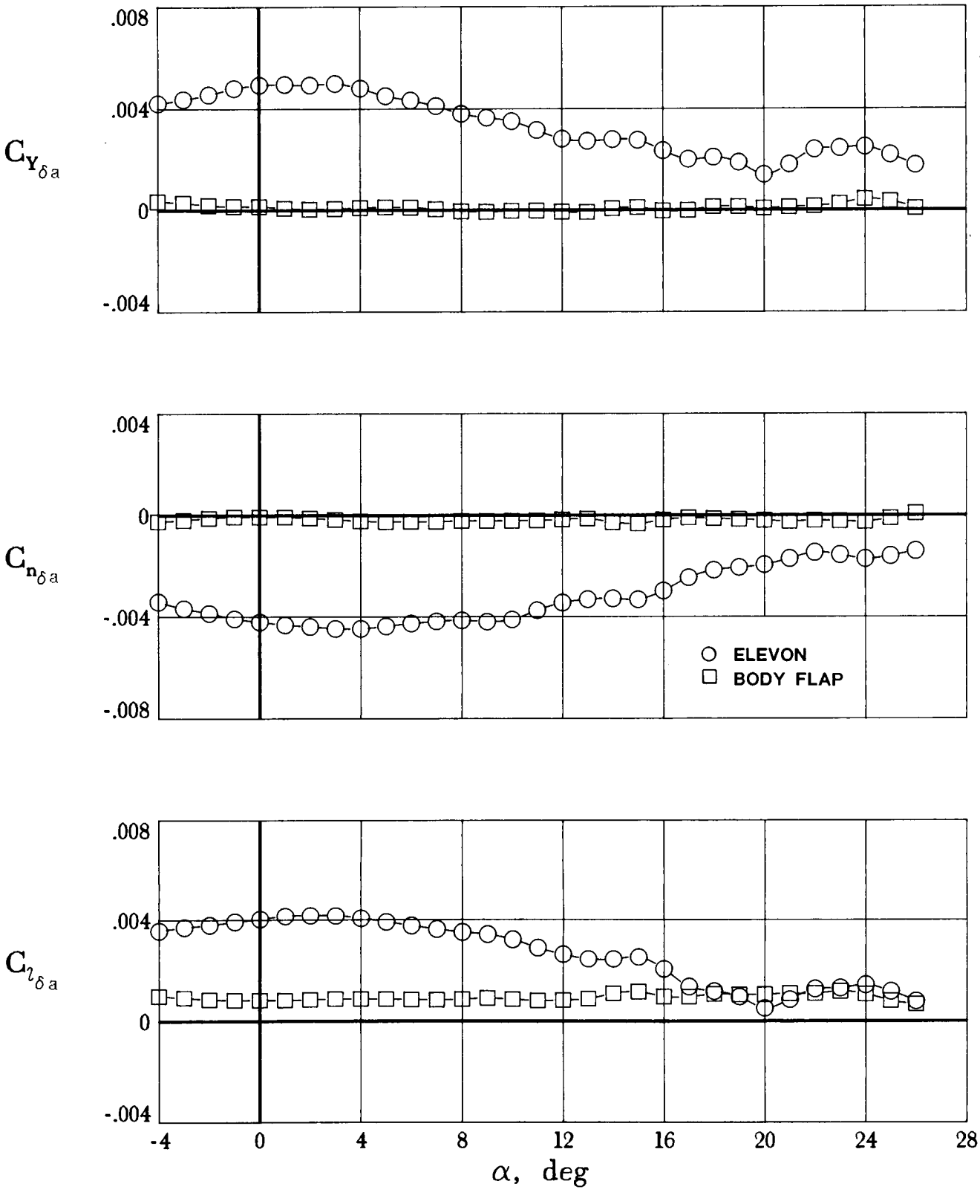

(c) $M = 0.9$.

Figure 13. Continued.

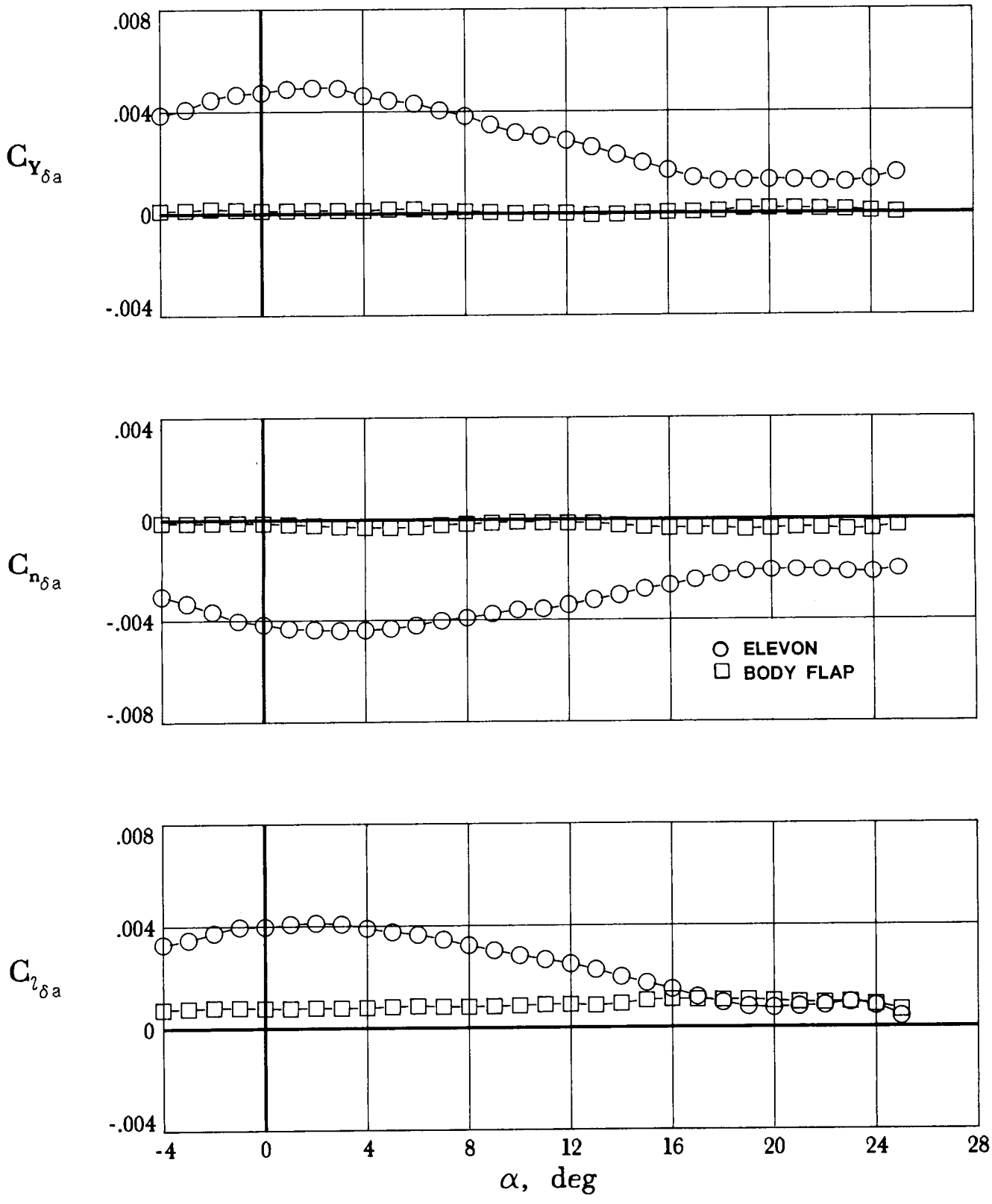

(d) $M = 0.95$.

Figure 13. Continued.

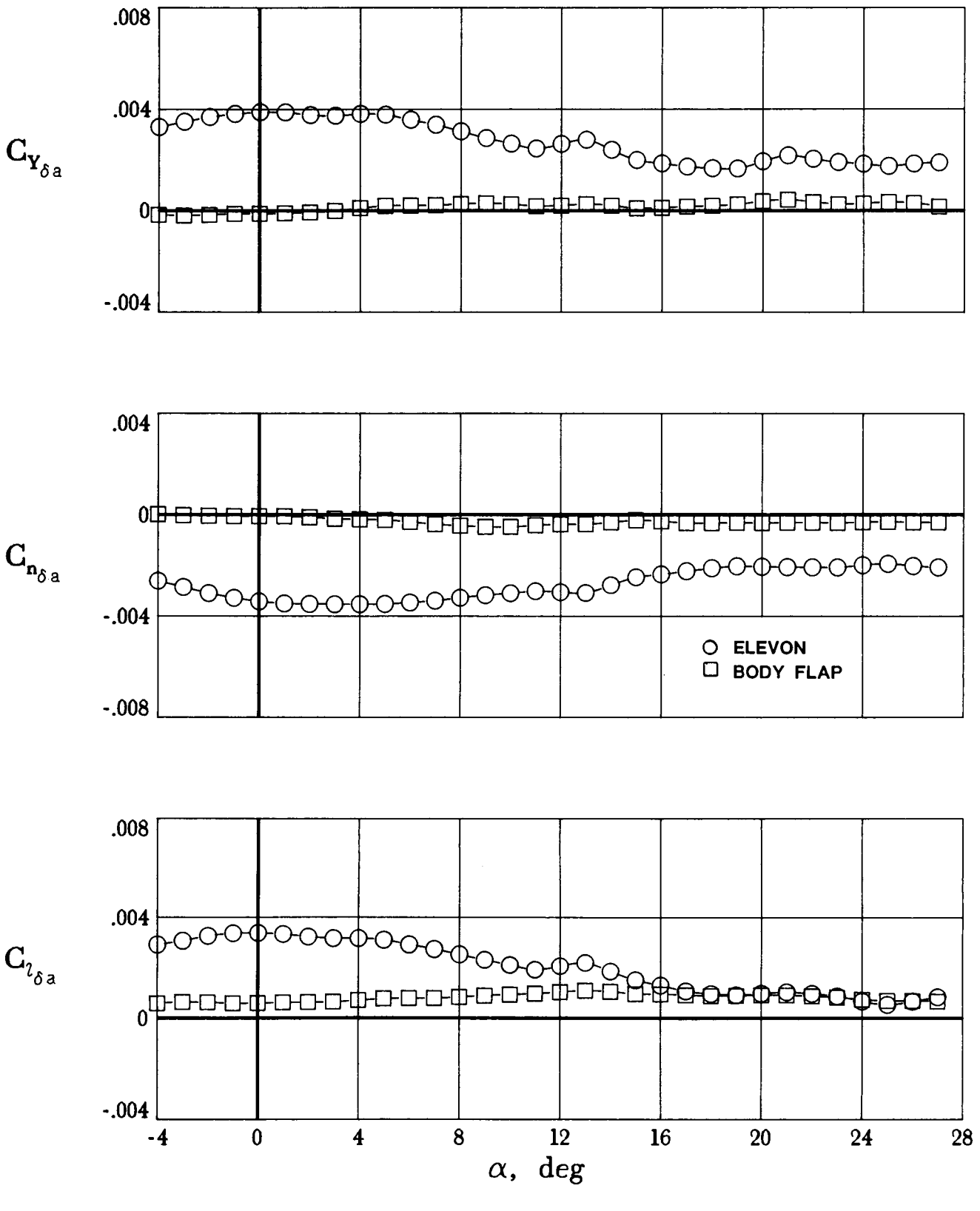

(e) $M = 1.1$.

Figure 13. Continued.

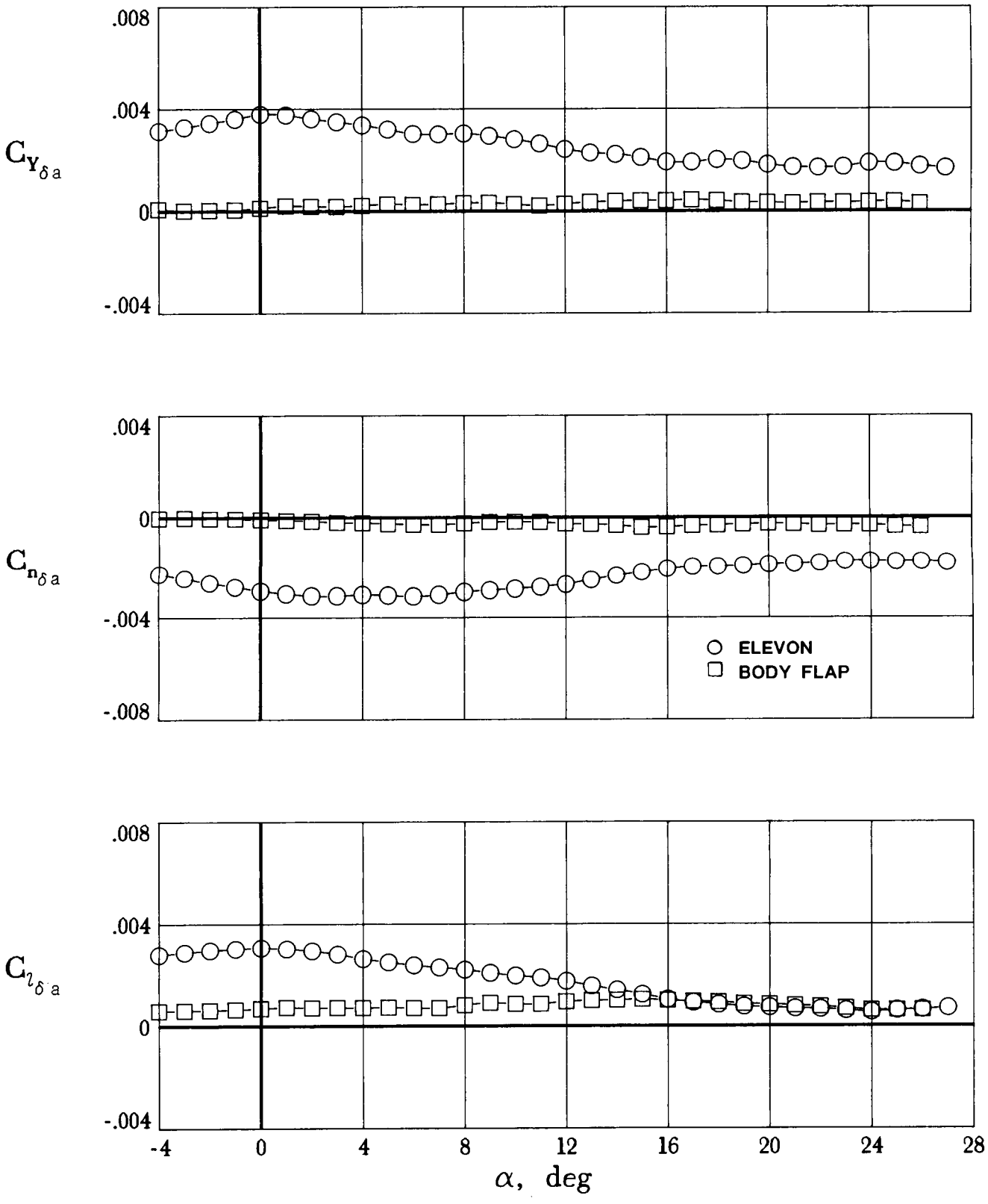

(f) $M = 1.2$.

Figure 13. Concluded.

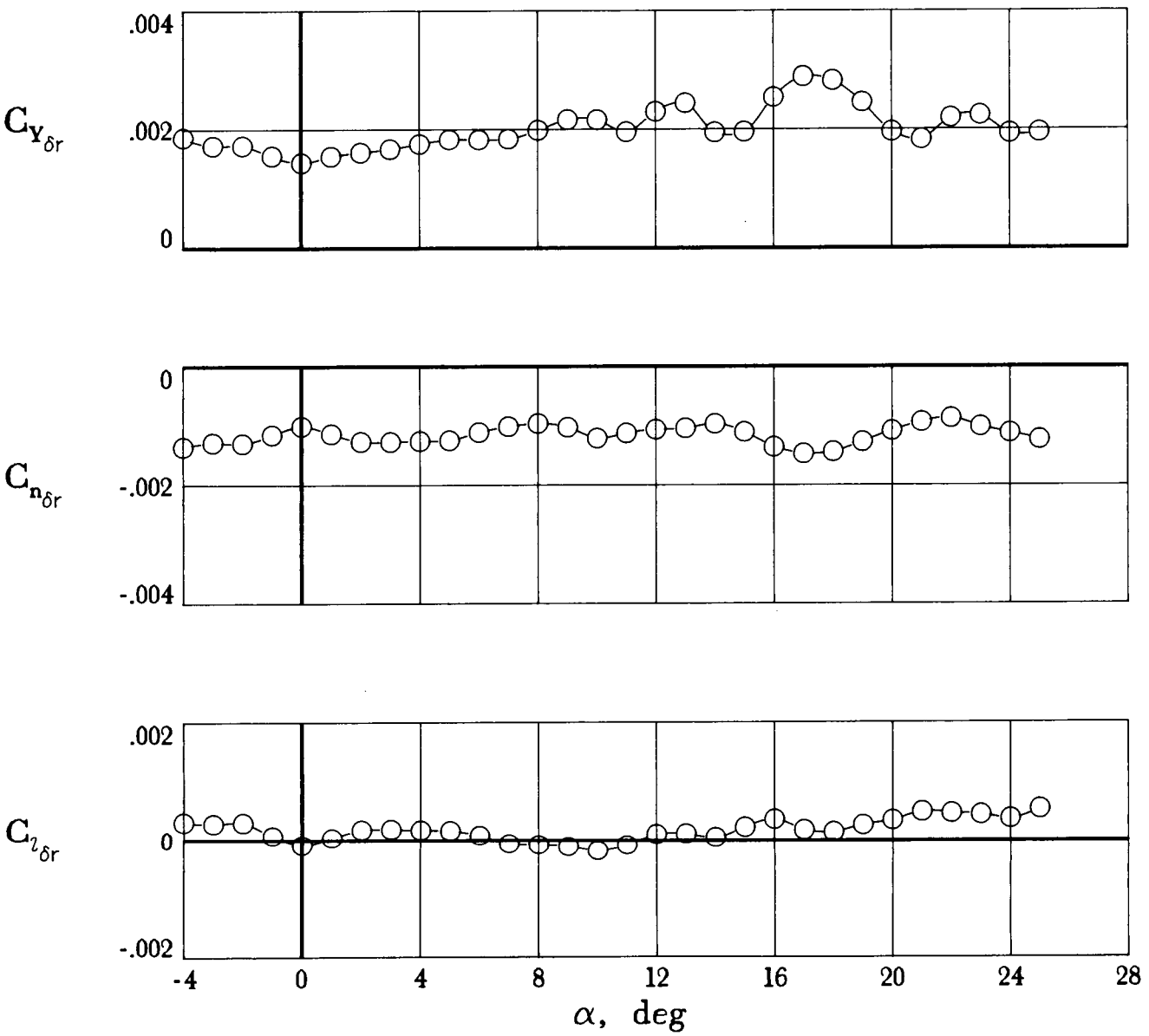

(a) $M = 0.6$.

Figure 14. Yaw control effectiveness.

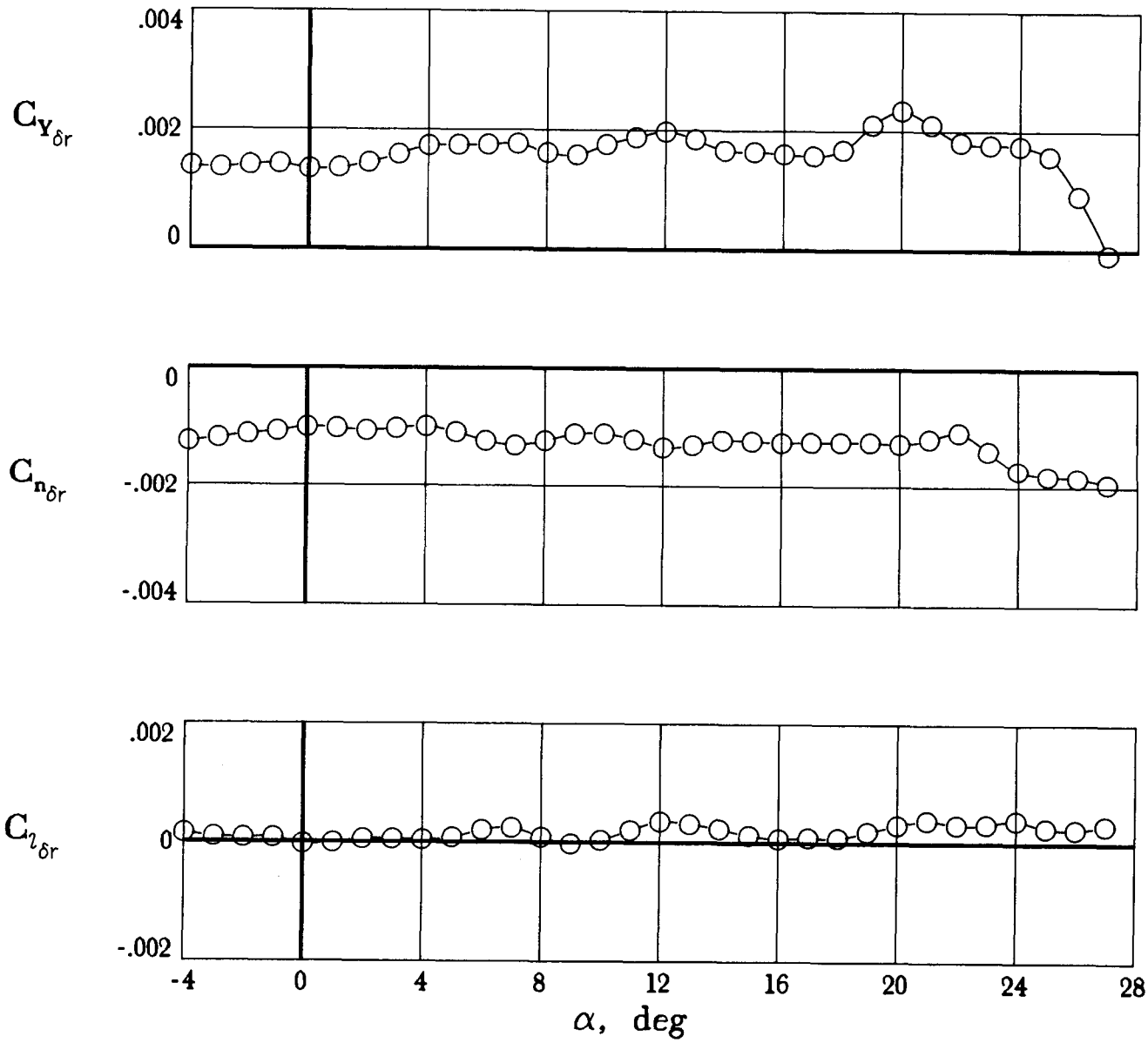

(b) $M = 0.8$.

Figure 14. Continued.

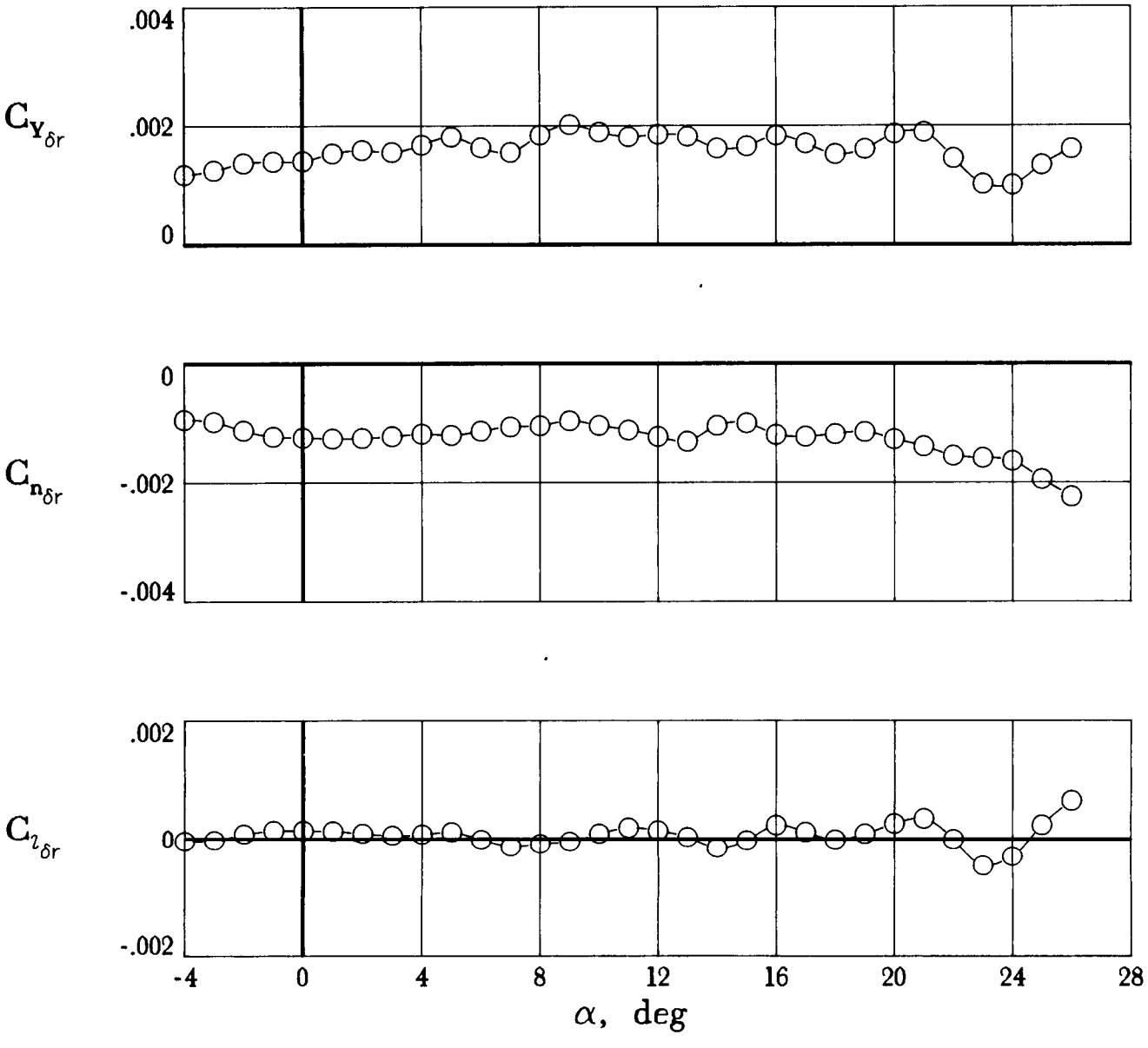

(c) $M = 0.9$.

Figure 14. Continued.

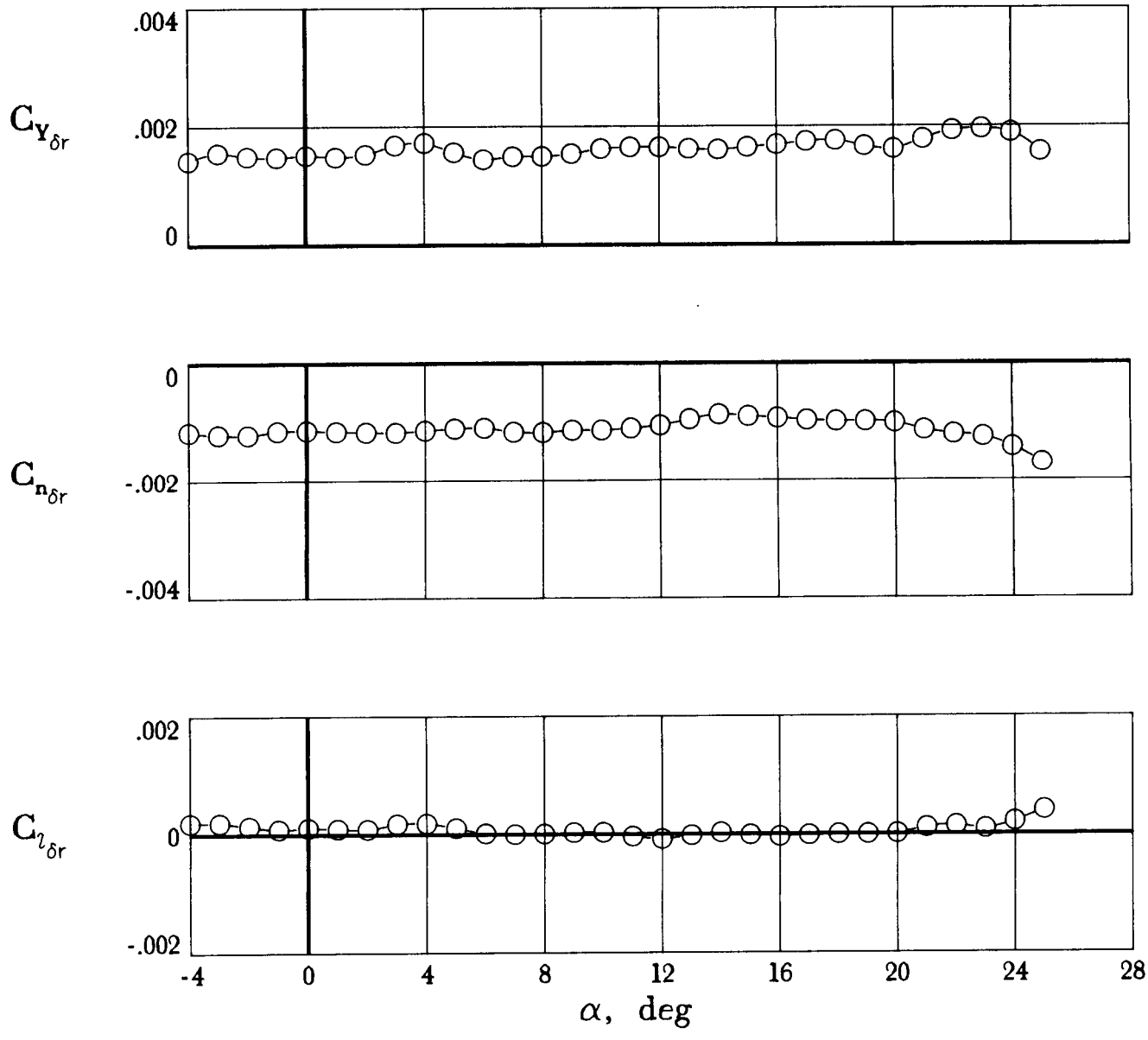

(d) $M = 0.95$.

Figure 14. Continued.

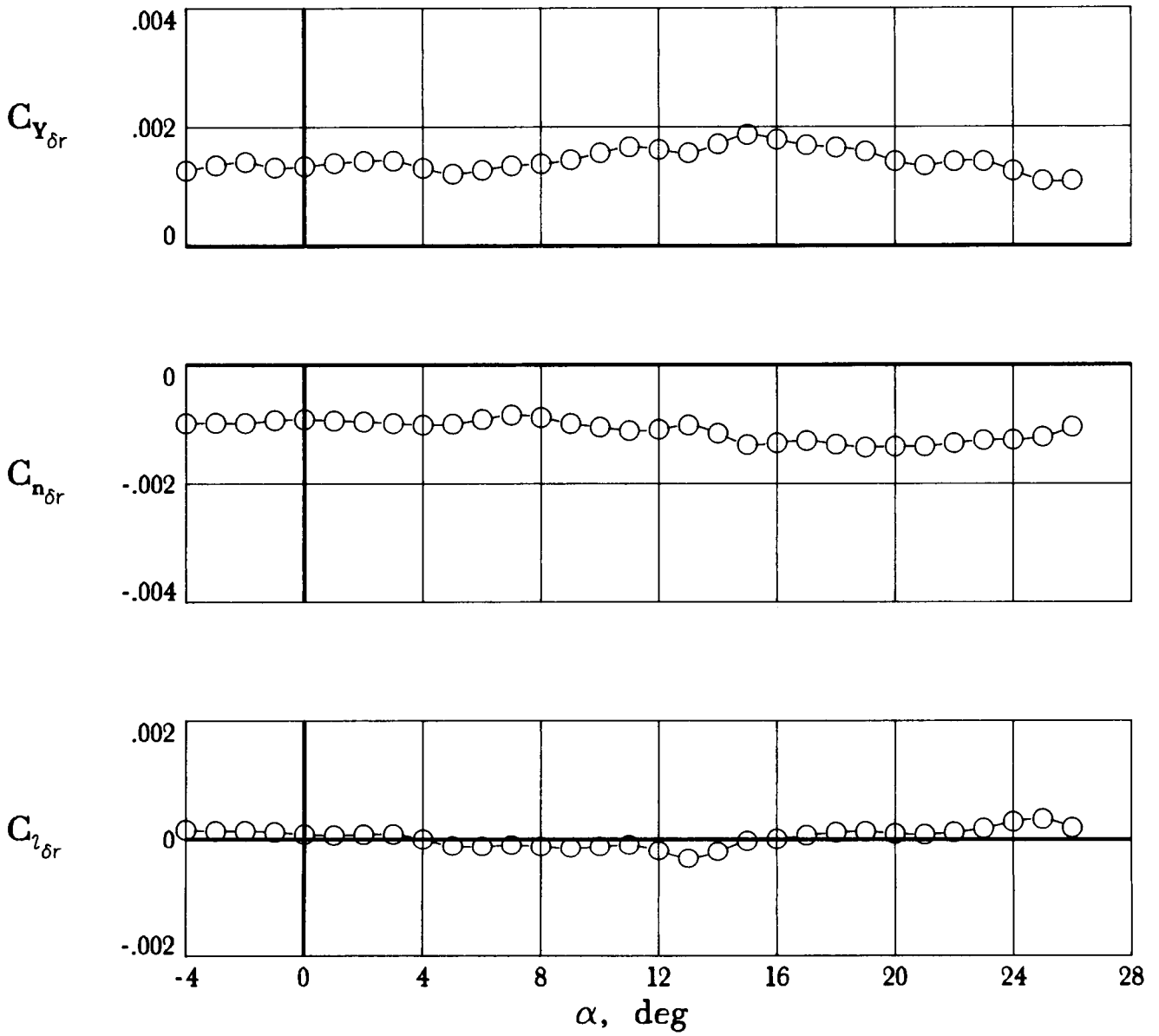

(e) $M = 1.1$.

Figure 14. Continued.

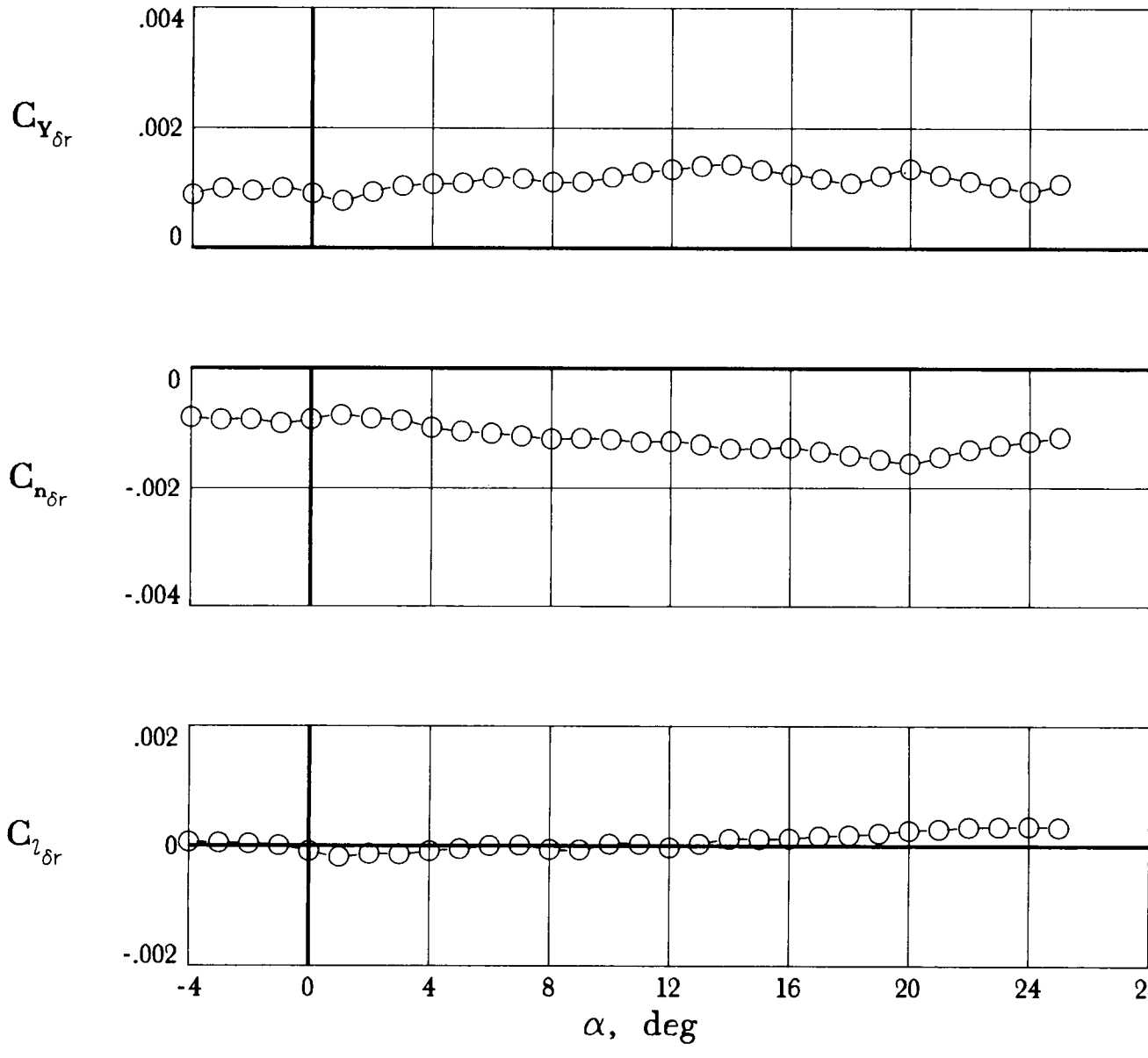

(f) $M = 1.2$.

Figure 14. Concluded.

NASA
National Aeronautics and Space Administration

Report Documentation Page

1. Report No.	2. Government Accession No.	3. Recipient's Catalog No.
NASA TM-4117		

4. Title and Subtitle	5. Report Date
Transonic Aerodynamic Characteristics of a Proposed Assured Crew Return Capability (ACRC) Lifting-Body Configuration	July 1989
	6. Performing Organization Code
7. Author(s)	8. Performing Organization Report No.
George M. Ware	L-16561
9. Performing Organization Name and Address	10. Work Unit No.
NASA Langley Research Center Hampton, VA 23665-5225	506-40-41-01
	11. Contract or Grant No.
12. Sponsoring Agency Name and Address	13. Type of Report and Period Covered
National Aeronautics and Space Administration Washington, DC 20546-0001	Technical Memorandum
	14. Sponsoring Agency Code

15. Supplementary Notes

16. Abstract

The investigation was conducted in the Calspan 8-Foot Transonic Wind Tunnel at Mach numbers from 0.6 to 1.2. The 0.07-scale model had a low-aspect-ratio body with a flat undersurface. A center fin and two tip fins were mounted on the aft upper body. The tip fins were rolled outboard 40° from the vertical. Elevon surfaces made up the trailing edges of the outboard fins, and body flaps were located on the upper and lower aft fuselage. Results of the investigation indicated that the model was longitudinally and laterally stable about a center-of-gravity position at 54 percent of the body length. The maximum trimmed lift/drag ratio was about 3.1 at a Mach number of 0.6. The small center fin contributed only a small positive increment to lateral stability but was effective as a yaw control device. The model with pitch controls undeflected had desirable longitudinal trim characteristics.

17. Key Words (Suggested by Authors(s))	18. Distribution Statement
Aerodynamics Lifting body Spacecraft	Unclassified—Unlimited Subject Category 02

19. Security Classif. (of this report)	20. Security Classif. (of this page)	21. No. of Pages	22. Price
Unclassified	Unclassified	73	A04

NASA FORM 1626 OCT 86

NASA-Langley, 1989

For sale by the National Technical Information Service, Springfield, Virginia 22161-2171